

18.357 Interfacial Phenomena, Fall 2010

taught by Prof. John W. M. Bush

June 3, 2013

Contents

1	Introduction, Notation	3
1.1	Suggested References	3
2	Definition and Scaling of Surface Tension	4
2.1	History: Surface tension in antiquity	4
2.2	Motivation: Who cares about surface tension?	5
2.3	Surface tension: a working definition	6
2.4	Governing Equations	7
2.5	The scaling of surface tension	7
2.6	A few simple examples	9
3	Wetting	11
4	Young's Law with Applications	12
4.1	Formal Development of Interfacial Flow Problems	12
5	Stress Boundary Conditions	14
5.1	Stress conditions at a fluid-fluid interface	14
5.2	Appendix A : Useful identity	16
5.3	Fluid Statics	17
5.4	Appendix B : Computing curvatures	21
5.5	Appendix C : Frenet-Serret Equations	21
6	More on Fluid statics	22
6.1	Capillary forces on floating bodies	23
7	Spinning, tumbling and rolling drops	24
7.1	Rotating Drops	24
7.2	Rolling drops	25
8	Capillary Rise	26
8.1	Dynamics	28
9	Marangoni Flows	30
10	Marangoni Flows II	34
10.1	Tears of Wine	34
10.2	Surfactants	35
10.3	Surfactant-induced Marangoni flows	38
10.4	Bubble motion	39

11 Fluid Jets	40
11.1 The shape of a falling fluid jet	40
11.2 The Plateau-Rayleigh Instability	41
11.3 Fluid Pipes	43
12 Instability Dynamics	45
12.1 Capillary Instability of a Fluid Coating on a Fiber	45
12.2 Dynamics of Instability (Rayleigh 1879)	46
12.3 Rupture of a Soap Film (Culick 1960, Taylor 1960)	47
13 Fluid Sheets	49
13.1 Fluid Sheets: shape and stability	49
13.2 Circular Sheet	50
13.3 Lenticular sheets with unstable rims (Taylor 1960)	51
13.4 Lenticular sheets with stable rims	51
13.5 Water Bells	53
13.6 Swirling Water Bell	54
14 Instability of Superposed Fluids	55
14.1 Rayleigh-Taylor Instability	57
14.2 Kelvin-Helmholtz Instability	58
15 Contact angle hysteresis, Wetting of textured solids	59
15.1 Contact Angle Hysteresis	59
15.2 Wetting of a Rough Surface	61
15.3 Wenzel State (1936)	62
15.4 Cassie-Baxter State	62
16 More forced wetting	64
16.1 Hydrophobic Case: $\theta_e > \pi/2$, $\cos \theta_e < 0$	64
16.2 Hydrophilic Case: $\theta_e < \pi/2$	65
16.3 Forced Wetting: the Landau-Levich-Derjaguin Problem	66
17 Coating: Dynamic Contact Lines	68
17.1 Contact Line Dynamics	71
18 Spreading	74
18.1 Spreading of small drops on solids	74
18.2 Immiscible Drops at an Interface <i>Pujado & Scriven 1972</i>	75
18.3 Oil Spill	76
18.4 Oil on water: A brief review	76
18.5 The Beating Heart <i>Stocker & Bush (JFM 2007)</i>	77
19 Water waves	79

1. Introduction, Notation

We consider fluid systems dominated by the influence of interfacial tension. The roles of curvature pressure and Marangoni stress are elucidated in a variety of situations. Particular attention will be given to the dynamics of drops and bubbles, soap films and minimal surfaces, wetting phenomena, water-repellency, surfactants, Marangoni flows, capillary origami and contact line dynamics. Theoretical developments will be accompanied by classroom demonstrations. The role of surface tension in biology will be highlighted.

Notation

Nomenclature: σ denotes surface tension (at fluid-gas interface)

γ denotes interfacial tension (at fluid-fluid or fluid-solid interface).

Note on units: we will use predominantly *cgs* system.

Unit of force: 1 dyne = 1 g cm s⁻² = 10⁻⁵N as the *cgs* unit of force, roughly the weight of 1 mosquito.

Pressure: 1 atm \approx 100kPa = 10⁵N/m²=10⁶ dynes/cm².

Units: $[\sigma]$ =dynes/cm=mN/m.

What is an interface?: roughness scale δ , from equality of surface and thermal energy get $\sigma\delta^2 \sim kT \Rightarrow \delta \sim (kT/\sigma)^{1/2}$. If $\delta \ll$ scales of experiment, can speak of a smooth interface.

1.1 Suggested References

While this list of relevant textbooks is far from complete, we include it as a source of additional reading for the interested student.

- **Capillarity and Wetting Phenomena: Drops, Bubbles, Pearls, Waves**
by P.G. de Gennes, F. Brochard-Wyart and D. Quéré. Springer Publishing.
A readable and accessible treatment of a wide range of capillary phenomena.
- **Molecular theory of capillarity**
by J.S. Rowlinson and B. Widom. Dover 1982.
- **Intermolecular and surface forces**
by J. Israelachvili. Academic Press, 2nd edition 1995.
- **Multimedia Fluid Mechanics**
Cambridge University Press, Ed. Bud Homsy.
A DVD with an extensive section devoted to capillary effects. Relevant videos will be used throughout the course.

2. Definition and Scaling of Surface Tension

These lecture notes have been drawn from many sources, including textbooks, journal articles, and lecture notes from courses taken by the author as a student. These notes are not intended as a complete discussion of the subject, or as a scholarly work in which all relevant references are cited. Rather, they are intended as an introduction that will hopefully motivate the interested student to learn more about the subject. Topics have been chosen according to their perceived value in developing the physical insight of the students.

2.1 History: Surface tension in antiquity

Hero of Alexandria (10 AD - 70 AD) Greek mathematician and engineer, “*the greatest experimentalist of antiquity*”. Exploited capillarity in a number of inventions described in his book *Pneumatics*, including the water clock.

Pliny the Elder (23 AD - 79 AD) Author, natural philosopher, army and naval commander of the early Roman Empire. Described the glassy wakes of ships. “*True glory comes in doing what deserves to be written; in writing what deserves to be read; and in so living as to make the world happier.*” “*Truth comes out in wine*”.

Leonardo da Vinci (1452-1519) Reported capillary rise in his notebooks, hypothesized that mountain streams are fed by capillary networks.

Francis Hauksbee (1666-1713) Conducted systematic investigation of capillary rise, his work was described in Newton’s *Opticks*, but no mention was made of him.

Benjamin Franklin (1706-1790) Polymath: scientist, inventor, politician; examined the ability of oil to suppress waves.

Pierre-Simon Laplace (1749-1827) French mathematician and astronomer, elucidated the concept and theoretical description of the meniscus, hence the term Laplace pressure.

Thomas Young (1773-1829) Polymath, solid mechanic, scientist, linguist. Demonstrated the wave nature of light with ripple tank experiments, described wetting of a solid by a fluid.

Joseph Plateau (1801-1883) Belgian physicist, continued his experiments after losing his sight. Extensive study of capillary phenomena, soap films, minimal surfaces, drops and bubbles.

2.2 Motivation: Who cares about surface tension?

As we shall soon see, surface tension dominates gravity on a scale less than the capillary length (roughly 2mm). It thus plays a critical role in a variety of small-scale processes arising in biology, environmental science and technology.

Biology

- all small creatures live in a world dominated by surface tension
- surface tension important for insects for many basic functions
- weight support and propulsion at the water surface
- adhesion and deadhesion via surface tension
- the pistol shrimp: hunting with bubbles
- underwater breathing and diving via surface tension
- natural strategies for water-repellency in plants and animals
- the dynamics of lungs and the role of surfactants and impurities
- early life: early vesicle formation, confinement to an interface
- oil recovery, carbon sequestration, groundwater flows
- design of insecticides intended to coat insects, leave plant unharmed
- chemical leaching and the water-repellency of soils
- oil spill dynamics and mitigation
- disease transmission via droplet exhalation
- dynamics of magma chambers and volcanoes
- the exploding lakes of Cameroon

Technology

- capillary effects dominant in microgravity settings: NASA
- cavitation-induced damage on propellers and submarines
- cavitation in medicine: used to damage kidney stones, tumours ...
- design of superhydrophobic surfaces e.g. self-cleaning windows, drag-reducing or erosion-resistant surfaces
- lab-on-a-chip technology: medical diagnostics, drug delivery
- microfluidics: continuous and discrete fluid transport and mixing
- tracking submarines with their surface signature
- inkjet printing
- the bubble computer

This image has been removed due to copyright restrictions. Please see the image on page <http://news.sciencemag.org/sciencenow/2011/06/spiders.html#panel-2>.

Figure 2.1: The diving bell spider

Geophysics and environmental science

- the dynamics of raindrops and their role in the biosphere
- most biomaterial is surface active, sticks to the surface of drops / bubbles
- chemical, thermal and biological transport in the surf zone

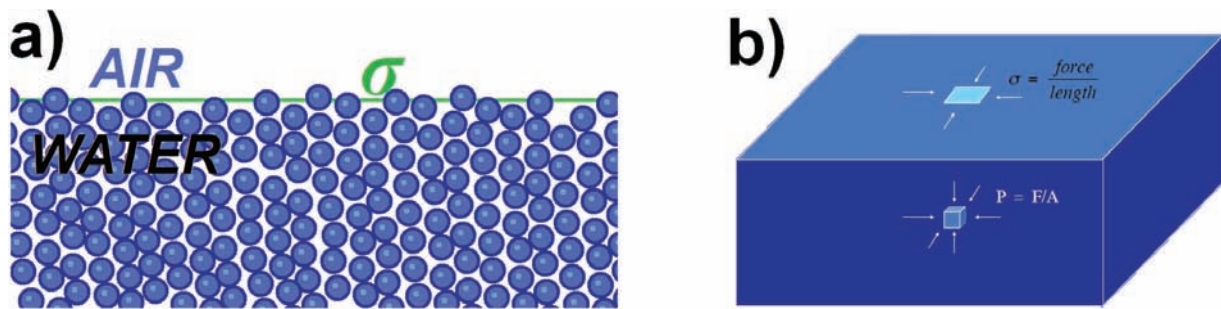


Figure 2.2: a) The free surface between air and water at a molecular scale. b) Surface tension is analogous to a negative surface pressure.

2.3 Surface tension: a working definition

Discussions of the molecular origins of surface or interfacial tension may be found elsewhere (e.g. *Israelachvili 1995, Rowlinson & Widom 1982*). Our discussion follows that of *de Gennes, Brochard-Wyart & Quéré 2003*.

Molecules in a fluid feel a mutual attraction. When this attractive force is overcome by thermal agitation, the molecules pass into a gaseous phase. Let us first consider a free surface, for example that between air and water (Fig. 2.2a). A water molecule in the fluid bulk is surrounded by attractive neighbours, while a molecule at the surface has a reduced number of such neighbours and so in an energetically unfavourable state. The creation of new surface is thus energetically costly, and a fluid system will act to minimize surface areas. It is thus that small fluid bodies tend to evolve into spheres; for example, a thin fluid jet emerging from your kitchen sink will generally pinch off into spherical drops in order to minimize the total surface area (see Lecture 5).

If U is the total cohesive energy per molecule, then a molecule at a free surface will lose $U/2$ relative to molecules in the bulk. Surface tension is a direct measure of this energy loss per unit area of surface. If the characteristic molecular dimension is R and its area thus R^2 , then the surface tension is $\sigma \sim U/(2R)^2$. Note that surface tension increases as the intermolecular attraction increases and the molecular size decreases. For most oils, $\sigma \sim 20$ dynes/cm, while for water, $\sigma \sim 70$ dynes/cm. The highest surface tensions are for liquid metals; for example, liquid mercury has $\sigma \sim 500$ dynes/cm. The origins of interfacial tension are analogous. Interfacial tension is a material property of a fluid-fluid interface whose origins lie in the different energy per area that acts to resist the creation of new interface. Fluids between which no interfacial tension arises are said to be miscible. For example, salt molecules will diffuse freely across a boundary between fresh and salt water; consequently, these fluids are miscible, and there is no interfacial tension between them. Our discussion will be confined to immiscible fluid-fluid interfaces (or fluid-gas surfaces), at which an effective interfacial (or surface) tension acts.

Surface tension σ has the units of force/length or equivalently energy/area, and so may be thought of as a negative surface pressure, or, equivalently, as a line tension acting in all directions parallel to the surface. Pressure is generally an isotropic force per area that acts throughout the bulk of a fluid: small surface element dS will feel a total force $p(\mathbf{x})dS$ owing to the local pressure field $p(\mathbf{x})$. If the surface S is closed, and the pressure uniform, the net pressure force acting on S is zero and the fluid remains static. Pressure gradients correspond to body forces (with units of force per unit volume) within a fluid, and so appear explicitly in the Navier-Stokes equations. Surface tension has the units of force per length, and its action is confined to the free surface. Consider for the sake of simplicity a perfectly flat interface. A surface line element $d\ell$ will feel a total force $\sigma d\ell$ owing to the local surface tension $\sigma(\mathbf{x})$. If the surface line element is a closed loop C , and the surface tension uniform, the net surface tension force acting on C is zero, and the fluid remains static. If surface tension gradients arise, there may be a net force on the surface element that acts to distort it through driving flow.

2.4 Governing Equations

The motion of a fluid of uniform density ρ and dynamic viscosity μ is governed by the Navier-Stokes equations, which represent a continuum statement of Newton's laws.

$$\rho \left(\frac{\partial \mathbf{u}}{\partial t} + \mathbf{u} \cdot \nabla \mathbf{u} \right) = -\nabla p + \mathbf{F} + \mu \nabla^2 \mathbf{u} \quad (2.1)$$

$$\nabla \cdot \mathbf{u} = 0 \quad (2.2)$$

This represents a system of 4 equations in 4 unknowns (the fluid pressure p and the three components of the velocity field \mathbf{u}). Here \mathbf{F} represents any body force acting on a fluid; for example, in the presence of a gravitational field, $\mathbf{F} = \rho \mathbf{g}$ where \mathbf{g} is the acceleration due to gravity.

Surface tension acts only at the free surface; consequently, it does not appear in the Navier-Stokes equations, but rather enters through the boundary conditions. The boundary conditions appropriate at a fluid-fluid interface are formally developed in Lecture 3. We here simply state them for the simple case of a free surface (such as air-water, in which one of the fluids is not dynamically significant) in order to get a feeling for the scaling of surface tension. The normal stress balance at a free surface must be balanced by the curvature pressure associated with the surface tension:

$$\mathbf{n} \cdot \mathbf{T} \cdot \mathbf{n} = \sigma (\nabla \cdot \mathbf{n}) \quad (2.3)$$

where $\mathbf{T} = -p\mathbf{I} + \mu [\nabla \mathbf{u} + (\nabla \mathbf{u})^T] = -p\mathbf{I} + 2\mu \mathbf{E}$ is the stress tensor, $\mathbf{E} = \frac{1}{2} [\nabla \mathbf{u} + (\nabla \mathbf{u})^T]$ is the deviatoric stress tensor, and \mathbf{n} is the unit normal to the surface. The tangential stress at a free surface must balance the local surface tension gradient:

$$\mathbf{n} \cdot \mathbf{T} \cdot \mathbf{t} = \nabla \sigma \cdot \mathbf{t} \quad (2.4)$$

where \mathbf{t} is the unit tangent to the interface.

2.5 The scaling of surface tension

Fundamental Concept The laws of Nature cannot depend on arbitrarily chosen system of units. Any physical system is most succinctly described in terms of dimensionless variables.

Buckingham's Theorem For a system with M physical variables (e.g. density, speed, length, viscosity) describable in terms of N fundamental units (e.g. mass, length, time, temperature), there are $M - N$ dimensionless groups that govern the system.

E.g. Translation of a rigid sphere through a viscous fluid:

Physical variables: sphere speed U and radius a , fluid viscosity ν and density ρ and sphere drag D ; $M = 5$.

Fundamental units: mass M , length L and time T ; $N = 3$.

Buckingham's Theorem: there are $M - N = 2$ dimensionless groups: $C_d = D/\rho U^2$ and $Re = Ua/\nu$. System is uniquely determined by a single relation between the two: $C_d = F(Re)$.

We consider a fluid of density ρ and viscosity $\mu = \rho\nu$ with a free surface characterized by a surface tension σ . The flow is marked by characteristic length- and velocity- scales of, respectively, a and U , and evolves in the presence of a gravitational field $\mathbf{g} = -g\hat{\mathbf{z}}$. We thus have a physical system defined in terms of six physical variables ($\rho, \nu, \sigma, a, U, g$) that may be expressed in terms of three fundamental units: mass, length and time. Buckingham's Theorem thus indicates that the system may be uniquely described in terms of three dimensionless groups. We choose

$$Re = \frac{Ua}{\nu} = \frac{\text{Inertia}}{\text{Viscosity}} = \text{Reynolds number} \quad (2.5)$$

$$Fr = \frac{U^2}{ga} = \frac{\text{Inertia}}{\text{Gravity}} = \text{Froude number} \quad (2.6)$$

$$Bo = \frac{\rho ga^2}{\sigma} = \frac{\text{Gravity}}{\text{Curvature}} = \text{Bond number} \quad (2.7)$$

The Reynolds number prescribes the relative magnitudes of inertial and viscous forces in the system, while the Froude number those of inertial and gravity forces. The Bond number indicates the relative importance of forces induced by gravity and surface tension. Note that these two forces are comparable when $\mathcal{Bo} = 1$, which arises at a lengthscale corresponding to the capillary length: $\ell_c = (\sigma/(\rho g))^{1/2}$. For an air-water surface, for example, $\sigma \approx 70$ dynes/cm, $\rho = 1\text{g/cm}^3$ and $g = 980\text{ cm/s}^2$, so that $\ell_c \approx 2\text{mm}$. Bodies of water in air are dominated by the influence of surface tension provided they are smaller than the capillary length. Roughly speaking, the capillary length prescribes the maximum size of pendant drops that may hang inverted from a ceiling, water-walking insects, and raindrops. Note that as a fluid system becomes progressively smaller, the relative importance of surface tension over gravity increases; it is thus that surface tension effects are critical in many in microscale engineering processes and in the lives of bugs.

Finally, we note that other frequently arising dimensionless groups may be formed from the products of \mathcal{Bo} , \mathcal{Re} and \mathcal{Fr} :

$$\mathcal{We} = \frac{\rho U^2 a}{\sigma} = \frac{\text{Inertia}}{\text{Curvature}} = \text{Weber number} \quad (2.8)$$

$$\mathcal{Ca} = \frac{\rho \nu U}{\sigma} = \frac{\text{Viscous}}{\text{Curvature}} = \text{Capillary number} \quad (2.9)$$

The Weber number indicates the relative magnitudes of inertial and curvature forces within a fluid, and the capillary number those of viscous and curvature forces. Finally, we note that if the flow is marked by a Marangoni stress of characteristic magnitude $\Delta\sigma/L$, then an additional dimensionless group arises that characterizes the relative magnitude of Marangoni and curvature stresses:

$$\mathcal{Ma} = \frac{a\Delta\sigma}{L\sigma} = \frac{\text{Marangoni}}{\text{Curvature}} = \text{Marangoni number} \quad (2.10)$$

We now demonstrate how these dimensionless groups arise naturally from the nondimensionalization of Navier-Stokes equations and the surface boundary conditions. We first introduce a dynamic pressure: $p_d = p - \rho \mathbf{g} \cdot \mathbf{x}$, so that gravity appears only in the boundary conditions. We consider the special case of high Reynolds number flow, for which the characteristic dynamic pressure is ρU^2 . We define dimensionless primed variables according to:

$$\mathbf{u} = U \mathbf{u}' , \quad p_d = \rho U^2 p'_d , \quad \mathbf{x} = a \mathbf{x}' , \quad t = \frac{a}{U} t' , \quad (2.11)$$

where a and U are characteristic length and velocity scales. Nondimensionalizing the Navier-Stokes equations and appropriate boundary conditions yields the following system:

$$\left(\frac{\partial \mathbf{u}'}{\partial t'} + \mathbf{u}' \cdot \nabla' \mathbf{u}' \right) = -\nabla' p'_d + \frac{1}{\mathcal{Re}} \nabla'^2 \mathbf{u}' , \quad \nabla' \cdot \mathbf{u}' = 0 \quad (2.12)$$

The normal stress condition assumes the dimensionless form:

$$-p'_d + \frac{1}{\mathcal{Fr}} z' + \frac{2}{\mathcal{Re}} \mathbf{n} \cdot \mathbf{E}' \cdot \mathbf{n} = \frac{1}{\mathcal{We}} \nabla' \cdot \mathbf{n} \quad (2.13)$$

The relative importance of surface tension to gravity is prescribed by the Bond number \mathcal{Bo} , while that of surface tension to viscous stresses by the capillary number \mathcal{Ca} . In the high \mathcal{Re} limit of interest, the normal force balance requires that the dynamic pressure be balanced by either gravitational or curvature stresses, the relative magnitudes of which are prescribed by the Bond number.

The nondimensionalization scheme will depend on the physical system of interest. Our purpose here was simply to illustrate the manner in which the dimensionless groups arise in the theoretical formulation of the problem. Moreover, we see that those involving surface tension enter exclusively through the boundary conditions.

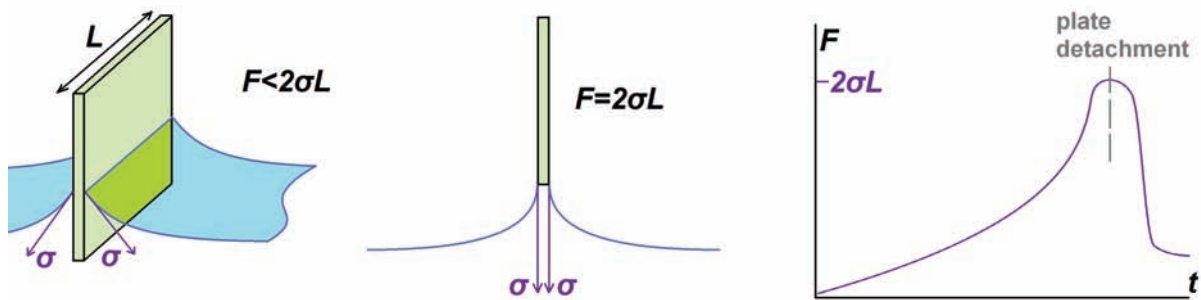


Figure 2.3: Surface tension may be measured by drawing a thin plate from a liquid bath.

2.6 A few simple examples

Measuring surface tension. Since σ is a tensile force per unit length, it is possible to infer its value by slowly drawing a thin plate out of a liquid bath and measure the resistive force (Fig. 2.3). The maximum measured force yields the surface tension σ .

Curvature/ Laplace pressure: consider an oil drop in water (Fig. 2.4a). Work is required to increase the radius from R to $R + dR$:

$$dW = \underbrace{-p_o dV_o - p_w dV_w}_{\text{mech. } E} + \underbrace{\gamma_{ow} dA}_{\text{surface } E} \quad (2.14)$$

where $dV_o = 4\pi R^2 dR = -dV_w$ and $dA = 8\pi R dR$.

For mechanical equilibrium, we require

$$dW = -(p_o - p_w)4\pi R^2 dR + \gamma_{ow}8\pi R dR = 0 \Rightarrow$$

$$\Delta P = (p_o - p_w) = 2\gamma_{ow}/R.$$

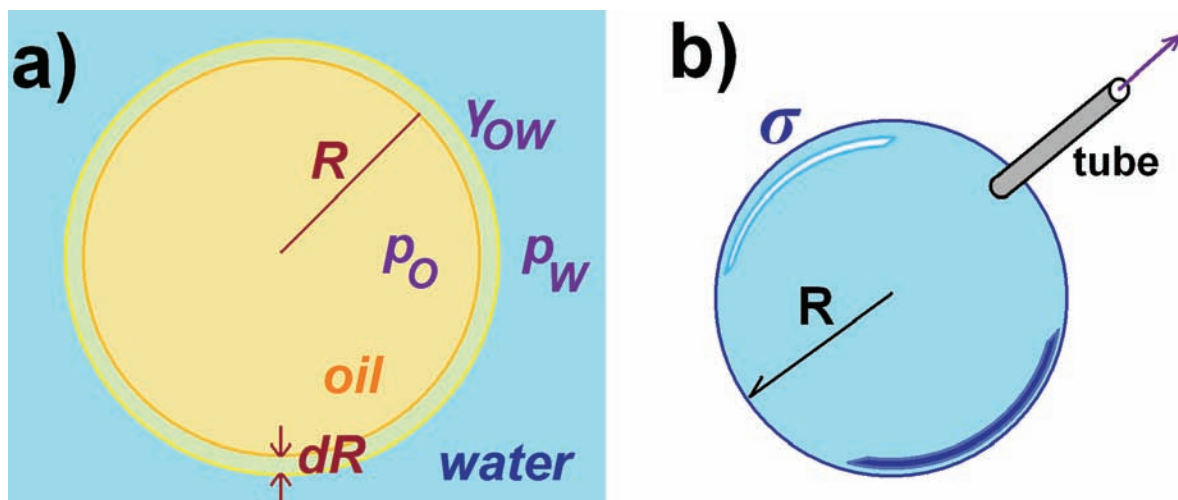


Figure 2.4: a) An oil drop in water b) When a soap bubble is penetrated by a cylindrical tube, air is expelled from the bubble by the Laplace pressure.

Note:

1. Pressure inside a drop / bubble is higher than that outside $\Delta P \sim 2\gamma/R \Rightarrow$ smaller bubbles have higher Laplace pressure \Rightarrow champagne is louder than beer.
Champagne bubbles $R \sim 0.1\text{mm}$, $\sigma \sim 50 \text{ dynes/cm}$, $\Delta P \sim 10^{-2} \text{ atm}$.
2. For a soap bubble (2 interfaces) $\Delta P = \frac{4\sigma}{R}$, so for $R \sim 5 \text{ cm}$, $\sigma \sim 35 \text{ dynes/cm}$ have $\Delta P \sim 3 \times 10^{-5} \text{ atm}$.

More generally, we shall see that there is a pressure jump across any curved interface:

Laplace pressure $\Delta p = \sigma \nabla \cdot \mathbf{n}$.

Examples:

1. **Soap bubble jet - Exit speed** (Fig. 2.4b)

$$\text{Force balance: } \Delta p = 4\sigma/R \sim \rho_{air} U^2 \Rightarrow U \sim \left(\frac{4\sigma}{\rho_{air} R} \right)^{1/2} \sim \left(\frac{4 \times 70 \text{ dynes/cm}}{0.001 \text{ g/cm}^3 \cdot 3 \text{ cm}} \right) \sim 300 \text{ cm/s}$$

2. **Ostwald Ripening:** The coarsening of foams (or emulsions) owing to diffusion of gas across interfaces, which is necessarily from small to large bubbles, from high to low Laplace pressure.

3. **Falling drops:** Force balance $Mg \sim \rho_{air} U^2 a^2$ gives

$$\text{fall speed } U \sim \sqrt{\rho g a / \rho_{air}}.$$

$$\text{drop integrity requires } \rho_{air} U^2 \sim \rho g a < \sigma / a$$

$$\text{raindrop size } a < \ell_c = \sqrt{\sigma / \rho g} \approx 2 \text{ mm}.$$

If a drop is small relative to the capillary length, σ maintains it against the destabilizing influence of aerodynamic stresses.

3. Wetting

Puddles. What sets their size?

Knowing nothing of surface chemistry, one anticipates that Laplace pressure balances hydrostatic pressure if $\sigma/H \geq \rho g H \Rightarrow H < \ell_c = \sqrt{\sigma/\rho g} = \text{capillary length}$.

Note:

1. Drops with $R < \ell_c$ remain heavily spherical
2. Large drops spread to depth $H \sim \ell_c$ so that Laplace + hydrostatic pressures balance at the drop's edge. A volume V will thus spread to a radius R s.t. $\pi R^2 \ell_c = V$, from which $R = (V/\pi \ell_c)^{1/2}$.
3. This is the case for H_2O on most surfaces, where a contact line exists.

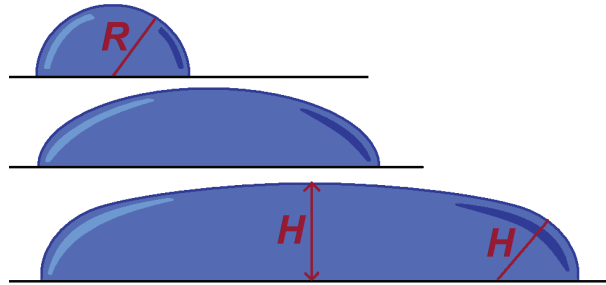


Figure 3.1: Spreading of drops of increasing size.

Note: In general, surface chemistry can dominate and one need not have a contact line.

More generally, **wetting** occurs at fluid-solid contact. Two possibilities exist: *partial wetting* or *total wetting*, depending on the surface energies of the 3 interfaces ($\gamma_{LV}, \gamma_{SV}, \gamma_{SL}$).

Now, just as $\sigma = \gamma_{LV}$ is a surface energy per area or tensile force per length at a liquid-vapour surface, γ_{SL} and γ_{SV} are analogous quantities at solid-liquid and solid-vapour interfaces.

The degree of wetting determined by *spreading parameters*:

$$S = [E_{\text{substrate}}]_{\text{dry}} - [E_{\text{substrate}}]_{\text{wet}} = \gamma_{SV} - (\gamma_{SL} + \gamma_{LV}) \quad (3.1)$$

where only γ_{LV} can be easily measured.

Total Wetting: $S > 0$, $\theta_e = 0$ liquid spreads completely in order to minimize its surface energy. e.g. silicon on glass, water on clean glass.

Note: Silicon oil is more likely to spread than H_2O since $\sigma_w \sim 70 \text{ dyn/cm} > \sigma_{s.o.} \sim 20 \text{ dyn/cm}$. Final result: a film of nanoscopic thickness resulting from competition between molecular and capillary forces.

Partial wetting: $S < 0$, $\theta_e > 0$. In absence of g , forms a spherical cap meeting solid at a contact angle θ_e . A liquid is “wetting” on a particular solid when $\theta_e < \pi/2$, non-wetting or weakly wetting when $\theta_e > \pi/2$. For H_2O , a surface is hydrophilic if $\theta_e < \pi/2$, hydrophobic if $\theta_e > \pi/2$ and superhydrophobic if $\theta_e > 5\pi/6$.

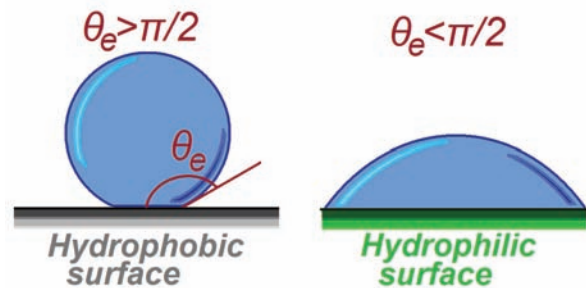


Figure 3.2: The same water drop on hydrophobic and hydrophilic surfaces.

Note: if $g = 0$, drops always take the form of a spherical cap \Rightarrow flattening indicates the effects of gravity.

4. Young's Law with Applications

Young's Law: what is the equilibrium contact angle θ_e ? Horizontal force balance at contact line:

$$\gamma_{LV} \cos \theta_e = \gamma_{SV} - \gamma_{SL}$$

$$\cos \theta_e = \frac{\gamma_{SV} - \gamma_{SL}}{\gamma_{LV}} = 1 + \frac{S}{\gamma_{LV}} \quad (\text{Young 1805}) \quad (4.1)$$

Note:

1. When $S \geq 0$, $\cos \theta_e \geq 1 \Rightarrow \theta_e$ undefined and spreading results.
2. Vertical force balance not satisfied at contact line \Rightarrow dimpling of soft surfaces.
E.g. bubbles in paint leave a circular rim.
3. The static contact angle need not take its equilibrium value \Rightarrow there is a finite range of possible static contact angles.

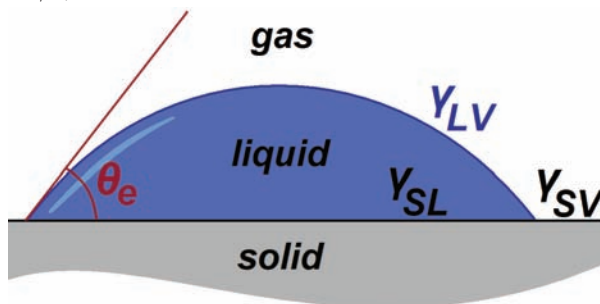


Figure 4.1: Three interfaces meet at the contact line.

Back to Puddles: Total energy:

$$E = \underbrace{(\gamma_{SL} - \gamma_{SV})A + \gamma_{LV}A}_{\text{surface energy}} + \underbrace{\frac{1}{2}\rho gh^2 A}_{\text{grav. pot. energy}} = -S\frac{V}{h} + \frac{1}{2}\rho gVh \quad (4.2)$$

Minimize energy w.r.t. h : $\frac{dE}{dh} = SV\frac{1}{h^2} + \frac{1}{2}\rho gV = 0$ when $-S/h^2 = \frac{1}{2}\rho g \Rightarrow$

$$h_0 = \sqrt{\frac{-2S}{\rho g}} = 2\ell_c \sin \frac{\theta_e}{2} \text{ gives puddle depth, where } \ell_c = \sqrt{\sigma/\rho g}.$$

Capillary Adhesion: Two wetted surfaces can stick together with great strength if $\theta_e < \pi/2$, e.g. Fig. 4.2.

Laplace Pressure:

$$\Delta P = \sigma \left(\frac{1}{R} - \frac{\cos \theta_e}{H/2} \right) \approx -\frac{2\sigma \cos \theta_e}{H}$$

i.e. low P inside film provided $\theta_e < \pi/2$.

If $H \ll R$, $F = \pi R^2 \frac{2\sigma \cos \theta_e}{H}$ is the attractive force between the plates.

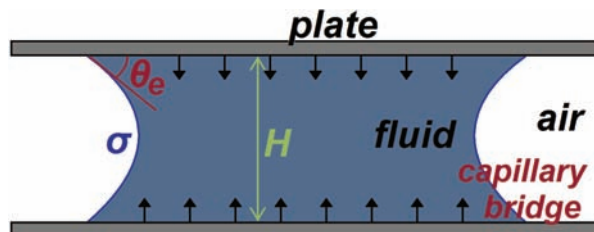


Figure 4.2: An oil drop forms a capillary bridge between two glass plates.

E.g. for H_2O , with $R = 1 \text{ cm}$, $H = 5 \mu\text{m}$ and $\theta_e = 0$, one finds $\Delta P \sim 1/3 \text{ atm}$ and an adhesive force $F \sim 10N$, the weight of 1l of H_2O .

Note: Such capillary adhesion is used by beetles in nature.

4.1 Formal Development of Interfacial Flow Problems

Governing Equations: Navier-Stokes. An incompressible, homogeneous fluid of density ρ and viscosity $\mu = \rho\nu$ (μ is dynamic and ν kinematic viscosity) acted upon by an external force per unit volume \mathbf{f} evolves according to

$$\nabla \cdot \mathbf{u} = 0 \quad (\text{continuity}) \quad (4.3)$$

$$\rho \left(\frac{\partial \mathbf{u}}{\partial t} + \mathbf{u} \cdot \nabla \mathbf{u} \right) = -\nabla p + \mathbf{f} + \mu \nabla^2 \mathbf{u} \quad (\text{Linear momentum conservation}) \quad (4.4)$$

This is a system of 4 equations in 4 unknowns (u_1, u_2, u_3, p) . These N-S equations must be solved subject to appropriate BCs.

Fluid-Solid BCs: “No-slip”: $\mathbf{u} = \mathbf{U}_{solid}$.

E.g.1 Falling sphere: $\mathbf{u} = \mathbf{U}$ on sphere surface, where \mathbf{U} is the sphere velocity.

E.g.2 Convection in a box: $\mathbf{u} = 0$ on the box surface.

But we are interested in flows dominated by interfacial effects. Here, in general, one must solve N-S equations in 2 domains, and match solutions together at the interface with appropriate BCs. Difficulty: These interfaces are free to move \Rightarrow Free boundary problems.

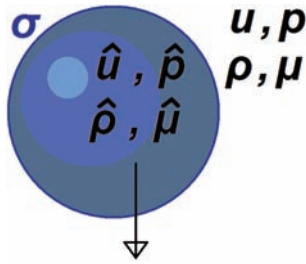


Figure 4.3: E.g.3 Drop motion within a fluid.



Figure 4.4: E.g.4 Water waves at an air-water interface.

Continuity of Velocity at an interface requires that $\mathbf{u} = \hat{\mathbf{u}}$.

And what about p ? We've seen $\Delta p \sim \sigma/R$ for a static bubble/drop, but to answer this question in general, we must develop stress conditions at a fluid-fluid interface.

Recall: Stress Tensor. The state of stress within an incompressible Newtonian fluid is described by the stress tensor: $\mathbf{T} = -p\mathbf{I} + 2\mu\mathbf{E}$ where $\mathbf{E} = \frac{1}{2}[(\nabla\mathbf{u}) + (\nabla\mathbf{u})^T]$ is the deviatoric stress tensor. The associated hydrodynamic force per unit volume within the fluid is $\nabla \cdot \mathbf{T}$.

One may thus write N-S eqns in the form: $\rho \frac{D\mathbf{u}}{Dt} = \nabla \cdot \mathbf{T} + \mathbf{f} = -\nabla p + \mu \nabla^2 \mathbf{u} + \mathbf{f}$.

Now: T_{ij} = force / area acting in the \mathbf{e}_j direction on a surface with a normal \mathbf{e}_i .

Note:

1. normal stresses (diagonals) T_{11}, T_{22}, T_{33} involve both p and u_i
2. tangential stresses (off-diagonals) T_{12}, T_{13} , etc., involve only velocity gradients, i.e. viscous stresses
3. T_{ij} is symmetric (Newtonian fluids)
4. $\mathbf{t}(\mathbf{n}) = \mathbf{n} \cdot \mathbf{T}$ = stress vector acting on a surface with normal \mathbf{n}

E.g. **Shear flow.** Stress in lower boundary is tangential. Force / area on lower boundary:

$T_{yx} = \mu \frac{\partial u_x}{\partial y} |_{y=0} = \mu k$ is the force/area that acts on y -surface in x -direction.

Note: the form of \mathbf{T} in arbitrary curvilinear coordinates is given in the Appendix of Batchelor.

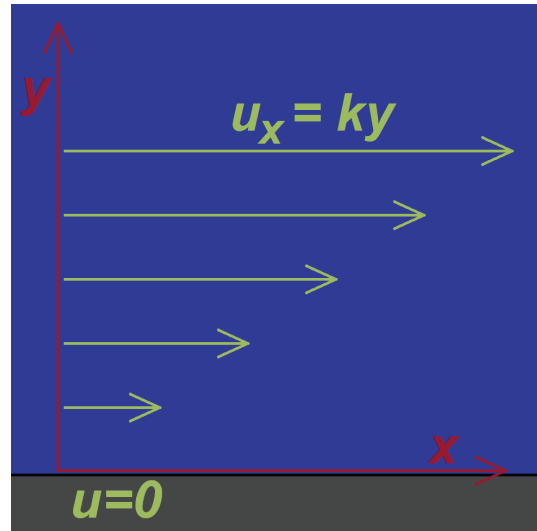
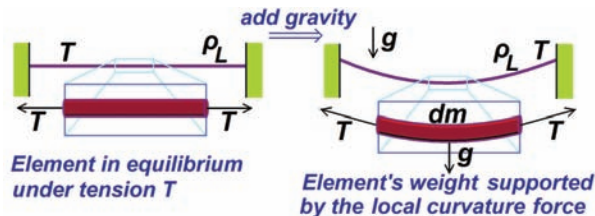


Figure 4.5: Shear flow above a rigid lower boundary.

5. Stress Boundary Conditions

Today:

1. Derive stress conditions at a fluid-fluid interface. Requires knowledge of $\mathbf{T} = -p\mathbf{I} + 2\mu\mathbf{E}$
2. Consider several examples of fluid statics



Recall: the curvature of a string under tension may support a normal force. (see right)

Figure 5.1: String under tension and the influence of gravity.

5.1 Stress conditions at a fluid-fluid interface

We proceed by deriving the normal and tangential stress boundary conditions appropriate at a fluid-fluid interface characterized by an interfacial tension σ .

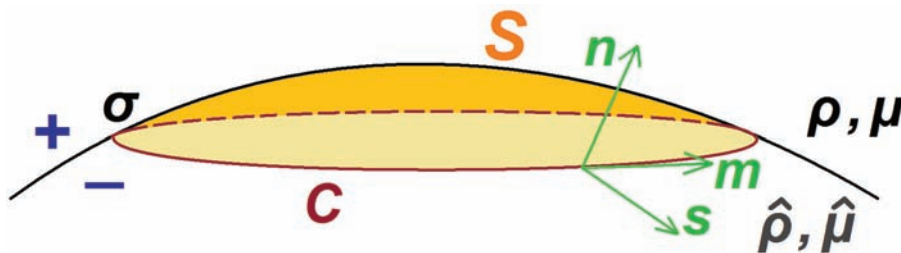


Figure 5.2: A surface S and bounding contour C on an interface between two fluids. Local unit vectors are \mathbf{n} , \mathbf{m} and \mathbf{s} .

Consider an interfacial surface S bounded by a closed contour C . One may think of there being a force per unit length of magnitude σ in the s -direction at every point along C that acts to flatten the surface S . Perform a force balance on a volume element V enclosing the interfacial surface S defined by the contour C :

$$\int_V \rho \frac{D\mathbf{u}}{Dt} dV = \int_V \mathbf{f} dV + \int_{S^*} [t(\mathbf{n}) + \hat{t}(\hat{\mathbf{n}})] dS + \int_C \sigma \mathbf{s} d\ell \quad (5.1)$$

Here ℓ indicates arc-length and so $d\ell$ a length increment along the curve C .

$\mathbf{t}(\mathbf{n}) = \mathbf{n} \cdot \mathbf{T}$ is the stress vector, the force/area exerted by the upper (+) fluid on the interface.

The stress tensor is defined in terms of the local fluid pressure and velocity field as $\mathbf{T} = -p\mathbf{I} + \mu [\nabla\mathbf{u} + (\nabla\mathbf{u})^T]$.

The stress exerted on the interface by the lower (-) fluid is $\hat{\mathbf{t}}(\hat{\mathbf{n}}) = \hat{\mathbf{n}} \cdot \hat{\mathbf{T}} = -\mathbf{n} \cdot \mathbf{T}$

where $\hat{\mathbf{T}} = -\hat{p}\mathbf{I} + \hat{\mu} [\nabla\hat{\mathbf{u}} + (\nabla\hat{\mathbf{u}})^T]$.

Physical interpretation of terms

$\int_V \rho \frac{D\mathbf{u}}{Dt} dV$: inertial force associated with acceleration of fluid in V

$\int_V \mathbf{f} dV$: body forces acting within V

$\int_S \mathbf{t}(\mathbf{n}) dS$: hydrodynamic force exerted by upper fluid

$\int_S \hat{\mathbf{t}}(\hat{\mathbf{n}}) dS$: hydrodynamic force exerted by lower fluid

$\int_C \sigma \mathbf{s} d\ell$: surface tension force exerted on perimeter.

Now if ϵ is the characteristic height of our volume V and R its characteristic radius, then the acceleration and body forces will scale as $R^2\epsilon$, while the surface forces will scale as R^2 . Thus, in the limit of $\epsilon \rightarrow 0$, the latter must balance.

$$\int_S \mathbf{t}(\mathbf{n}) + \hat{\mathbf{t}}(\hat{\mathbf{n}}) \, dS + \int_C \sigma \mathbf{s} \, d\ell = 0 \quad (5.2)$$

Now we have that

$$\mathbf{t}(\mathbf{n}) = \mathbf{n} \cdot \mathbf{T} \quad , \quad \hat{\mathbf{t}}(\hat{\mathbf{n}}) = \hat{\mathbf{n}} \cdot \hat{\mathbf{T}} = -\mathbf{n} \cdot \mathbf{T} \quad (5.3)$$

Moreover, the application of Stokes Theorem (see below) allows us to write

$$\int_C \sigma \mathbf{s} \, d\ell = \int_S \nabla_S \sigma - \sigma \mathbf{n} (\nabla_S \cdot \mathbf{n}) \, dS \quad (5.4)$$

where the tangential (surface) gradient operator, defined

$$\nabla_S = [\mathbf{I} - \mathbf{nn}] \cdot \nabla = \nabla - \mathbf{n} \frac{\partial}{\partial \mathbf{n}} \quad (5.5)$$

appears because σ and \mathbf{n} are only defined on the surface S . We proceed by dropping the subscript s on ∇ , with this understanding. The surface force balance thus becomes

$$\int_S \left(\mathbf{n} \cdot \mathbf{T} - \mathbf{n} \cdot \hat{\mathbf{T}} \right) dS = \int_S \sigma \mathbf{n} (\nabla \cdot \mathbf{n}) - \nabla \sigma \, dS \quad (5.6)$$

Now since the surface S is arbitrary, the integrand must vanish identically. One thus obtains the interfacial stress balance equation, which is valid at every point on the interface:

Stress Balance Equation

$$\mathbf{n} \cdot \mathbf{T} - \mathbf{n} \cdot \hat{\mathbf{T}} = \sigma \mathbf{n} (\nabla \cdot \mathbf{n}) - \nabla \sigma \quad (5.7)$$

Interpretation of terms:

- $\mathbf{n} \cdot \mathbf{T}$ stress (force/area) exerted by + on - (will generally have both \perp and \parallel components)
- $\mathbf{n} \cdot \hat{\mathbf{T}}$ stress (force/area) exerted by - on + (will generally have both \perp and \parallel components)
- $\sigma \mathbf{n} (\nabla \cdot \mathbf{n})$ normal curvature force per unit area associated with local curvature of interface, $\nabla \cdot \mathbf{n}$
- $\nabla \sigma$ tangential stress associated with gradients in σ

Normal stress balance Taking $\mathbf{n} \cdot (5.7)$ yields the normal stress balance

$$\mathbf{n} \cdot \mathbf{T} \cdot \mathbf{n} - \mathbf{n} \cdot \hat{\mathbf{T}} \cdot \mathbf{n} = \sigma (\nabla \cdot \mathbf{n}) \quad (5.8)$$

The jump in the normal stress across the interface is balanced by the curvature pressure.

Note: If $\nabla \cdot \mathbf{n} \neq 0$, there must be a normal stress jump there, which generally involves both pressure and viscous terms.

Tangential stress balance Taking \mathbf{d} (5.7), where \mathbf{d} is any linear combination of \mathbf{s} and \mathbf{m} (any tangent to S), yields the tangential stress balance at the interface:

$$\mathbf{n} \cdot \mathbf{T} \cdot \mathbf{d} - \mathbf{n} \cdot \hat{\mathbf{T}} \cdot \mathbf{d} = \nabla \sigma \cdot \mathbf{d} \quad (5.9)$$

Physical Interpretation

- LHS represents the jump in tangential components of the hydrodynamic stress at the interface
- RHS represents the tangential stress (Marangoni stress) associated with gradients in σ , as may result from gradients in temperature θ or chemical composition c at the interface since in general $\sigma = \sigma(\theta, c)$
- LHS contains only the non-diagonal terms of \mathbf{T} - only the velocity gradients, not pressure; therefore any non-zero $\nabla \sigma$ at a fluid interface must *always* drive motion.

5.2 Appendix A : Useful identity

Recall Stokes Theorem:

$$\int_C \mathbf{F} \cdot d\mathbf{l} = \int_S \mathbf{n} \cdot (\nabla \wedge \mathbf{F}) dS \quad (5.10)$$

Along the contour C , $d\mathbf{l} = \mathbf{m} d\ell$, so that we have

$$\int_C \mathbf{F} \cdot \mathbf{m} d\ell = \int_S \mathbf{n} \cdot (\nabla \wedge \mathbf{F}) dS \quad (5.11)$$

Now let $\mathbf{F} = \mathbf{f} \wedge \mathbf{b}$, where \mathbf{b} is an arbitrary *constant* vector. We thus have

$$\int_C (\mathbf{f} \wedge \mathbf{b}) \cdot \mathbf{m} d\ell = \int_S \mathbf{n} \cdot (\nabla \wedge (\mathbf{f} \wedge \mathbf{b})) dS \quad (5.12)$$

Now use standard vector identities to see $(\mathbf{f} \wedge \mathbf{b}) \cdot \mathbf{m} = -\mathbf{b} \cdot (\mathbf{f} \wedge \mathbf{m})$ and

$$\nabla \wedge (\mathbf{f} \wedge \mathbf{b}) = \mathbf{f} (\nabla \cdot \mathbf{b}) - \mathbf{b} (\nabla \cdot \mathbf{f}) + \mathbf{b} \cdot \nabla \mathbf{f} - \mathbf{f} \cdot \nabla \mathbf{b} = -\mathbf{b} (\nabla \cdot \mathbf{f}) + \mathbf{b} \cdot \nabla \mathbf{f} \quad (5.13)$$

since \mathbf{b} is a constant vector. We thus have

$$\mathbf{b} \cdot \int_C (\mathbf{f} \wedge \mathbf{m}) d\ell = \mathbf{b} \cdot \int_S [\mathbf{n} (\nabla \cdot \mathbf{f}) - (\nabla \mathbf{f}) \cdot \mathbf{n}] dS \quad (5.14)$$

Since \mathbf{b} is arbitrary, we thus have

$$\int_C (\mathbf{f} \wedge \mathbf{m}) d\ell = \int_S [\mathbf{n} (\nabla \cdot \mathbf{f}) - (\nabla \mathbf{f}) \cdot \mathbf{n}] dS \quad (5.15)$$

We now choose $\mathbf{f} = \sigma \mathbf{n}$, and recall that $\mathbf{n} \wedge \mathbf{m} = -\mathbf{s}$. One thus obtains

$$-\int_C \sigma \mathbf{s} d\ell = \int_S [\mathbf{n} \nabla \cdot (\sigma \mathbf{n}) - \nabla (\sigma \mathbf{n}) \cdot \mathbf{n}] dS = \int_S [\mathbf{n} \nabla \sigma \cdot \mathbf{n} + \sigma \mathbf{n} (\nabla \cdot \mathbf{n}) - \nabla \sigma - \sigma (\nabla \mathbf{n}) \cdot \mathbf{n}] dS.$$

We note that $\nabla \sigma \cdot \mathbf{n} = 0$ since $\nabla \sigma$ must be tangent to the surface S and $(\nabla \mathbf{n}) \cdot \mathbf{n} = \frac{1}{2} \nabla (\mathbf{n} \cdot \mathbf{n}) = \frac{1}{2} \nabla (1) = 0$, and so obtain the desired result:

$$\int_C \sigma \mathbf{s} d\ell = \int_S [\nabla \sigma - \sigma \mathbf{n} (\nabla \cdot \mathbf{n})] dS \quad (5.16)$$

5.3 Fluid Statics

We begin by considering static fluid configurations, for which the stress tensor reduces to the form $\mathbf{T} = -p\mathbf{I}$, so that $\mathbf{n} \cdot \mathbf{T} \cdot \mathbf{n} = -p$, and the normal stress balance equation (5.8) assumes the simple form:

$$\hat{p} - p = \sigma \nabla \cdot \mathbf{n} \tag{5.17}$$

The pressure jump across a static interface is balanced by the curvature force at the interface. Now since $\mathbf{n} \cdot \mathbf{T} \cdot \mathbf{d} = 0$ for a static system, the tangential stress balance indicates that $\nabla \sigma = 0$. This leads to the following important conclusion: *There cannot be a static system in the presence of surface tension gradients.* While pressure jumps can sustain normal stress jumps across a fluid interface, they do not contribute to the tangential stress jump. Consequently, tangential surface (Marangoni) stresses can only be balanced by viscous stresses associated with fluid motion. We proceed by applying equation (5.17) to describe a number of static situations.

1. Stationary Bubble : We consider a spherical air bubble of radius R submerged in a static fluid. What is the pressure drop across the bubble surface?

The divergence in spherical coordinates of $\mathbf{F} = (F_r, F_\theta, F_\phi)$ is given by

$$\nabla \cdot \mathbf{F} = \frac{1}{r^2} \frac{\partial}{\partial r} (r^2 F_r) + \frac{1}{r \sin \theta} \frac{\partial}{\partial \theta} (\sin \theta F_\theta) + \frac{1}{r \sin \phi} \frac{\partial}{\partial \phi} F_\phi.$$

Hence $\nabla \cdot \mathbf{n}|_S = \frac{1}{r^2} \frac{\partial}{\partial r} r^2|_{r=R} = \frac{2}{R}$ so the normal stress jump (5.17) indicates that

$$\Delta P = \hat{p} - p = \frac{2\sigma}{R} \tag{5.18}$$

The pressure within the bubble is higher than that outside by an amount proportional to the surface tension, and inversely proportional to the bubble size. As noted in Lec. 2, it is thus that small bubbles are louder than large ones when they burst at a free surface: champagne is louder than beer. We note that soap bubbles in air have two surfaces that define the inner and outer surfaces of the soap film; consequently, the pressure differential is twice that across a single interface.

2. The static meniscus ($\theta_e < \pi/2$)

Consider a situation where the pressure within a static fluid varies owing to the presence of a gravitational field, $p = p_0 + \rho g z$, where p_0 is the constant ambient pressure, and $\mathbf{g} = -g\hat{z}$ is the grav. acceleration. The normal stress balance thus requires that the interface satisfy the *Young-Laplace Equation*:

$$\rho g z = \sigma \nabla \cdot \mathbf{n} \tag{5.19}$$

The vertical gradient in fluid pressure must be balanced by the curvature pressure; as the gradient is constant, the curvature must likewise increase lin-

early with z . Such a situation arises in the static meniscus (*below*).

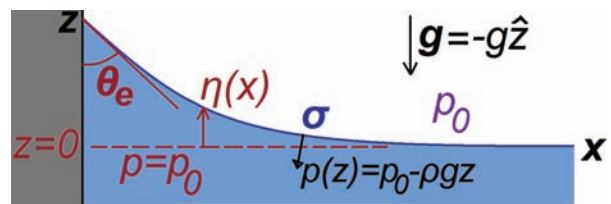


Figure 5.3: Static meniscus near a wall.

The shape of the meniscus is prescribed by two factors: the contact angle between the air-water interface and the wall, and the balance between hydrostatic pressure and curvature pressure. We treat the contact angle θ_e as given; noting that it depends in general on the surface energy. The normal force balance is expressed by the Young-Laplace equation, where now $\rho = \rho_w - \rho_{air} \approx \rho_w$ is the density difference between water and air. We define the free surface by $z = \eta(x)$; equivalently, we define a functional $f(x, z) = z - \eta(x)$ that vanishes on the surface. The normal to the surface $z = \eta(x)$ is thus

$$\mathbf{n} = \frac{\nabla f}{|\nabla f|} = \frac{\hat{z} - \eta'(x)\hat{x}}{[1 + \eta'(x)^2]^{1/2}} \tag{5.20}$$

As deduced in Appendix B, the curvature of the free surface $\nabla \cdot \hat{\mathbf{n}}$, may be expressed as

$$\nabla \cdot \hat{\mathbf{n}} = \frac{-\eta_{xx}}{(1 + \eta_x^2)^{3/2}} \approx -\eta_{xx} \quad (5.21)$$

Assuming that the slope of the meniscus remains sufficiently small, $\eta_x^2 \ll 1$, allows one to linearize equation (5.21), so that (5.19) assumes the form

$$\rho g \eta = \sigma \eta_{xx} \quad (5.22)$$

Applying the boundary condition $\eta(\infty) = 0$ and the contact condition $\eta_x(0) = -\cot \theta$, and solving (5.22) thus yields

$$\eta(x) = \ell_c \cot \theta e^{-x/\ell_c} \quad (5.23)$$

where $\ell_c = \sqrt{\sigma/\rho g}$ is the capillary length. The meniscus formed by an object floating in water is exponential, decaying over a length scale ℓ_c . Note that this behaviour may be rationalized as follows: the system arranges itself so that its total energy (grav. potential + surface) is minimized.

3. Floating Bodies

Floating bodies must be supported by some combination of buoyancy and curvature forces. Specifically, since the fluid pressure beneath the interface is related to the atmospheric pressure p_0 above the interface by

$$p = p_0 + \rho g z + \sigma \nabla \cdot \mathbf{n} , \quad (5.24)$$

one may express the vertical force balance as

$$Mg = \mathbf{z} \cdot \int_C -p \mathbf{n} d\ell = \underbrace{F_b}_{\text{buoyancy}} + \underbrace{F_c}_{\text{curvature}} . \quad (5.25)$$

The buoyancy force

$$F_b = \mathbf{z} \cdot \int_C \rho g z \mathbf{n} d\ell = \rho g V_b \quad (5.26)$$

is thus simply the weight of the fluid displaced above the object and inside the line of tangency (see figure below). We note that it may be deduced by integrating the curvature pressure over the contact area C using the first of the Frenet-Serret equations (see Appendix C).

$$F_c = \mathbf{z} \cdot \int_C \sigma (\nabla \cdot \mathbf{n}) \mathbf{n} d\ell = \sigma \mathbf{z} \cdot \int_C \frac{d\mathbf{t}}{d\ell} d\ell = \sigma \mathbf{z} \cdot (\mathbf{t}_1 - \mathbf{t}_2) = 2\sigma \sin \theta \quad (5.27)$$

At the interface, the buoyancy and curvature forces must balance precisely, so the Young-Laplace relation is satisfied:

$$0 = \rho g z + \sigma \nabla \cdot \mathbf{n} \quad (5.28)$$

Integrating this equation over the meniscus and taking the vertical component yields the vertical force balance:

$$F_b^m + F_c^m = 0 \quad (5.29)$$

where

$$F_b^m = \mathbf{z} \cdot \int_{C_m} \rho g z \mathbf{n} d\ell = \rho g V_m \quad (5.30)$$

$$F_c^m = \mathbf{z} \cdot \int_{C_m} \sigma (\nabla \cdot \mathbf{n}) \mathbf{n} d\ell = \sigma \mathbf{z} \cdot \int_{C_m} \frac{d\mathbf{t}}{d\ell} d\ell = \sigma \mathbf{z} \cdot (\mathbf{t}_1 - \mathbf{t}_2) = -2\sigma \sin \theta \quad (5.31)$$

where we have again used the Frenet-Serret equations to evaluate the curvature force.

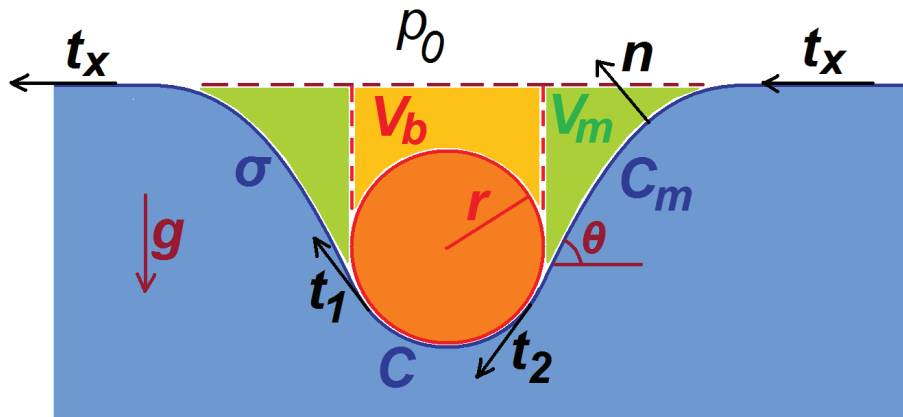


Figure 5.4: A floating non-wetting body is supported by a combination of buoyancy and curvature forces, whose relative magnitude is prescribed by the ratio of displaced fluid volumes V_b and V_m .

Equations (5.27-5.31) thus indicate that the curvature force acting on the floating body is expressible in terms of the fluid volume displaced *outside* the line of tangency:

$$F_c = \rho g V_m \quad (5.32)$$

The relative magnitude of the buoyancy and curvature forces supporting a floating, non-wetting body is thus prescribed by the relative magnitudes of the volumes of the fluid displaced inside and outside the line of tangency:

$$\frac{F_b}{F_c} = \frac{V_b}{V_m} \quad (5.33)$$

For 2D bodies, we note that since the meniscus will have a length comparable to the capillary length, $\ell_c = (\sigma/(\rho g))^{1/2}$, the relative magnitudes of the buoyancy and curvature forces,

$$\frac{F_b}{F_c} \approx \frac{r}{\ell_c}, \quad (5.34)$$

is prescribed by the relative magnitudes of the body size and capillary length. Very small floating objects ($r \ll \ell_c$) are supported principally by curvature rather than buoyancy forces. This result has been extended to three-dimensional floating objects by Keller 1998, *Phys. Fluids*, 10, 3009-3010.

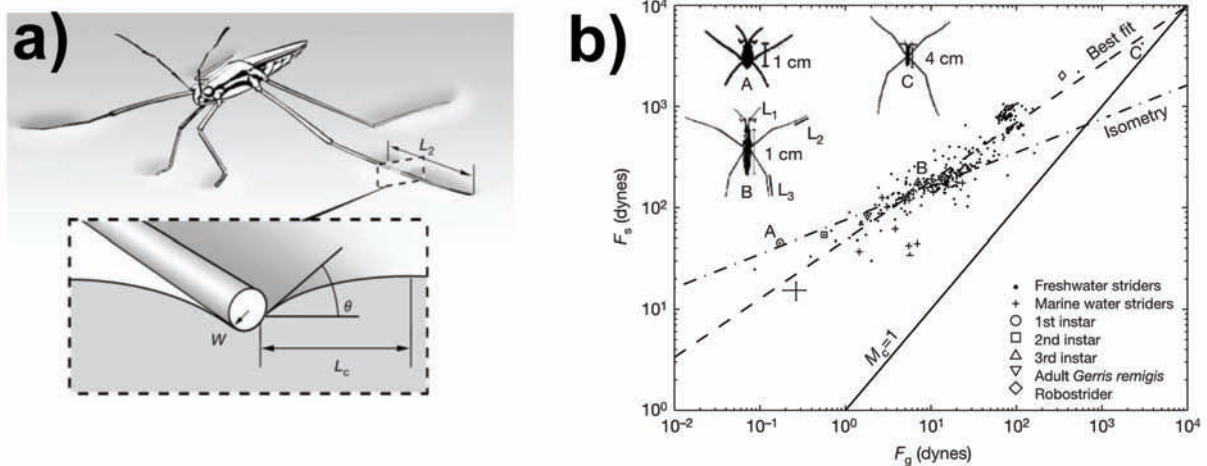


Figure 5.5: **a)** Water strider legs are covered with hair, rendering them effectively non-wetting. The tarsal segment of its legs rest on the free surface. The free surface makes an angle θ with the horizontal, resulting in an upward curvature force per unit length $2\sigma \sin \theta$ that bears the insect's weight. **b)** The relation between the maximum curvature force $F_s = 2\sigma P$ and body weight $F_g = Mg$ for 342 species of water striders. $P = 2(L_1 + L_2 + L_3)$ is the combined length of the tarsal segments. From *Hu, Chan & Bush; Nature 424, 2003*.

4. Water-walking Insects

Small objects such as paper clips, pins or insects may reside at rest on a free surface provided the curvature force induced by their deflection of the free surface is sufficient to bear their weight (Fig. 5.5a). For example, for a body of contact length L and total mass M , static equilibrium on the free surface requires that:

$$\frac{Mg}{2\sigma L \sin \theta} < 1, \quad (5.35)$$

where θ is the angle of tangency of the floating body.

This simple criterion is an important geometric constraint on water-walking insects. Fig. 5.5b indicates the dependence of contact length on body weight for over 300 species of water-striders, the most common water walking insect. Note that the solid line corresponds to the requirement (5.35) for static equilibrium. Smaller insects maintain a considerable margin of safety, while the larger striders live close to the edge. The maximum size of water-walking insects is limited by [the constraint \(5.35\)](#).

If body proportions were independent of size L , one would expect the body weight to scale as L^3 and the curvature force as L . Isometry would thus suggest a dependence of the form $F_c \sim F_g^{1/3}$, represented as the dashed line. The fact that the best fit line has a slope considerably larger than $1/3$ indicates a variance from isometry: the legs of large water striders are proportionally longer.

5.4 Appendix B : Computing curvatures

We see the appearance of the divergence of the surface normal, $\nabla \cdot \mathbf{n}$, in the normal stress balance. We proceed by briefly reviewing how to formulate this curvature term in two common geometries.

In cartesian coordinates (x, y, z) , we consider a surface defined by $z = h(x, y)$. We define a functional $f(x, y, z) = z - h(x, y)$ that necessarily vanishes on the surface. The normal to the surface is defined by

$$\mathbf{n} = \frac{\nabla f}{|\nabla f|} = \frac{\hat{\mathbf{z}} - h_x \hat{\mathbf{x}} - h_y \hat{\mathbf{y}}}{(1 + h_x^2 + h_y^2)^{1/2}} \quad (5.36)$$

and the local curvature may thus be computed:

$$\nabla \cdot \mathbf{n} = \frac{-(h_{xx} + h_{yy}) - (h_{xx} h_y^2 + h_{yy} h_x^2) + 2h_x h_y h_{xy}}{(1 + h_x^2 + h_y^2)^{3/2}} \quad (5.37)$$

In the simple case of a two-dimensional interface, $z = h(x)$, these results assume the simple forms:

$$\mathbf{n} = \frac{\hat{\mathbf{z}} - h_x \hat{\mathbf{x}}}{(1 + h_x^2)^{1/2}}, \quad \nabla \cdot \mathbf{n} = \frac{-h_{xx}}{(1 + h_x^2)^{3/2}} \quad (5.38)$$

Note that \mathbf{n} is dimensionless, while $\nabla \cdot \mathbf{n}$ has the units of $1/L$.

In 3D polar coordinates (r, θ, z) , we consider a surface defined by $z = h(r, \theta)$. We define a functional $g(r, \theta, z) = z - h(r, \theta)$ that vanishes on the surface, and compute the normal:

$$\mathbf{n} = \frac{\nabla g}{|\nabla g|} = \frac{\hat{\mathbf{z}} - h_r \hat{\mathbf{r}} - \frac{1}{r} h_\theta \hat{\boldsymbol{\theta}}}{(1 + h_r^2 + \frac{1}{r^2} h_\theta^2)^{1/2}}, \quad (5.39)$$

from which the local curvature is computed:

$$\nabla \cdot \mathbf{n} = \frac{-h_{\theta\theta} - h_r^2 h_{\theta\theta} + h_r h_{\theta r} - r h_r - \frac{2}{r} h_r h_\theta^2 - r^2 h_{rr} - h_{rr} h_\theta^2 + h_r h_\theta h_{r\theta}}{r^2 (1 + h_r^2 + \frac{1}{r^2} h_\theta^2)^{1/2}} \quad (5.40)$$

In the case of an axisymmetric interface, $z = h(r)$, these reduce to:

$$\mathbf{n} = \frac{\hat{\mathbf{z}} - h_r \hat{\mathbf{r}}}{(1 + h_r^2)^{1/2}}, \quad \nabla \cdot \mathbf{n} = \frac{-r h_r - r^2 h_{rr}}{r^2 (1 + h_r^2)^{3/2}} \quad (5.41)$$

5.5 Appendix C : Frenet-Serret Equations

Differential geometry yields relations that are often useful in computing curvature forces on 2D interfaces.

$$(\nabla \cdot \mathbf{n}) \mathbf{n} = \frac{d\mathbf{t}}{d\ell} \quad (5.42)$$

$$-(\nabla \cdot \mathbf{n}) \mathbf{t} = \frac{d\mathbf{n}}{d\ell} \quad (5.43)$$

Note that the LHS of (5.42) is proportional to the curvature pressure acting on an interface. Therefore the net force acting on surface S as a result of curvature / Laplace pressures:

$\mathbf{F} = \int_C \sigma (\nabla \cdot \mathbf{n}) \mathbf{n} d\ell = \sigma \int_C \frac{d\mathbf{t}}{d\ell} d\ell = \sigma (\mathbf{t}_2 - \mathbf{t}_1)$ and so the net force on an interface resulting from curvature pressure can be deduced in terms of the geometry of the end points.

6. More on Fluid statics

Last time, we saw that the balance of curvature and hydrostatic pressures requires $-\rho g \eta = \sigma \nabla \cdot \mathbf{n} = \sigma \frac{-\eta_{xx}}{(1+\eta_x^2)^{3/2}}$.

We linearized, assuming $\eta_x \ll 1$, to find $\eta(x)$. Note: we can integrate directly

$$\begin{aligned} \rho g \eta \eta_x &= \sigma \frac{\eta_x \eta_{xx}}{(1+\eta_x^2)^{3/2}} \rho g \Rightarrow \frac{d}{dx} \left(\frac{\eta^2}{2} \right) = \sigma \frac{d}{dx} \frac{1}{(1+\eta_x^2)^{1/2}} \Rightarrow \\ \frac{1}{2\sigma} \rho g \eta^2 &= \int_x^\infty \frac{d}{dx} \frac{1}{(1+\eta_x^2)^{1/2}} dx = 1 - \frac{1}{(1+\eta_x^2)^{1/2}} = 1 - \sin \theta \\ \sigma \sin \theta + \frac{1}{2} \rho g \eta^2 &= \sigma \end{aligned} \tag{6.1}$$

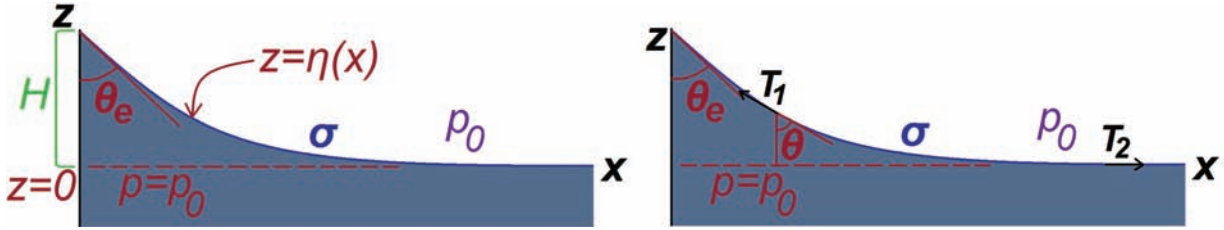


Figure 6.1: Calculating the shape and maximal rise height of a static meniscus.

Maximal rise height: At $z = h$ we have $\theta = \theta_e$, so from (6.1) $\frac{1}{2} \rho g h^2 = \sigma(1 - \sin \theta_e)$, from which

$$h = \sqrt{2} \ell_c (1 - \sin \theta_e)^{1/2} \quad \text{where } \ell_c = \sqrt{\sigma / \rho g} \tag{6.2}$$

Alternative perspective: Consider force balance on the meniscus.

Horizontal force balance:

$$\underbrace{\sigma \sin \theta}_{\text{horiz. proj. of } T_1} + \underbrace{\frac{1}{2} \rho g z^2}_{\text{hydrostatic suction}} = \underbrace{\sigma}_{T_2} \tag{6.3}$$

Vertical force balance:

$$\underbrace{\sigma \cos \theta}_{\text{vert. proj. of } T_1} = \underbrace{\int_x^\infty \rho g z dx}_{\text{weight of fluid}} \tag{6.4}$$

At $x = 0$, where $\theta = \theta_e$, gives $\sigma \cos \theta_e =$ weight of fluid displaced above $z = 0$.

Note: $\sigma \cos \theta_e =$ weight of displaced fluid is +/- according to whether θ_e is smaller or larger than $\frac{\pi}{2}$.

Floating Bodies Without considering interfacial effects, one anticipates that heavy things sink and light things float. This doesn't hold for objects small relative to the capillary length.

Recall: Archimedean force on a submerged body $F_A = \int_S p \mathbf{n} dS = \rho g V_B$.

In general, the hydrodynamic force acting on a body in a fluid

$\mathbf{F}_h = \int_S \mathbf{T} \cdot \mathbf{n} dS$, where $\mathbf{T} = -p\mathbf{I} + 2\mu\mathbf{E} = -p\mathbf{I}$ for static fluid.

Here $\mathbf{F}_h = -\int_S p \mathbf{n} dS = -\int_S \rho g z \mathbf{n} dS = -\rho g \int_V \nabla z dV$ by divergence theorem. This is equal to $-\rho g \int_V dV \hat{\mathbf{z}} = -\rho g V \hat{\mathbf{z}} =$ weight of displaced fluid. The archimedean force can thus support weight of a body $Mg = \rho_B g V$ if $\rho_F > \rho_B$ (fluid density larger than body density); otherwise, it sinks.

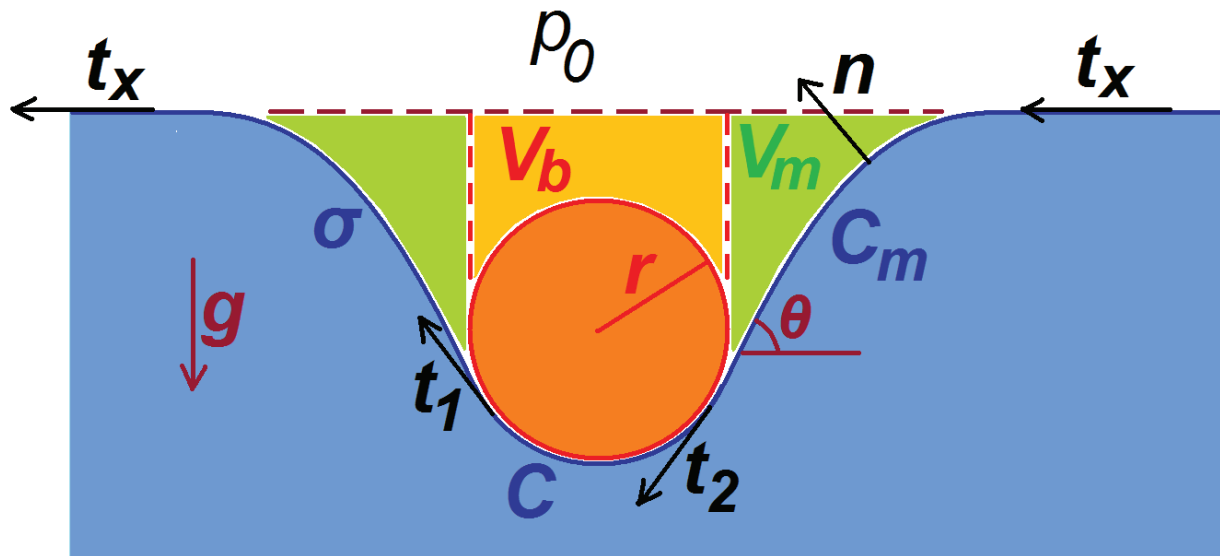


Figure 6.2: A heavy body may be supported on a fluid surface by a combination of buoyancy and surface tension.

6.1 Capillary forces on floating bodies

- arise owing to interaction of the menisci of floating bodies
- attractive or repulsive depending on whether the menisci are of the same or opposite sense
- explains the formation of bubble rafts on champagne
- explains the mutual attraction of Cheerios and their attraction to the walls
- utilized in technology for self-assembly on the microscale

Capillary attraction Want to calculate the attractive force between two floating bodies separated by a distance R . Total energy of the system is given by

$$E_{tot} = \sigma \oint dA(R) + \int_{-\infty}^{\infty} dx \int_0^{h(x)} \rho g z dz \quad (6.5)$$

where the first term in (6.5) corresponds to the total surface energy when the two bodies are a distance R apart, and the second term is the total gravitational potential energy of the fluid. Differentiating (6.5) yields the force acting on each of the bodies:

$$F(R) = -\frac{dE_{tot}(R)}{dR} \quad (6.6)$$

Such capillary forces are exploited by certain water walking insects to climb menisci. By deforming the free surface, they generate a lateral force that drives them up menisci (Hu & Bush 2005).

7. Spinning, tumbling and rolling drops

7.1 Rotating Drops

We want to find $z = h(r)$ (see right). Normal stress balance on S :

$$\Delta P + \underbrace{\frac{1}{2}\Delta\rho\Omega^2 r^2}_{\text{centrifugal}} = \underbrace{\sigma\nabla\cdot\mathbf{n}}_{\text{curvature}}$$

Nondimensionalize:

$$\Delta p' + 4B_0 \left(\frac{r}{a}\right)^2 = \nabla\cdot\mathbf{n},$$

where $\Delta p' = \frac{a\Delta p}{\sigma}$, $\Sigma = \frac{\Delta\rho\Omega^2 a^3}{8\sigma} = \frac{\text{centrifugal}}{\text{curvature}} = =$
 Rotational Bond number = const. Define surface functional: $f(r, \theta) = z - h(r) \Rightarrow$ vanishes on the surface. Thus

$$\mathbf{n} = \frac{\nabla f}{|\nabla f|} = \frac{\hat{z} - h_r(r)\hat{r}}{(1+h_r^2(r))^{1/2}} \text{ and } \nabla\cdot\mathbf{n} = \frac{-rh_r - r^2 h_{rr}}{r^2(1+h_r^2)^{3/2}}$$

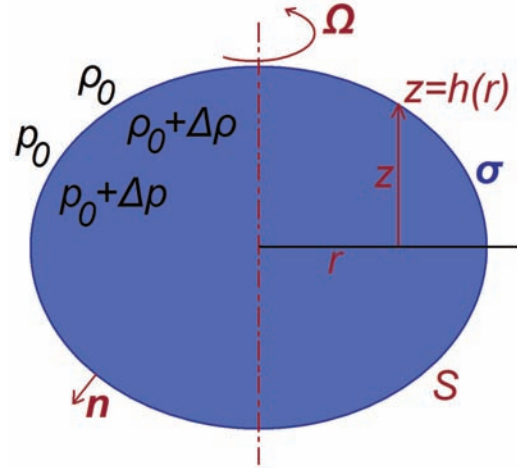


Figure 7.1: The radial profile of a rotating drop.

Brown + Scriven (1980) computed drop shapes and stability for $B_0 > 0$:

1. for $\Sigma < 0.09$, only axisymmetric solutions, oblate ellipsoids
2. for $0.09 < \Sigma < 0.31$, both axisymmetric and lobed solutions possible, stable
3. for $\Sigma > 0.31$ no stable solution, only lobed forms

Tektites: centimetric metallic ejecta formed from spinning cooling silica droplets generated by meteorite impact.

Q1: Why are they so much bigger than raindrops? From raindrop scaling, we expect $\ell_c \sim \sqrt{\frac{\sigma}{\Delta\rho g}}$ but both σ , $\Delta\rho$ higher by a factor of 10 \Rightarrow large tektite size suggests they are not equilibrium forms, but froze into shape during flight.

Q2: Why are their shapes so different from those of raindrops? Owing to high ρ of tektites, the internal dynamics (esp. rotation) dominates the aerodynamics \Rightarrow drop shape set by its rotation.

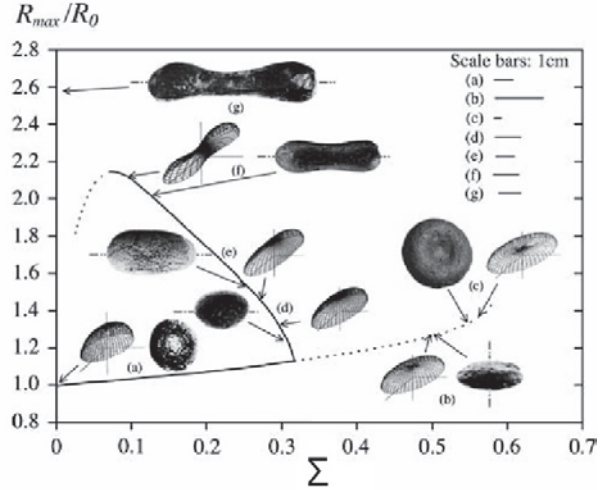


Figure 7.2: The ratio of the maximum radius to the unperturbed radius is indicated as a function of Σ . Stable shapes are denoted by the solid line, their metastable counterparts by dashed lines. Predicted 3-dimensional forms are compared to photographs of natural tektites. From *Elkins-Tanton, Ausillous, Bico, Quéré and Bush (2003)*.

Light drops: For the case of $\Sigma < 0$, $\Delta\rho < 0$, a spinning drop is stabilized on axis by centrifugal pressures. For high $|\Sigma|$, it is well described by a cylinder with spherical caps. Drop energy:

$$E = \underbrace{\frac{1}{2}I\Omega^2}_{\text{Rotational K.E.}} + \underbrace{2\pi rL\gamma}_{\text{Surface energy}}$$

Neglecting the end caps, we write volume $V = \pi r^2 L$ and moment of inertia $I = \frac{\Delta m r^2}{2} = \Delta\rho \frac{\pi}{2} L r^4$.

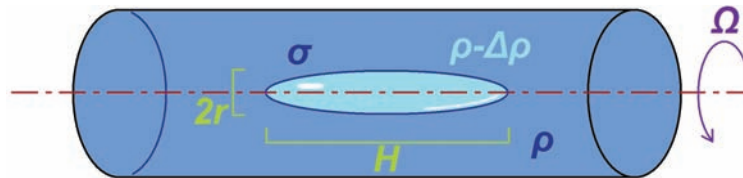


Figure 7.3: A bubble or a drop suspended in a denser fluid, spinning with angular speed Ω .

The energy per unit drop volume is thus $\frac{E}{V} = \frac{1}{4}\Delta\rho\Omega^2 r^2 + \frac{2\gamma}{r}$.

Minimizing with respect to r :

$$\frac{d}{dr} \left(\frac{E}{V} \right) = \frac{1}{2}\Delta\rho\Omega^2 r - \frac{2\gamma}{r^2} = 0, \text{ which occurs when } r = \left(\frac{4\gamma}{\Delta\rho\Omega^2} \right)^{1/3}. \text{ Now } r = \left(\frac{V}{\pi L} \right)^{1/2} = \left(\frac{4\gamma}{\Delta\rho\Omega^2} \right)^{1/3} \Rightarrow$$

Vonnegut's Formula: $\gamma = \frac{1}{4\pi^{3/2}}\Delta\rho\Omega^2 \left(\frac{V}{L} \right)^{3/2}$ allows inference of γ from L , useful technique for small γ as it avoids difficulties associated with fluid-solid contact.

Note: r grows with σ and decreases with Ω .

7.2 Rolling drops

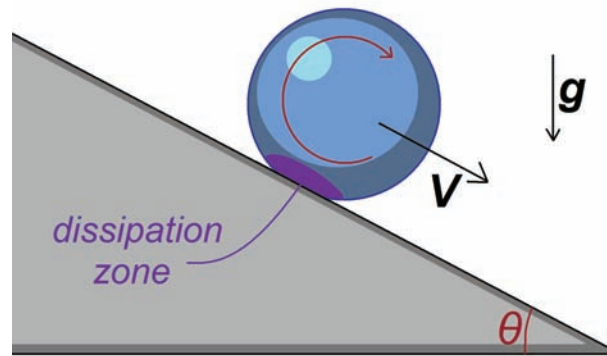


Figure 7.4: A liquid drop rolling down an inclined plane.

(Aussillous and Quere 2003) Energetics: for steady descent at speed V , $MgV \sin\theta = \text{Rate of viscous dissipation} = 2\mu \int_{V_d} (\nabla \mathbf{u})^2 dV$, where V_d is the dissipation zone, so this sets $V \Rightarrow \Omega = V/R$ is the angular speed. Stability characteristics different: bioconcave oblate ellipsoids now stable.

8. Capillary Rise

Capillary rise is one of the most well-known and vivid illustrations of capillarity. It is exploited in a number of biological processes, including drinking strategies of insects, birds and bats and plays an important role in a number of geophysical settings, including flow in porous media such as soil or sand.

Historical Notes:

- *Leonardo da Vinci* (1452 - 1519) recorded the effect in his notes and proposed that mountain streams may result from capillary rise through a fine network of cracks
- *Jacques Rohault* (1620-1675): erroneously suggested that capillary rise is due to suppression of air circulation in narrow tube and creation of a vacuum
- *Geovanni Borelli* (1608-1675): demonstrated experimentally that $h \sim 1/r$
- *Geminiano Montanari* (1633-87): attributed circulation in plants to capillary rise
- *Francis Hauksbee* (1700s): conducted an extensive series of capillary rise experiments reported by Newton in his *Opticks* but was left unattributed
- *James Jurin* (1684-1750): an English physiologist who independently confirmed $h \sim 1/r$; hence “Jurin’s Law”.

Consider capillary rise in a cylindrical tube of inner radius a (Fig. 8.2)

Recall:

Spreading parameter: $S = \gamma_{SV} - (\gamma_{SL} + \gamma_{LV})$.

We now define Imbibition / Impregnation parameter:

$$I = \gamma_{SV} - \gamma_{SL} = \gamma_{LV} \cos \theta$$

via force balance at contact line.

Note: in capillary rise, I is the relevant parameter, since motion of the contact line doesn’t change the energy of the liquid-vapour interface.

Imbibition Condition: $I > 0$.

Note: since $I = S + \gamma_{LV}$, the imbibition condition $I > 0$ is always more easily met than the spreading condition, $S > 0$

\Rightarrow most liquids soak sponges and other porous media, while complete spreading is far less common.

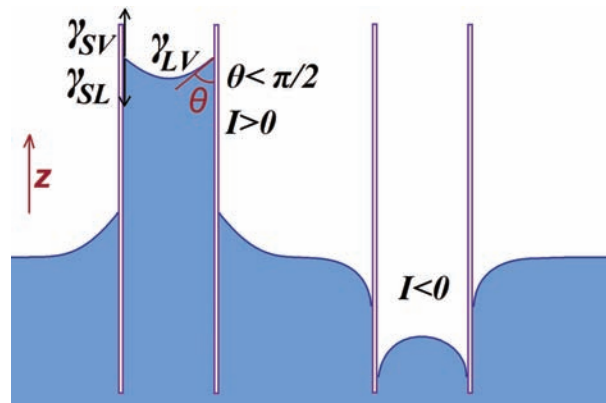


Figure 8.1: Capillary rise and fall in a tube for two values of the imbibition parameter I : $I > 0$ (left) and $I < 0$ (right).

We want to predict the dependence of rise height H on both tube radius a and wetting properties. We do so by minimizing the total system energy, specifically the surface and gravitational potential energies. The energy of the water column:

$$E = \underbrace{(\gamma_{SL} - \gamma_{SV})2\pi aH}_{\text{surface energy}} + \underbrace{\frac{1}{2}\rho g a^2 \pi H^2}_{\text{grav.P.E.}} = -2\pi aHI + \frac{1}{2}\rho g a^2 \pi H^2$$

will be a minimum with respect to H when $\frac{dE}{dH} = 0$
 $\Rightarrow H = 2\frac{\gamma_{SV} - \gamma_{SL}}{\rho g a} = 2\frac{l_c}{\rho g a}$, from which we deduce

Jurin's Law

$$H = 2\frac{\gamma_{LV} \cos \theta}{\rho g r} \quad (8.1)$$

Note:

1. describes both capillary rise and descent: sign of H depends on whether $\theta > \pi/2$ or $\theta < \pi/2$
2. H increases as θ decreases. H_{max} for $\theta = 0$
3. we've implicitly assumed $R \ll H$ & $R \ll l_c$.

The same result may be deduced via pressure or force arguments.

By Pressure Argument

Provided $a \ll l_c$, the meniscus will take the form of a spherical cap with radius $R = \frac{a}{\cos \theta}$. Therefore
 $p_A = p_B - \frac{2\sigma \cos \theta}{a} = p_0 - \frac{2\sigma \cos \theta}{a} = p_0 - \rho g H$
 $\Rightarrow H = \frac{2\sigma \cos \theta}{\rho g a}$ as previously.

By Force Argument

The weight of the column supported by the tensile force acting along the contact line:

$\rho \pi a^2 H g = 2\pi a (\gamma_{SV} - \gamma_{SL}) = 2\pi a \sigma \cos \theta$, from which Jurin's Law again follows.

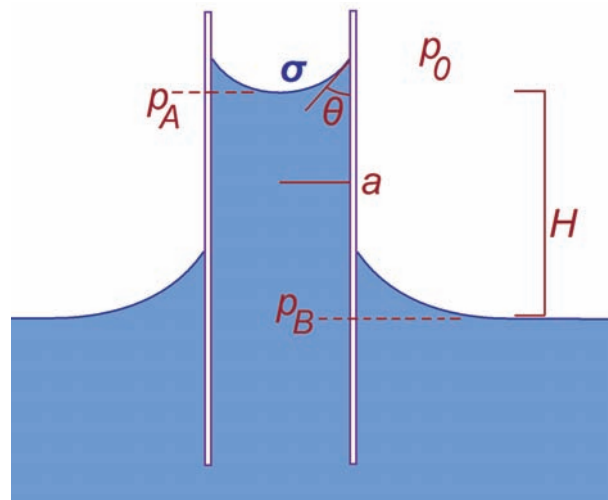


Figure 8.2: Deriving the height of capillary rise in a tube via pressure arguments.

8.1 Dynamics

The column rises due to capillary forces, its rise being resisted by a combination of gravity, viscosity, fluid inertia and dynamic pressure. Conservation of momentum dictates $\frac{d}{dt}(m(t)\dot{z}(t)) = F_{TOT} + \int_S \rho \mathbf{v} \mathbf{v} \cdot \mathbf{n} dA$, where the second term on the right-hand side is the total momentum flux, which evaluates to $\pi a^2 \rho \dot{z}^2 = \dot{m} \dot{z}$, so the force balance on the column may be expressed as

$$\left(\underbrace{m}_{\text{Inertia}} + \underbrace{m_a}_{\text{Added mass}} \right) \ddot{z} = \underbrace{2\pi a \sigma \cos \theta}_{\text{capillary force}} - \underbrace{mg}_{\text{weight}} - \underbrace{\pi a^2 \frac{1}{2} \rho \dot{z}^2}_{\text{dynamic pressure}} - \underbrace{2\pi a z \cdot \tau_v}_{\text{viscous force}} \quad (8.2)$$

where $m = \pi a^2 z \rho$. Now assume the flow in the tube is fully developed Poiseuille flow, which will be established after a diffusion time $\tau = \frac{a^2}{\nu}$. Thus, $u(r) = 2\dot{z} \left(1 - \frac{r^2}{a^2}\right)$, and $F = \pi a^2 \dot{z}$ is the flux along the tube.

The stress along the outer wall: $\tau_v = \mu \frac{du}{dr} \Big|_{r=a} = -\frac{4\mu}{a} \dot{z}$.

Finally, we need to estimate m_a , which will dominate the dynamics at short time. We thus estimate the change in kinetic energy as the column rises from z to $z + \Delta z$. $\Delta E_k = \Delta \left(\frac{1}{2} m U^2\right)$, where $m = m_c + m_0 + m_\infty$ (mass in the column, in the spherical cap, and all the other mass, respectively). In the column, $m_c = \pi a^2 z \rho$, $u = U$. In the spherical cap, $m_0 = \frac{2\pi}{3} a^3 \rho$, $u = U$. In the outer region, radial inflow extends to ∞ , but $u(r)$ decays.

Volume conservation requires: $\pi a^2 U = 2\pi a^2 u_r(a) \Rightarrow u_r(a) = U/2$.

Continuity thus gives: $2\pi a^2 u_r(a) = 2\pi r^2 u_r(r) \Rightarrow u_r(r) = \frac{a^2}{r^2} u_r(a) = \frac{a^2}{2r^2} U$.

Thus, the K.E. in the far field: $\frac{1}{2} m_\infty^{eff} U^2 = \frac{1}{2} \int_a^\infty u_r(r)^2 dm$, where $dm = \rho 2\pi r^2 dr$.

Hence

$$\begin{aligned} m_\infty^{eff} &= \frac{1}{U^2} \int_a^\infty \rho \left(\frac{a^2}{2r^2} U\right)^2 2\pi r^2 dr = \\ &= \pi \rho a^4 \int_a^\infty \frac{1}{2r^2} dr = \frac{1}{2} \rho \pi a^3 \end{aligned}$$

Now

$$\begin{aligned} \Delta E_k &= \frac{1}{2} \Delta (m_c + m_0 + m_\infty) U^2 + \frac{1}{2} m 2U \Delta U = \\ &= \frac{1}{2} \Delta m_c U^2 + \frac{1}{2} (m_c + m_0 + m_\infty^{eff}) 2U \Delta U = \\ &= \frac{1}{2} (\pi a^2 \rho \Delta z) U^2 + (\pi a^2 \rho z + \frac{2}{3} \pi a^3 \rho + \frac{1}{2} \pi a^3 \rho) U \Delta U \end{aligned}$$

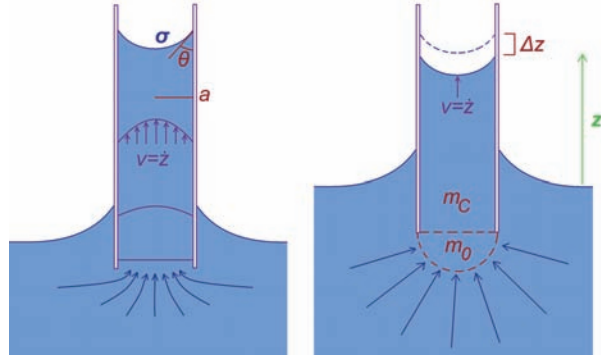


Figure 8.3: The dynamics of capillary rise.

Substituting for $m = \pi a^2 z \rho$, $m_a = \frac{7}{6} \pi a^3 \rho$ (added mass) and $\tau_v = -\frac{4\mu}{a} \dot{z}$ into (8.2) we arrive at

$$\left(z + \frac{7}{6} a\right) \ddot{z} = \frac{2\sigma \cos \theta}{\rho a} - \frac{1}{2} \dot{z}^2 - \frac{8\mu z \dot{z}}{\rho a^2} - gz \quad (8.3)$$

The static balance clearly yields the rise height, i.e. Jurin's Law. But how do we get there?

Inertial Regime

1. the timescale of establishment of Poiseuille flow is $\tau^* = \frac{4a^2}{\nu}$, the time required for boundary effects to diffuse across the tube
2. until this time, viscous effects are negligible and the capillary rise is resisted primarily by fluid inertia

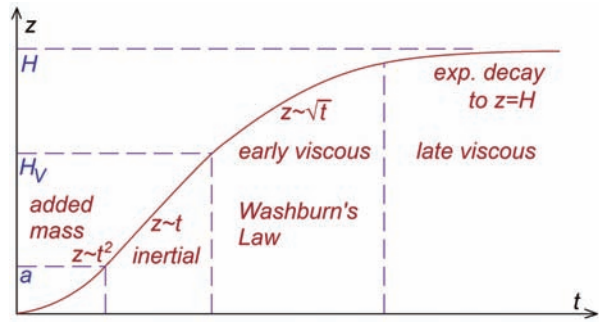


Figure 8.4: The various scaling regimes of capillary rise.

Initial Regime: $z \sim 0, \dot{z} \sim 0$, so the force balance assumes the form $\frac{7}{6}a\ddot{z} = \frac{2\sigma \cos \theta}{\rho a}$ We thus infer

$$z(t) = \frac{6}{7} \frac{\sigma \cos \theta}{\rho a^2} t^2.$$

Once $z \geq \frac{7}{6}a$, one must also consider the column mass, and so solve $(z + \frac{7}{6}a)\ddot{z} = \frac{2\sigma \cos \theta}{\rho a}$. As the column accelerates from $\dot{z} = 0$, \dot{z}^2 becomes important, and the force balance becomes: $\frac{1}{2}\dot{z}^2 = \frac{2\sigma \cos \theta}{\rho a} \Rightarrow$

$$\dot{z} = U = \left(\frac{4\sigma \cos \theta}{\rho a} \right)^{1/2} \text{ is independent of } g, \mu.$$

$$z = \left(\frac{4\sigma \cos \theta}{\rho a} \right)^{1/2} t.$$

Viscous Regime ($t \gg \tau^*$) Here, inertial effects become negligible, so the force balance assumes the form:

$$\frac{2\sigma \cos \theta}{\rho a} - \frac{8\mu z \dot{z}}{\rho a^2} - gz = 0. \text{ We thus infer } H - z = \frac{8\mu z \dot{z}}{\rho g a^2}, \text{ where } H = \frac{2\sigma \cos \theta}{\rho g a}, \dot{z} = \frac{\rho g a^2}{8\mu} \left(\frac{H}{z} - 1 \right)$$

Nondimensionalizing: $z^* = z/H, t^* = t/\tau, \tau = \frac{8\mu H}{\rho g a^2};$

We thus have $\dot{z}^* = \frac{1}{z^* - 1} \Rightarrow dt^* = \frac{z^*}{1 - z^*} dz^* = (-1 - \frac{1}{1 - z^*}) dz^* \Rightarrow t^* = -z^* - \ln(1 - z^*).$

Note: at $t^* \rightarrow \infty, z^* \rightarrow 1.$

Early Viscous Regime: When $z^* \ll 1$, we consider $\ln(z^* - 1) = -z^* - \frac{1}{2}z^{*2}$ and so infer $z^* = \sqrt{2t^*}.$

Redimensionalizing thus yields *Washburn's Law*: $z = \left[\frac{\sigma a \cos \theta}{2\mu} t \right]^{1/2}$

Note that \dot{z} is independent of g .

Late Viscous Regime: As z approaches $H, z^* \approx 1$. Thus, we consider $t^* = [-z^* - \ln(1 - z^*)] = \ln(1 - z^*)$ and so infer $z^* = 1 - \exp(-t^*).$

Redimensionalizing yields $z = H [1 - \exp(-t/\tau)],$ where $H = \frac{2\sigma \cos \theta}{\rho g a}$ and $\tau = \frac{8\mu H}{\rho g a^2}.$

Note: if rise timescale $\ll \tau^* = \frac{4a^2}{\nu}$, inertia dominates, i.e. $H \ll U_{inertial} \tau^* = \left(\frac{4\sigma \cos \theta}{\rho a} \right)^{1/2} \frac{4a^2}{\nu} \Rightarrow$ inertial overshoot arises, giving rise to oscillations of the water column about its equilibrium height H .

Wicking In the viscous regime, we have $\frac{2\sigma \cos \theta}{\rho a} = \frac{8\mu z \dot{z}}{\rho a^2} + \rho g$. What if the viscous stresses dominate gravity? This may arise, for example, for predominantly horizontal flow (Fig. 8.5).

Force balance: $\frac{2\sigma a \cos \theta}{8\mu} = z \dot{z} = \frac{1}{2} \frac{d}{dt} z^2 \Rightarrow z = \left(\frac{\sigma a \cos \theta}{2\mu} t \right)^{1/2} \sim \sqrt{t}$ (*Washburn's Law*).

Note: Front slows down, not due to g , but owing to increasing viscous dissipation with increasing column length.

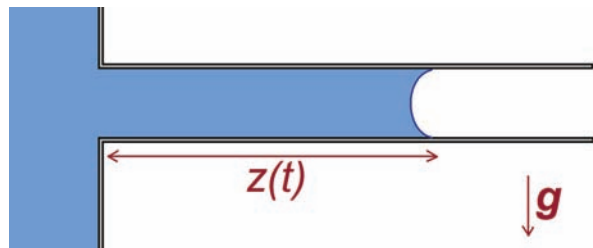


Figure 8.5: Horizontal flow in a small tube.

9. Marangoni Flows

Marangoni flows are those driven by surface gradients. In general, surface tension σ depends on both the temperature and chemical composition at the interface; consequently, Marangoni flows may be generated by gradients in either temperature or chemical composition at an interface. We previously derived the tangential stress balance at a free surface:

$$\mathbf{n} \cdot \mathbf{T} \cdot \mathbf{t} = -\mathbf{t} \cdot \nabla \sigma \quad , \quad (9.1)$$

where \mathbf{n} is the unit outward normal to the surface, and \mathbf{t} is any unit tangent vector. The tangential component of the hydrodynamic stress at the surface must balance the tangential stress associated with gradients in σ . Such Marangoni stresses may result from gradients in temperature or chemical composition at the interface. For a static system, since $\mathbf{n} \cdot \mathbf{T} \cdot \mathbf{t} = 0$, the tangential stress balance equation indicates that: $0 = \nabla \sigma$. This leads us to the following important conclusion:

There cannot be a static system in the presence of surface tension gradients.

While pressure jumps can arise in static systems characterized by a normal stress jump across a fluid interface, they do not contribute to the tangential stress jump. Consequently, tangential surface stresses can only be balanced by viscous stresses associated with fluid motion.

Thermocapillary flows: Marangoni flows induced by temperature gradients $\sigma(T)$.

Note that in general $\frac{d\sigma}{dT} < 0$ Why? A warmer gas phase has more liquid molecules, so the creation of surface is less energetically unfavourable; therefore, σ is lower.

Approach Through the interfacial BCs (and $\sigma(T)$'s appearance therein), N-S equations must be coupled

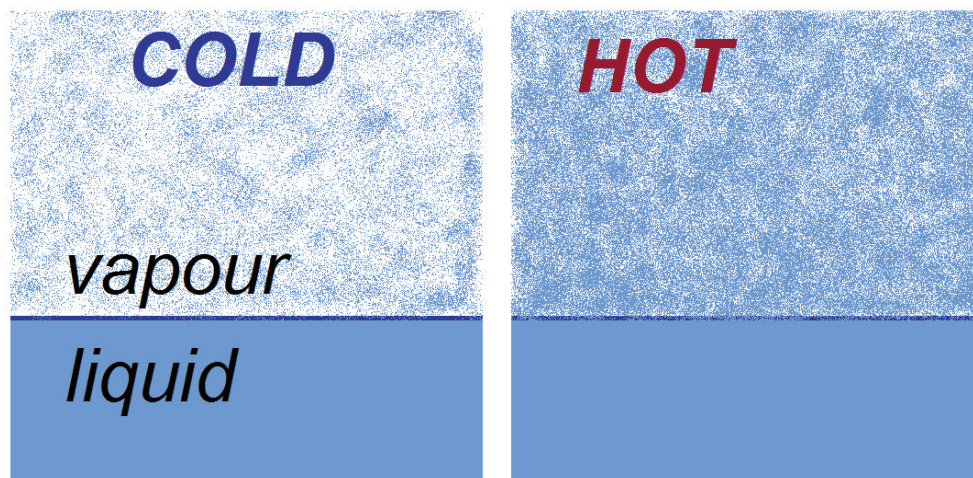


Figure 9.1: Surface tension of a gas-liquid interface decreases with temperature since a warmer gas phase contains more suspended liquid molecules. The energetic penalty of a liquid molecule moving to the interface is thus decreased.

to the heat equation

$$\frac{\partial T}{\partial t} + \mathbf{u} \cdot \nabla T = \kappa \nabla^2 T \quad (9.2)$$

Note:

1. the heat equation must be solved subject to appropriate BCs at the free surface. Doing so can be complicated, especially if the fluid is evaporating.
2. Analysis may be simplified when the **Peclet number** $\mathcal{P}e = \frac{Ua}{\kappa} \ll 1$. Nondimensionalize (9.2): $\mathbf{x} = a\mathbf{x}'$, $t = \frac{a}{\nu}t'$, $\mathbf{u} = U\mathbf{u}'$ to get

$$\mathcal{P}e \left(\frac{\partial T'}{\partial t'} + \mathbf{u}' \cdot \nabla' T' \right) = \nabla'^2 T' \quad (9.3)$$

Note:

$\mathcal{P}e = \mathcal{R}e \cdot \mathcal{P}r = \frac{Ua}{\nu} \cdot \frac{\nu}{\kappa} \ll 1$ if $\mathcal{R}e \ll 1$, so one has $\nabla^2 T = 0$.

The **Prandtl number** $\mathcal{P}r = O(1)$ for many common (e.g. aqueous) fluids.

E.g.1 Thermocapillary flow in a slot (Fig.9.2a)

Surface Tangential BCs $\tau = \frac{\Delta\sigma}{L} = \frac{d\sigma}{dT} \frac{\Delta T}{L} \approx \mu \frac{U}{H}$ viscous stress $U \sim \frac{1}{\mu} \frac{H}{L} \Delta\sigma$.

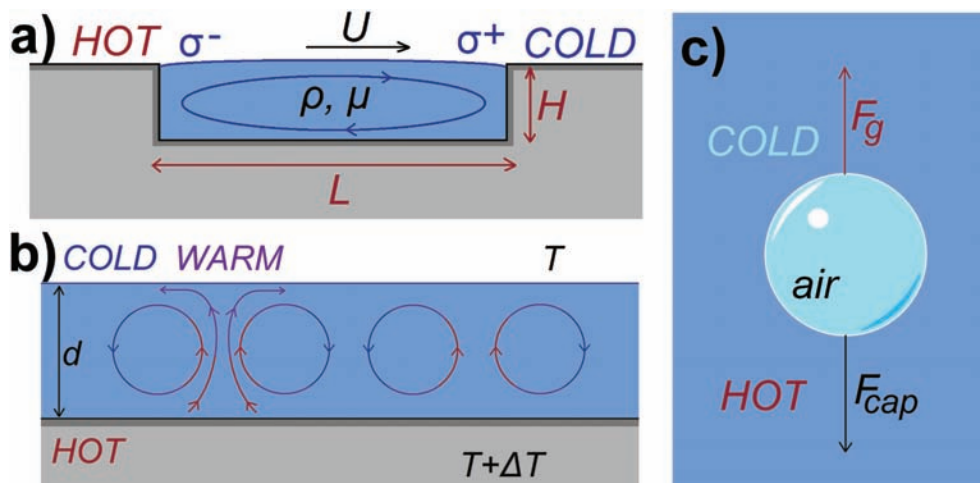


Figure 9.2: a) Thermocapillary flow in a slot b) Thermal convection in a plane layer c) Thermocapillary drop motion.

E.g.2 Thermocapillary Drop Motion (Young, Goldstein & Block 1962)

can trap bubbles in gravitational field via thermocapillary forces. (Fig.9.2c).

E.g.3 Thermal Marangoni Convection in a Plane Layer (Fig.9.2b).

Consider a horizontal fluid layer heated from below. Such a layer may be subject to either buoyancy- or Marangoni-induced convection.

Recall: Thermal buoyancy-driven convection (Rayleigh-Bernard) $\rho(T) = \rho_0 (1 + \alpha(T - T_0))$, where α is the thermal expansivity. Consider a buoyant blob of characteristic scale d . Near the onset of convection, one expects it to rise with a Stokes velocity $U \sim \frac{g\Delta\rho}{\rho} \frac{d^2}{\nu} = \frac{g\alpha\Delta T d^2}{\nu}$. The blob will rise, and so convection will occur, provided its rise time $\tau_{rise} = \frac{d}{U} = \frac{d\nu}{g\alpha\Delta T d^2}$ is less than the time required for it to lose its heat and buoyancy by diffusion, $\tau_{diff} = \frac{d^2}{\kappa}$.

Criterion for Instability: $\frac{\tau_{diff}}{\tau_{rise}} \sim \frac{g\alpha\Delta T d^3}{\kappa\nu} \equiv \mathcal{R}a > \mathcal{R}a_c \sim 10^3$, where $\mathcal{R}a$ is the Rayleigh number.

Note: for $\mathcal{R}a < \mathcal{R}a_c$, heat is transported solely through diffusion, so the layer remains static. For $\mathcal{R}a > \mathcal{R}a_c$, convection arises.

The subsequent behaviour depends on $\mathcal{R}a$ and $\mathcal{P}r$. Generally, as $\mathcal{R}a$ increases, steady convection rolls \Rightarrow time-dependency \Rightarrow chaos \Rightarrow turbulence.

Thermal Marangoni Convection

Arises because of the dependence of σ on temperature: $\sigma(T) = \sigma_0 - \Gamma(T - T_0)$

Mechanism:

- Imagine a warm spot on surface \Rightarrow prompts surface divergence \Rightarrow upwelling.
- Upwelling blob is warm, which reinforces the perturbation provided it rises before losing its heat via diffusion.
- Balance Marangoni and viscous stress: $\frac{\Delta\sigma}{d} \sim \frac{\mu U}{d}$
- Rise time: $\frac{d}{U} \sim \frac{\mu d}{\Delta\sigma}$
- Diffusion time $\tau_{diff} = \frac{d^2}{\kappa}$

Criterion for instability: $\frac{\tau_{diff}}{\tau_{rise}} \sim \frac{\Gamma\Delta T d}{\mu\kappa} \equiv Ma > Ma_c$, where Ma is the Marangoni number.

Note:

1. Since $Ma \sim d$ and $Ra \sim d^3$, thin layers are most unstable to Marangoni convection.
2. Bénard's original experiments performed in millimetric layers of spermaceti were visualizing Marangoni convection, but were misinterpreted by Rayleigh as being due to buoyancy \Rightarrow not recognized until *Block (Nature 1956)*.
3. *Pearson (1958)* performed stability analysis with flat surface \Rightarrow deduced $Ma_c = 80$.
4. *Scriven & Sternling (1964)* considered a deformable interface, which renders the system unstable at all Ma . Downwelling beneath peaks in Marangoni convection, upwelling between peaks in Rayleigh-Bénard convection (Fig. 9.3a).
5. *Smith (1966)* showed that the destabilizing influence of the surface may be mitigated by gravity. Stability Criterion: $\frac{d\sigma}{dT} \frac{dT}{dz} < \frac{2}{3}\rho g d \Rightarrow$ thin layers prone to instability.

E.g.4 Marangoni Shear Layer (Fig. 9.3)

Lateral $\nabla\theta$ leads to Marangoni stress \Rightarrow shear flow. The resulting $T(x, y)$ may destabilize the layer to

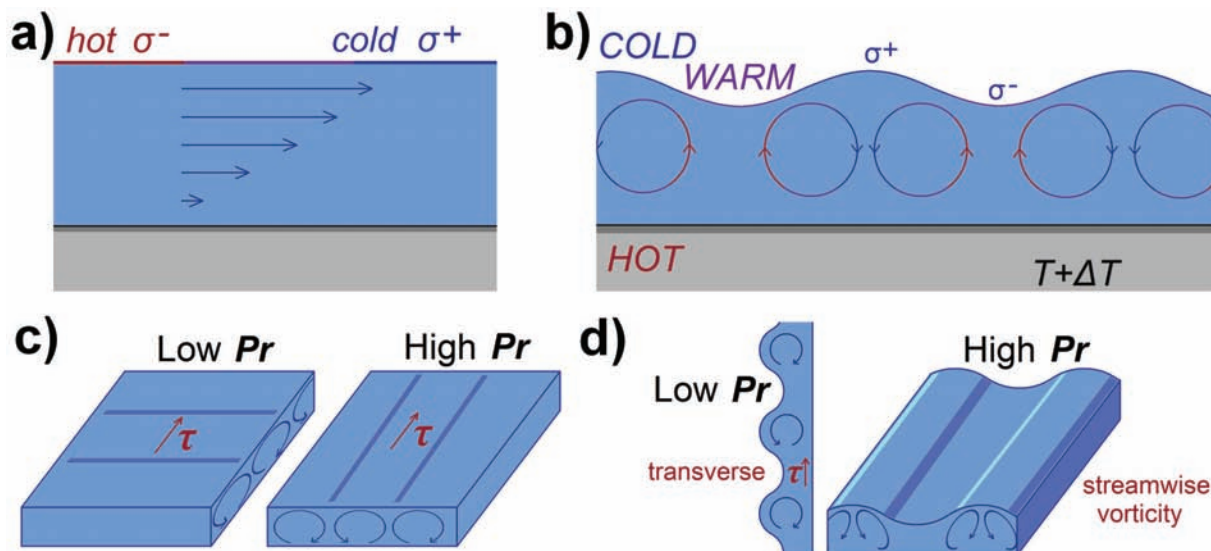


Figure 9.3: a) Marangoni convection in a shear layer may lead to transverse surface waves or streamwise rolls (c). Surface deflection may accompany both instabilities (b,d).

Marangoni convection.

Smith & Davis (1983ab) considered the case of flat free surface. System behaviour depends on $Pr = \nu/\kappa$.

Low Pr : Hydrothermal waves propagate in direction of τ .

High Pr : Streamwise vortices (Fig. 9.3c).

Hosoi & Bush (2001) considered a deformable free surface (Fig. 9.3d)

E.g.5 Evaporatively-driven convection

e.g. for an alcohol- H_2O solution, evaporation affects both the alcohol concentration c and temperature θ . The density $\rho(c, \theta)$ and surface tension $\sigma(c, \theta)$ are such that $\frac{\partial\rho}{\partial\theta} < 0$, $\frac{\partial\rho}{\partial c} < 0$, $\frac{d\sigma}{d\theta} < 0$, $\frac{d\sigma}{dc} < 0$. Evaporation results in surface cooling and so may generate either Rayleigh-Bénard or Marangoni thermal convection. Since it also induces a change in surface chemistry, it may likewise generate either $Ra - B$ or Marangoni chemical convection.

E.g.6 Coffee Drop

Marangoni flows are responsible for the ring-like stain left by a coffee drop.

- coffee grounds stick to the surface
- evaporation leads to surface cooling, which is most pronounced near the edge, where surface area per volume ratio is highest
- resulting thermal Marangoni stresses drive radial outflow on surface \Rightarrow radial ring

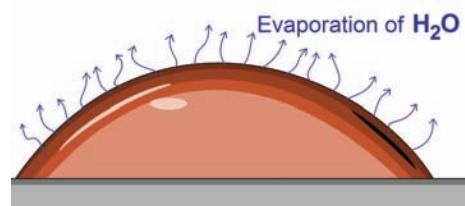


Figure 9.4: Evaporation of water from a coffee drop drives a Marangoni flow.

10. Marangoni Flows II

10.1 Tears of Wine

The first Marangoni flow considered was the tears of wine phenomenon (*Thomson 1885*), which actually predates Marangoni's first published work on the subject by a decade. The tears of wine phenomenon is readily observed in a wine glass following the establishment of a thin layer of wine on the walls of the glass.

An illustration of the tears of wine phenomenon is shown in Fig. 10.1. Evaporation of alcohol occurs everywhere along the free surface. The alcohol concentration in the thin layer is thus reduced relative to that in the bulk owing to the enhanced surface area to volume ratio. As surface tension decreases with alcohol concentration, the surface tension is higher in the thin film than the bulk; the associated Marangoni stress drives upflow throughout the thin film. The wine climbs until reaching the top of the film, where it accumulates in a band of fluid that thickens until eventually becoming gravitationally unstable and releasing the tears of wine. The tears or "legs" roll back to replenish the bulk reservoir, but with fluid that is depleted in alcohol.

The flow relies on the transfer of chemical potential energy to kinetic and ultimately gravitational potential energy. The process continues until the fuel for the process, the alcohol is completely depleted. For certain liquors (e.g. port), the climbing film, a Marangoni shear layer, goes unstable to streamwise vortices and an associated radial corrugation - the "tear ducts of wine" (*Hosoi & Bush, JFM 2001*). When the descending tears reach the bath, they appear to recoil in response to the abrupt change in σ . The tears or legs of wine are taken by sommeliers to be an indicator of the quality of wine.

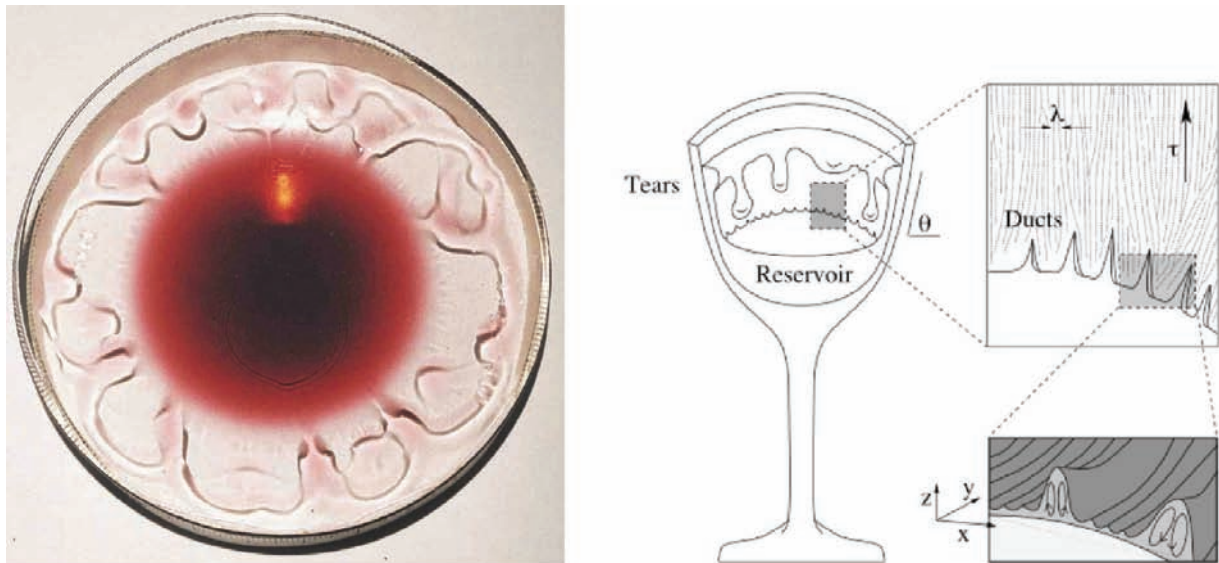


Figure 10.1: The tears of wine. Fluid is drawn from the bulk up the thin film adjoining the walls of the glass by Marangoni stresses induced by evaporation of alcohol from the free surface.

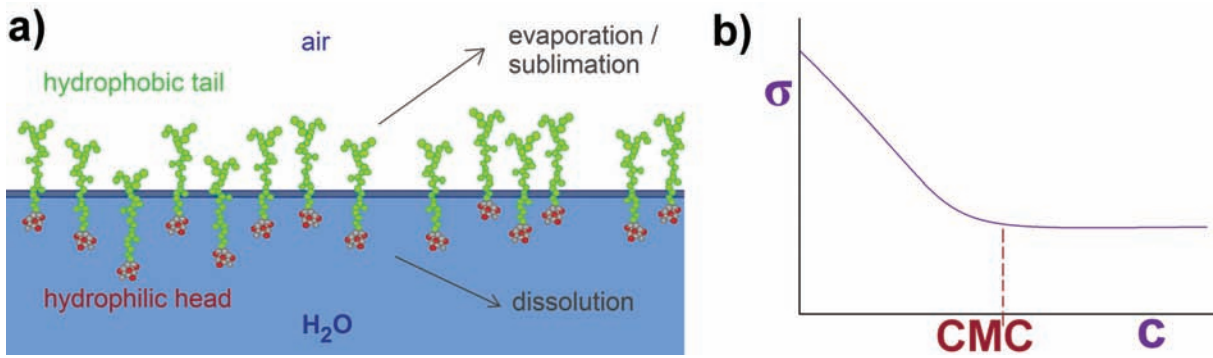


Figure 10.2: a) A typical molecular structure of surfactants. b) The typical dependence of σ on surfactant concentration c .

10.2 Surfactants

Surfactants are molecules that have an affinity for interfaces; common examples include soap and oil. Owing to their molecular structure (e.g. a hydrophilic head and hydrophobic tail, Fig. 10.2a), they find it energetically favourable to reside at the free surface. Their presence reduces the surface tension; consequently, gradients in surfactant concentration Γ result in surface tension gradients. Surfactants thus generate a special class of Marangoni flows. There are many different types of surfactants, some of which are insoluble (and so remain on the surface), others of which are soluble in the suspending fluid and so diffuse into the bulk. For a wide range of common surfactants, surface tension is a monotonically decreasing function of Γ until a critical micell concentration (CMC) is achieved, beyond CMC there is no further dependence of σ on Γ (Fig. 10.2b).

Surfactant properties:

- **Diffusivity** prescribes the rate of diffusion, D_s (bulk diffusivity D_b), of a surfactant along an interface
- **Solubility** prescribes the ease with which surfactant passes from the surface to the bulk. An insoluble surfactant cannot dissolve into the bulk, must remain on the surface.
- **Volatility** prescribes the ease with which surfactant sublimates.

Theoretical Approach: because of the dependence of σ on the surfactant concentration, and the appearance of σ in the boundary conditions, N-S equations must be augmented by an equation governing the evolution of Γ . In the bulk,

$$\frac{\partial c}{\partial t} + \mathbf{u} \cdot \nabla c = D_b \nabla^2 c \quad (10.1)$$

The concentration of surfactant Γ on a free surface evolves according to

$$\frac{\partial \Gamma}{\partial t} + \nabla_s \cdot (\Gamma \mathbf{u}_s) + \Gamma (\nabla_s \cdot \mathbf{n}) (\mathbf{u} \cdot \mathbf{n}) = J(\Gamma, C_s) + D_s \nabla_s^2 \Gamma \quad (10.2)$$

where \mathbf{u}_s is the surface velocity, ∇_s is the surface gradient operator and D_s is the surface diffusivity of the surfactant (Stone 1999). J is a surfactant source term associated with adsorption onto or desorption from the surface, and depends on both the surface surfactant concentration Γ and the concentration in the bulk C_s . Tracing the evolution of a contaminated free surface requires the use of Navier-Stokes equations, relevant boundary conditions and the surfactant evolution equation (10.2). The dependence of surface tension on surfactant concentration, $\sigma(\Gamma)$, requires the coupling of the flow field and surfactant field. In certain special cases, the system may be made more tractable. For example, for insoluble surfactants, $J = 0$. Many surfactants have sufficiently small D_s that surface diffusivity may be safely neglected.



Figure 10.3: The footprint of a whale, caused by the whales sweeping biomaterial to the sea surface. The biomaterial acts as a surfactant in locally suppressing the capillary waves evident elsewhere on the sea surface. Observed in the wake of a whale on a Whale Watch from Boston Harbour.

Special case: expansion of a spherical surfactant-laden bubble.

$\frac{\partial \Gamma}{\partial t} + \Gamma (\nabla \cdot \mathbf{n}) u_r = 0$. Here $\nabla \cdot \mathbf{n} = 2/R$, $u_r = \frac{dR}{dt}$ so $\frac{d\Gamma}{dt} + \Gamma \frac{2}{R} \frac{dR}{dt} = 0 \Rightarrow \frac{d\Gamma}{\Gamma} = -2 \frac{dR}{R}$ $4\pi R^2 \Gamma = \text{const.}$, so the surfactant is conserved.

Marangoni Elasticity The principal dynamical influence of surfactants is to impart an effective elasticity to the interface. One can think of a clean interface as a “slippery trampoline” that resists deformation through generation of normal curvature pressures. However, such a surface cannot generate traction on the interface. However, a surface-laden interface, like a trampoline, resists surface deformation as does a clean interface, but can also support tangential stresses via Marangoni elasticity. Specifically, the presence of surfactants will serve not only to alter the normal stress balance (through the reduction of σ), but also the tangential stress balance through the generation of Marangoni stresses.

The presence of surfactants will act to suppress any fluid motion characterized by non-zero surface divergence. For example, consider a fluid motion characterized by a radially divergent surface motion. The presence of surfactants results in the redistribution of surfactants: Γ is reduced near the point of divergence. The resulting Marangoni stresses act to suppress the surface motion, resisting it through an effective surface elasticity. Similarly, if the flow is characterized by a radial convergence, the resulting accumulation of surfactant in the region of convergence will result in Marangoni stresses that serve to resist it. It is this effective elasticity that gives soap films their longevity: the divergent motions that would cause a pure liquid film to rupture are suppressed by the surfactant layer on the soap film surface.

The ability of surfactant to suppress flows with non-zero surface divergence is evident throughout the natural world. It was first remarked upon by Pliny the Elder, who rationalized that the absence of capillary waves in the wake of ships is due to the ships stirring up surfactant. This phenomenon was also widely known to spear-fishermen, who poured oil on the water to increase their ability to see their prey, and by sailors, who would do similarly in an attempt to calm troubled seas. Finally, the suppression of capillary waves by surfactant is at least partially responsible for the ‘footprints of whales’ (see Fig. 10.3). In the wake of whales, even in turbulent roiling seas, one sees patches on the sea surface (of characteristic width 5-10m) that are perfectly flat. These are generally acknowledged to result from the whales sweeping biomaterial to the surface with their tails, this biomaterial serving as a surfactant that suppresses capillary waves.

Surfactants and a murder mystery. From *Nature*, 22, 1880:

*“In the autumn of 1878 a man committed a terrible crime in Somerset, which was for some time involved in deep mystery. His wife, a handsome and decent mulatto woman, disappeared suddenly and entirely from sight, after going home from church on Sunday, October 20. Suspicion immediately fell upon the husband, a clever young fellow of about thirty, but no trace of the missing woman was left behind, and there seemed a strong probability that the crime would remain undetected. On Sunday, however, October 27, a week after the woman had disappeared, some Somerville boatmen looking out towards the sea, as is their custom, were struck by observing in the Long Bay Channel, the surface of which was ruffled by a slight breeze, a **streak of calm such as, to use their own illustration, a cask of oil usually diffuses around it when in the water.** The feverish anxiety about the missing woman suggested some strange connection between this singular calm and the mode of her disappearance. Two or three days after - why not sooner I cannot tell you - her brother and three other men went out to the spot where it was observed, and from which it had not disappeared since Sunday, and with a series of fish-hooks ranged along a long line dragged the bottom of the channel, but at first without success. Shifting the position of the boat, they dragged a little further to windward, and presently the line was caught. With water glasses the men discovered that it had caught in a skeleton which was held down by some heavy weight. They pulled on the line; something suddenly gave way, and up came the skeleton of the trunk, pelvis, and legs of a human body, from which almost every vestige of flesh had disappeared, but which, from the minute fragments remaining, and the terrible stench, had evidently not lain long in the water. The husband was a fisherman, and Long Bay Channel was a favourite fishing ground, and he calculated, truly enough, that the fish would very soon destroy all means of identification; but it never entered into his head that as they did so their ravages, combined with the process of decomposition, **set free the matter which was to write the traces of his crime on the surface of the water.** The case seems to be an exceedingly interesting one; the calm is not mentioned in any book on medical jurisprudence that I have, and the doctors seem not to have had experience of such an occurrence. A diver went down and found a stone with a rope attached, by which the body had been held down, and also portions of the scalp and of the skin of the sole of the foot, and of clothing, by means of which the body was identified. The husband was found guilty and executed.”*

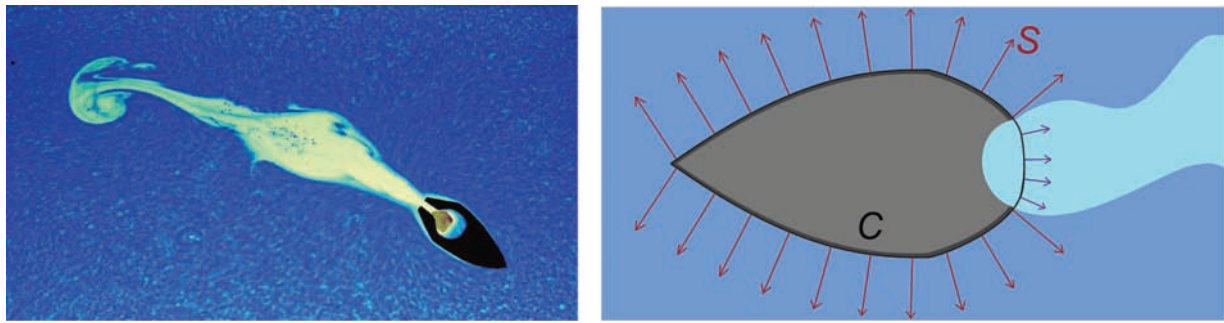


Figure 10.4: The soap boat. A floating body (length 2.5cm) contains a small volume of soap, which serves as its fuel in propelling it across the free surface. The soap exits the rear of the boat, decreasing the local surface tension. The resulting fore-to-aft surface tension gradient propels the boat forward. The water surface is covered with Thymol blue, which parts owing to the presence of soap, which is thus visible as a white streak.

10.3 Surfactant-induced Marangoni flows

1. Marangoni propulsion

Consider a floating body with perimeter C in contact with the free surface, which we assume for the sake of simplicity to be flat. Recalling that σ may be thought of as a force per unit length in a direction tangent to the surface, we see that the total surface tension force acting on the body is:

$$F_c = \int_C \sigma \mathbf{s} dl \quad (10.3)$$

where \mathbf{s} is the unit vector tangent to the free surface and normal to C , and dl is an increment of arc length along C . If σ is everywhere constant, then this line integral vanishes identically by the divergence theorem. However, if $\sigma = \sigma(\mathbf{x})$, then it may result in a net propulsive force. The ‘soap boat’ may be simply generated by coating one end of a toothpick with soap, which acts to reduce surface tension (see *right*). The concomitant gradient in surface tension results in a net propulsive force that drives the boat away from the soap. We note that an analogous Marangoni propulsion technique arises in the natural world: certain water-walking insects eject surfactant and use the resulting surface tension gradients as an emergency mechanism for avoiding predation. Moreover, when a pine needle falls into a lake or pond, it is propelled across the surface in an analogous fashion owing to the influence of the resin at its base decreasing the local surface tension.

2. Soap film stability

Pinching a film increases the surface area, decreases Γ and so increases σ . Fluid is thus drawn in and the film is stabilized by the Marangoni elasticity.

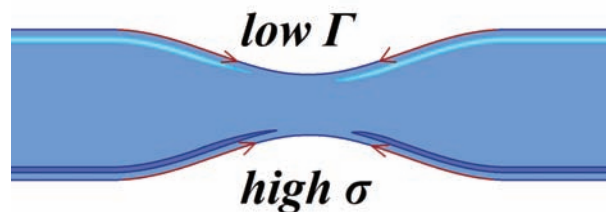


Figure 10.5: Fluid is drawn to a pinched area of a soap film through induced Marangoni stresses.

3. Vertical Soap Film

- Vertical force balance: $\rho gh(z) = \frac{d\sigma}{dz}$. The weight of a soap film is supported by Marangoni stress.
- Internal dynamics: note that film is dynamic (as are all Marangoni flows), if it were static, its max height would be ℓ_c . It is constantly drying due to the influence of gravity.
- On the surface: $\frac{d\sigma}{dz} \sim \mu \frac{du}{dx}$ balance of Marangoni and viscous stresses.
- Inside: $\rho g \sim \mu \frac{d^2u}{dx^2}$ Gravity-viscous.

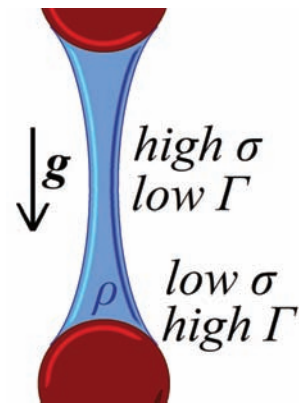


Figure 10.6: The weight of a vertical soap film is supported by Marangoni stresses on its surface.

10.4 Bubble motion

Theoretical predictions for the rise speed of small drops or bubbles do not adequately describe observations. Specifically, air bubbles rise at low Reynolds number at rates appropriate for rigid spheres with equivalent buoyancy in all but the most carefully cleaned fluids. This discrepancy may be rationalized through consideration of the influence of surfactants on the surface dynamics. The flow generated by a clean spherical bubble of radius a rising at low $Re = Ua/\nu$ is intuitively obvious. The interior flow is toroidal, while the surface motion is characterized by divergence and convergence at, respectively, the leading and trailing surfaces. The presence of surface contamination changes the flow qualitatively.

The effective surface elasticity imparted by the surfactants acts to suppress the surface motion. Surfactant is generally swept to the trailing edge of the bubble, where it accumulates, giving rise to a local decrease in surface tension. The resulting fore-to-aft surface tension gradient results in a Marangoni stress that resists surface motion, and so rigidifies the bubble surface. The air bubble thus moves as if its surface were stagnant, and it is thus that its rise speed is commensurate with that predicted for a rigid sphere: the no-slip boundary condition is more appropriate than the free-slip. Finally, we note that the characteristic Marangoni stress $\Delta\sigma/a$ is most pronounced for small bubbles. It is thus that the influence of surfactants is greatest on small bubbles.

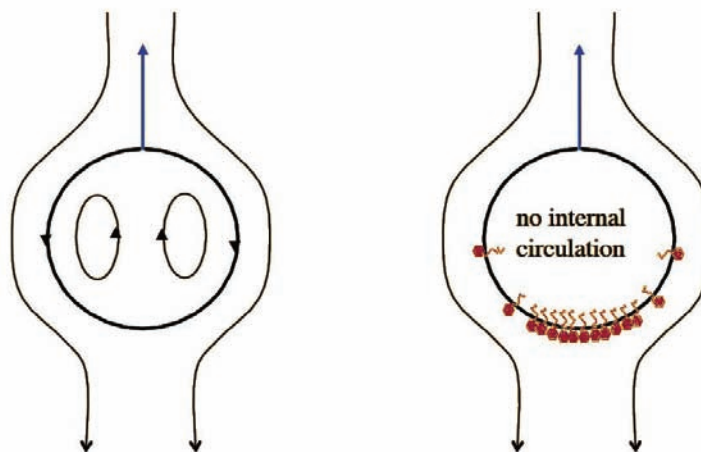


Figure 10.7: A rising drop or bubble (*left*) is marked by internal circulation in a clean system that is absent in a contaminated, surfactant-laden fluid (*right*). Surfactant sticks to the surface, and the induced Marangoni stress rigidifies the drop surface.

11. Fluid Jets

11.1 The shape of a falling fluid jet

Consider a circular orifice of a radius a ejecting a flux Q of fluid density ρ and kinematic viscosity ν (see Fig. 11.1). The resulting jet accelerates under the influence of gravity $-g\hat{z}$. We assume that the jet Reynolds number $\mathcal{R}e = Q/(a\nu)$ is sufficiently high that the influence of viscosity is negligible; furthermore, we assume that the jet speed is independent of radius, and so adequately described by $U(z)$. We proceed by deducing the shape $r(z)$ and speed $U(z)$ of the evolving jet.

Applying Bernoulli's Theorem at points A and B:

$$\frac{1}{2}\rho U_0^2 + \rho g z + P_A = \frac{1}{2}\rho U^2(z) + P_B \quad (11.1)$$

The local curvature of slender threads may be expressed in terms of the two principal radii of curvature, R_1 and R_2 :

$$\nabla \cdot \mathbf{n} = \frac{1}{R_1} + \frac{1}{R_2} \approx \frac{1}{r} \quad (11.2)$$

Thus, the fluid pressures within the jet at points A and B may be simply related to that of the ambient, P_0 :

$$P_A \approx P_0 + \frac{\sigma}{a}, \quad P_B \approx P_0 + \frac{\sigma}{r} \quad (11.3)$$

Substituting into (11.1) thus yields

$$\frac{1}{2}\rho U_0^2 + \rho g z + P_0 + \frac{\sigma}{a} = \frac{1}{2}\rho U^2(z) + P_0 + \frac{\sigma}{r} \quad (11.4)$$

from which one finds

$$\frac{U(z)}{U_0} = \left[1 + \underbrace{\frac{2}{\mathcal{F}r} \frac{z}{a}}_{\text{acc. due to } g} + \underbrace{\frac{2}{\mathcal{W}e} \left(1 - \frac{a}{r}\right)}_{\text{dec. due to } \sigma} \right]^{1/2} \quad (11.5)$$

where we define the dimensionless groups

$$\mathcal{F}r = \frac{U_0^2}{ga} = \frac{INERTIA}{GRAVITY} = \text{Froude Number} \quad (11.6)$$

$$\mathcal{W}e = \frac{\rho U_0^2 a}{\sigma} = \frac{INERTIA}{CURVATURE} = \text{Weber Number} \quad (11.7)$$

Now flux conservation requires that

$$Q = 2\pi \int_0^r U(z)r(z)dr = \pi a^2 U_0 = \pi r^2 U(z) \quad (11.8)$$

from which one obtains

$$\frac{r(z)}{a} = \left(\frac{U_0}{U(z)} \right)^{1/2} = \left[1 + \frac{2}{\mathcal{F}r} \frac{z}{a} + \frac{2}{\mathcal{W}e} \left(1 - \frac{a}{r}\right) \right]^{-1/4} \quad (11.9)$$

This may be solved algebraically to yield the thread shape $r(z)/a$, then this result substituted into (11.5) to deduce the velocity profile $U(z)$. In the limit of $\mathcal{W}e \rightarrow \infty$, one obtains

$$\frac{r}{a} = \left(1 + \frac{2gz}{U_0^2} \right)^{-1/4}, \quad \frac{U(z)}{U_0} = \left(1 + \frac{2gz}{U_0^2} \right)^{1/2} \quad (11.10)$$

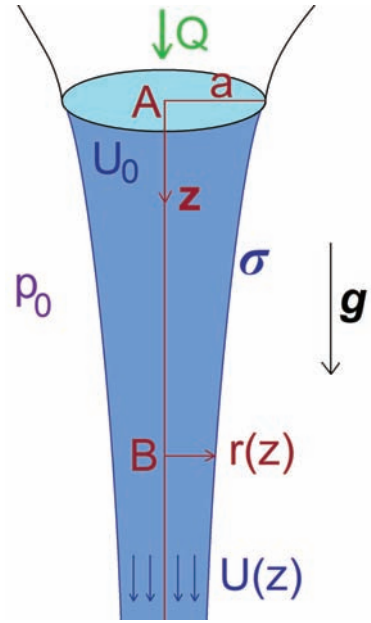


Figure 11.1: A fluid jet extruded from an orifice of radius a accelerates under the influence of gravity. Its shape is influenced both by the gravitational acceleration \mathbf{g} and the surface tension σ . Note that σ gives rise to a gradient in curvature pressure within the jet, $\sigma/r(z)$, that opposes the acceleration due to \mathbf{g} .

11.2 The Plateau-Rayleigh Instability

We here summarize the work of Plateau and Rayleigh on the instability of cylindrical fluid jets bound by surface tension. It is precisely this Rayleigh-Plateau instability that is responsible for the pinch-off of thin water jets emerging from kitchen taps (see Fig. 11.2).

The equilibrium base state consists of an infinitely long quiescent cylindrical inviscid fluid column of radius R_0 , density ρ and surface tension σ (see Fig. 11.3). The influence of gravity is neglected. The pressure p_0 is constant inside the column and may be calculated by balancing the normal stresses with surface tension at the boundary. Assuming zero external pressure yields

$$p_0 = \sigma \nabla \cdot \mathbf{n} \Rightarrow p_0 = \frac{\sigma}{R_0} . \quad (11.11)$$

We consider the evolution of infinitesimal varicose perturbations on the interface, which enables us to linearize the governing equations. The perturbed columnar surface takes the form:

$$\tilde{R} = R_0 + \epsilon e^{\omega t + ikz} , \quad (11.12)$$

where the perturbation amplitude $\epsilon \ll R_0$, ω is the growth rate of the instability and k is the wave number of the disturbance in the z -direction. The corresponding wavelength of the varicose perturbations is necessarily $2\pi/k$. We denote by \tilde{u}_r the radial component of the perturbation velocity, \tilde{u}_z the axial component, and \tilde{p} the perturbation pressure. Substituting these perturbation fields into the N-S equations and retaining terms only to order ϵ yields:

$$\frac{\partial \tilde{u}_r}{\partial t} = -\frac{1}{\rho} \frac{\partial \tilde{p}}{\partial r} \quad (11.13)$$

$$\frac{\partial \tilde{u}_z}{\partial t} = -\frac{1}{\rho} \frac{\partial \tilde{p}}{\partial z} \quad (11.14)$$

The linearized continuity equation becomes:

$$\frac{\partial \tilde{u}_r}{\partial r} + \frac{\tilde{u}_r}{r} + \frac{\partial \tilde{u}_z}{\partial z} = 0 . \quad (11.15)$$

We anticipate that the disturbances in velocity and pressure will have the same form as the surface disturbance (11.12), and so write the perturbation velocities and pressure as:

$$(\tilde{u}_r, \tilde{u}_z, \tilde{p}) = (R(r), Z(r), P(r)) e^{\omega t + ikz} . \quad (11.16)$$

Substituting (11.16) into equations (11.13-11.15) yields the linearized equations governing the perturbation fields:

Momentum equations : $\omega R = -\frac{1}{\rho} \frac{dP}{dr}$ (11.17)

$$\omega Z = -\frac{ik}{\rho} P \quad (11.18)$$

Continuity: $\frac{dR}{dr} + \frac{R}{r} + ikZ = 0 .$ (11.19)

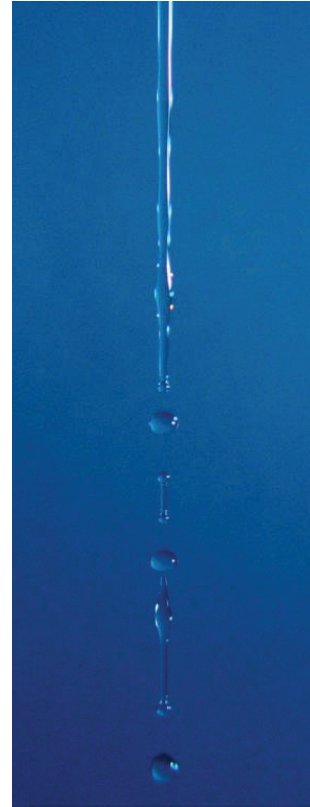
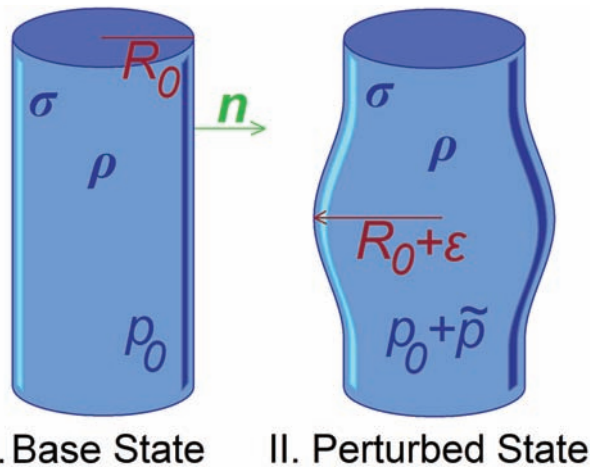


Figure 11.2: The capillary-driven instability of a water thread falling under the influence of gravity. The initial jet diameter is approximately 3 mm.



I. Base State II. Perturbed State

Figure 11.3: A cylindrical column of initial radius R_0 comprised of an inviscid fluid of density ρ , bound by surface tension σ .

Eliminating $Z(r)$ and $P(r)$ yields a differential equation for $R(r)$:

$$r^2 \frac{d^2 R}{dr^2} + r \frac{dR}{dr} - (1 + (kr)^2) R = 0 \quad . \quad (11.20)$$

This corresponds to the modified Bessel Equation of order 1, whose solutions may be written in terms of the modified Bessel functions of the first and second kind, respectively, $I_1(kr)$ and $K_1(kr)$. We note that $K_1(kr) \rightarrow \infty$ as $r \rightarrow 0$; therefore, the well-behavedness of our solution requires that $R(r)$ take the form

$$R(r) = CI_1(kr) \quad , \quad (11.21)$$

where C is an as yet unspecified constant to be determined later by application of appropriate boundary conditions. The pressure may be obtained from (11.21) and (11.17), and by using the Bessel function identity $I'_0(\xi) = I_1(\xi)$:

$$P(r) = -\frac{\omega\rho C}{k} I_0(kr) \quad \text{and} \quad Z(r) = -\frac{ik}{\omega\rho} P(r). \quad (11.22)$$

We proceed by applying appropriate boundary conditions. The first is the kinematic condition on the free surface:

$$\frac{\partial \tilde{R}}{\partial t} = \tilde{\mathbf{u}} \cdot \mathbf{n} \approx \tilde{u}_r \quad . \quad (11.23)$$

Substitution of (11.21) into this condition yields

$$C = \frac{\epsilon\omega}{I_1(kR_0)} \quad . \quad (11.24)$$

Second, we require a normal stress balance on the free surface:

$$p_0 + \tilde{p} = \sigma \nabla \cdot \mathbf{n} \quad (11.25)$$

We write the curvature as $\sigma \nabla \cdot \mathbf{n} = \left(\frac{1}{R_1} + \frac{1}{R_2} \right)$, where R_1 and R_2 are the principal radii of curvature of the jet surface:

$$\frac{1}{R_1} = \frac{1}{R_0 + \epsilon e^{\omega t + ikz}} \approx \frac{1}{R_0} - \frac{\epsilon}{R_0^2} e^{\omega t + ikz} \quad (11.26)$$

$$\frac{1}{R_2} = \epsilon k^2 e^{\omega t + ikz} \quad . \quad (11.27)$$

Substitution of (11.26) and (11.27) into equation (11.25) yields:

$$p_0 + \tilde{p} = \frac{\sigma}{R_0} - \frac{\epsilon\sigma}{R_0^2} (1 - k^2 R_0^2) e^{\omega t + ikz} \quad (11.28)$$

Cancellation via (11.11) yields the equation for \tilde{p} accurate to order ϵ :

$$\tilde{p} = -\frac{\epsilon\sigma}{R_0^2} (1 - k^2 R_0^2) e^{\omega t + ikz} \quad . \quad (11.29)$$

Combining (11.22), (11.24) and (11.29) yields the dispersion relation, that indicates the dependence of the growth rate ω on the wavenumber k :

$$\omega^2 = \frac{\sigma}{\rho R_0^3} k R_0 \frac{I_1(kR_0)}{I_0(kR_0)} (1 - k^2 R_0^2) \quad (11.30)$$

We first note that unstable modes are only possible when

$$kR_0 < 1 \quad (11.31)$$

The column is thus unstable to disturbances whose wavelengths exceed the circumference of the cylinder. A plot of the dependence of the growth rate ω on the wavenumber k for the Rayleigh-Plateau instability is shown in Fig. 11.4.

The fastest growing mode occurs for $kR_0 = 0.697$, i.e. when the wavelength of the disturbance is

$$\lambda_{max} \approx 9.02R_0 \quad (11.32)$$

By inverting the maximum growth rate ω_{max} one may estimate the characteristic break-up time:

$$t_{breakup} \approx 2.91 \sqrt{\frac{\rho R_0^3}{\sigma}} \quad (11.33)$$

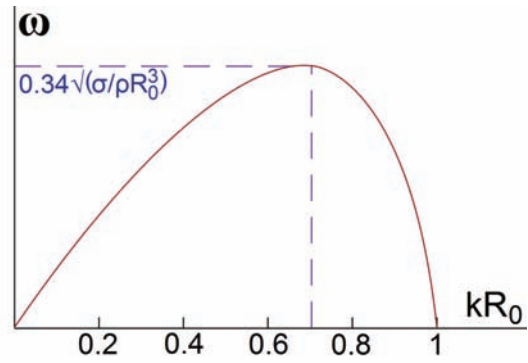


Figure 11.4: The dependence of the growth rate ω on the wavenumber k for the Rayleigh-Plateau instability.

Note: In general, pinch-off depends on $\mathcal{O}h = \frac{\mu\nu}{\sigma R}$.

At low $\mathcal{O}h$, we have seen that $\tau_{pinch} \sim \left(\frac{\rho R^2}{\sigma}\right)^{1/2}$, $\lambda = 9.02R$.

At high $\mathcal{O}h$, when viscosity is important, $\tau_{pinch} \sim \frac{\mu R}{\sigma}$, λ increases with μ .

A water jet of diameter 1cm has a characteristic break-up time of about 1/8s, which is consistent with casual observation of jet break-up in a kitchen sink.

Related Phenomena: Waves on jets

When a vertical water jet impinges on a horizontal reservoir of water, a field of standing waves may be excited on the base of the jet (see Fig. 11.5). The wavelength is determined by the requirement that the wave speed correspond to the local jet speed: $U = -\omega/k$. Using our dispersion relation (11.30) thus yields

$$U^2 = \frac{\omega^2}{k^2} = \frac{\sigma}{\rho k R_0^2} \frac{I_1(kR_0)}{I_0(kR_0)} (1 - k^2 R_0^2) \quad (11.34)$$

Provided the jet speed U is known, this equation may be solved in order to deduce the wavelength of the waves that will travel at U and so appear to be stationary in the lab frame. For jets falling from a nozzle, the result (11.5) may be used to deduce the local jet speed.

11.3 Fluid Pipes

The following system may be readily observed in a kitchen sink. When the volume flux exiting the tap is such that the falling stream has a diameter of 2 – 3mm, obstructing the stream with a finger at a distance of several centimeters from the tap gives rise to a stationary field of varicose capillary waves upstream of the finger. If the finger is dipped in liquid detergent (soap) before insertion into the stream, the capillary waves begin at some critical distance above the finger, below which the stream is cylindrical. Closer inspection reveal that the surface of the jet's cylindrical base is quiescent.

An analogous phenomenon arises when a vertical fluid jet impinges on a deep water reservoir (see Fig. 11.5). When the reservoir is contaminated by surfactant, the surface tension of the reservoir is diminished relative to that of the jet. The associated surface tension gradient draws surfactant a finite distance up the jet, prompting two salient alterations in the jet surface. First, the surfactant suppresses surface waves, so that the base of the jet surface assumes a cylindrical form (Fig. 11.5b). Second, the jet surface at its base becomes stagnant: the Marangoni stresses associated with the surfactant gradient are balanced by the viscous stresses generated within the jet. The quiescence of the jet surface may be simply demonstrated by sprinkling a small amount of talc or lycopodium powder onto the jet. The fluid jet thus enters a contaminated reservoir as if through a rigid pipe.

A detailed theoretical description of the fluid pipe is given in *Hancock & Bush (JFM, 466, 285-304)*. We here present a simple scaling that yields the dependence of the vertical extent H of the fluid pipe on

Note: Surface area of rim/ length: $p = 2\pi R$ where $m = \rho hx = \pi\rho R^2 \Rightarrow R = \sqrt{\frac{hx}{\pi}}$ where R is the rim radius. Therefore the rim surface energy is $\sigma P = \sigma 2\pi\sqrt{\frac{hx}{\pi}} = 2\sigma\sqrt{hx\pi}$. Total surface energy of the system is $\sigma [2x + 2(\pi hx)^{1/2}]$.

Scale: $\frac{SA_{rim}}{SA_{sheet}} \sim \frac{2\sqrt{hx\pi}}{2x} \sim \left(\frac{hx}{x}\right)^{1/2} \ll 1$ for $x \gg h$.

The rim surface area is thus safely neglected once the sheet has retracted a distance comparable to its thickness.

Some final comments on soap film rupture.

1. for dependence on geometry and influence of μ , see *Savva & Bush (JFM 2009)*.
2. form of sheet depends on $\sqrt{\mathcal{O}h} = \frac{\mu}{\sqrt{2h\rho\sigma}}$.
3. The growing rim at low $\mathcal{O}h$ is subject to Ra-Plateau \Rightarrow scalloping of the retracting rim \Rightarrow rim pinches off into drops
4. At very high speed, air-induced shear stress leads to flapping. The sheet thus behaves like a flapping flag, but with Marangoni elasticity.

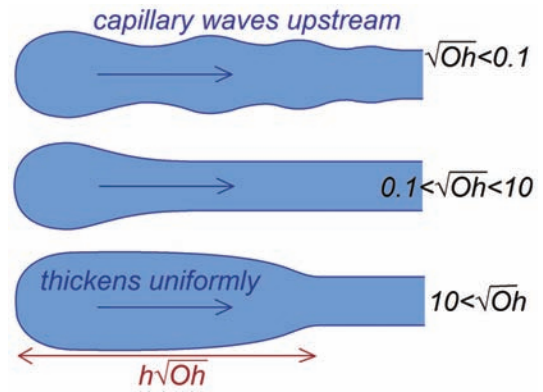


Figure 12.5: The different shapes of a retracting sheet and rim depend on the value of $\mathcal{O}h$.

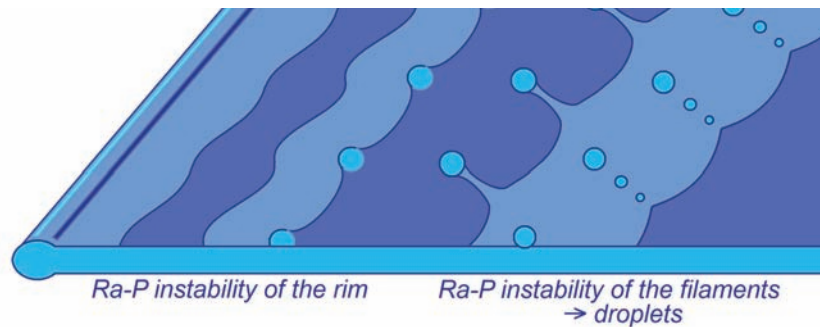


Figure 12.6: The typical evolution of a retracting sheet. As the rim retracts and engulfs fluid, it eventually becomes Rayleigh-Plateau unstable. Thus, it develops variations in radius along its length, and the retreating rim becomes scalloped. Filaments are eventually left by the retracting rim, and pinch off through a Rayleigh-Plateau instability, the result being droplets.

12. Instability Dynamics

12.1 Capillary Instability of a Fluid Coating on a Fiber

We proceed by considering the surface tension-induced instability of a fluid coating on a cylindrical fiber. Define mean thickness

$$h^* = \frac{1}{\lambda} \int_0^\lambda h(x) dx \quad (12.1)$$

Local interfacial thickness

$$h(x) = h^* + \epsilon \cos kx \quad (12.2)$$

Volume conservation requires:

$$\begin{aligned} \int_0^\lambda \pi(r+h)^2 dx &= \int_0^\lambda \pi(r+h_0)^2 dx \Rightarrow \int_0^\lambda (r+h^* + \epsilon \cos kx)^2 dx = (r+h_0)^2 \lambda \Rightarrow \\ (r+h^*)^2 \lambda + \epsilon^2 \frac{\lambda}{2} &= (r+h_0)^2 \lambda \Rightarrow (r+h^*)^2 = (r+h_0)^2 - \frac{\epsilon^2}{2} = (r+h_0)^2 \left[1 - \frac{1}{2} \frac{\epsilon^2}{(r+h_0)^2} \right] \end{aligned}$$

which implies

$$h^* = h_0 - \frac{1}{4} \frac{\epsilon^2}{r+h_0} \quad (12.3)$$

Note:

$h^* < h_0$ which suggests instability.

So, when does perturbation reduce surface energy? i.e. when is $\int_0^\lambda 2\pi(r+h) ds < 2\pi(r+h_0)\lambda$?

Note: $ds^2 = dh^2 + dx^2 \Rightarrow ds = dx \sqrt{1 + \left(\frac{dh}{dx}\right)^2} \approx dx \left[1 + \frac{1}{2} \epsilon^2 k^2 \sin^2 kx \right]^{1/2}$

$$\int_0^\lambda (r+h) ds = \int_0^\lambda (r+h^* + \epsilon \cos kx) \left(1 + \frac{1}{2} \epsilon^2 k^2 \sin^2 kx \right)^{1/2} dx = (r+h^*)\lambda + \frac{1}{4} (r+h^*) \epsilon^2 k^2 \lambda.$$

So the inequality holds provided $(r+h^*)\lambda + \frac{1}{4} (r+h^*) \epsilon^2 k^2 \lambda < (r+h_0)\lambda$.

Substitute for h^* from (12.3):

$$-\frac{1}{4} \frac{\epsilon^2}{r+h_0} + \frac{1}{4} (r+h^*) \epsilon^2 k^2 < 0 \quad (12.4)$$

We note that the result is independent of ϵ :

$$k^2 < (r+h_0)^{-1} (r+h^*)^{-1} \approx \frac{1}{(r+h_0)^2} \quad (12.5)$$

i.e. unstable wavelengths are prescribed by

$$\lambda = \frac{2\pi}{k} > 2\pi(r+h_0) \quad (12.6)$$

as in standard inviscid Ra-P. All long wavelength disturbances will grow. Which grows the fastest? That is determined by the *dynamics* (not just geometry). We proceed by considering the dynamics in the thin film limit, $h_0 \ll r$, for which we obtain the lubrication limit.

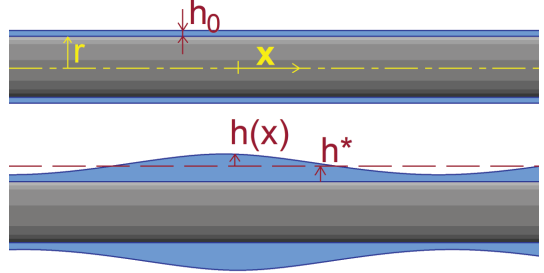


Figure 12.1: Instability of a fluid coating on a cylindrical fiber.

12.2 Dynamics of Instability (Rayleigh 1879)

Physical picture: Curvature pressure induced by perturbation drives Couette flow that is resisted by viscosity

$$\eta \frac{d^2 v}{dy^2} - \frac{dp}{dx} = 0 \tag{12.7}$$

where $\frac{dp}{dx}$ is the gradient in curvature pressure, which is independent of y (a generic feature of lubrication problems), so we can integrate the above equation to obtain

$$v(y) = \frac{1}{\mu} \frac{dp}{dx} \left(\frac{y^2}{2} - hy \right) \tag{12.8}$$

Flux per unit length:

$$Q = \int_0^h v(y) dy = -\frac{1}{3\mu} \frac{dp}{dx} h^3 \tag{12.9}$$

Conservation of volume in lubrication problems requires that $Q(x + dx) - Q(x) = -\frac{\partial h}{\partial t} dx \Rightarrow$

$$\frac{dQ}{dx} = -\frac{h_0^3}{3\mu} \frac{d^2 p}{dx^2} = -\frac{\partial h}{\partial t} \tag{12.10}$$

Curvature pressure

$$p(x) = \sigma \left(\frac{1}{R_1} + \frac{1}{R_2} \right) = \sigma \left(\frac{1}{r+h} - h_{xx} \right) \tag{12.11}$$

Substitute (12.11) into (12.10):

$$\frac{\partial h}{\partial t} = \frac{\sigma h_0^3}{3\mu} \frac{\partial^2}{\partial x^2} \left[\frac{1}{r+h(x)} - \sigma h_{xx} \right] \tag{12.12}$$

Now $h(x, t) = h^* + \epsilon(t) \cos kx \Rightarrow h_x = -\epsilon k \sin kx, h_{xx} = -\epsilon^2 k \cos kx, h_t = \frac{d\epsilon}{dt} \cos kx$

So $\cos kx \frac{d\epsilon}{dt} = \frac{\sigma h_0^3}{3\mu} \epsilon \cos kx \left[\frac{k^2}{(r+h)^2} - k^4 \right] \Rightarrow \frac{d\epsilon}{dt} = \beta \epsilon$ where $\beta = \frac{\sigma h_0^3}{3\mu} \left[\frac{k^2}{(r+h_0)^2} - k^4 \right]$

Fastest growing mode when $\frac{d\beta}{dk} = 0 = \frac{2k^5}{(r+h_0)^2} - 4k^*3$ so

$$\lambda^* = 2\sqrt{2}\pi (r + h_0) \tag{12.13}$$

is the most unstable wavelength for the viscous mode.

Note:

- Recall that for classic Ra-P on a cylindrical fluid thread $\lambda^* \sim 9R$.
- We see here the timescale of instability: $\tau^* = \frac{12\mu(r+h_0)^4}{\sigma h_0^3}$.
- Scaling Argument for Pinch-off time.

When $h \ll r, \nabla p \sim \frac{\sigma h_0}{r^2} \frac{1}{r} \sim \mu \frac{v}{h_0^2} \Rightarrow v \sim \frac{r}{\tau} \sim \frac{h_0^3}{\mu} \frac{\sigma h_0}{r^3} \Rightarrow$

$$\tau_{pinch} \sim \frac{\mu r^4}{\sigma h_0^3} \tag{12.14}$$

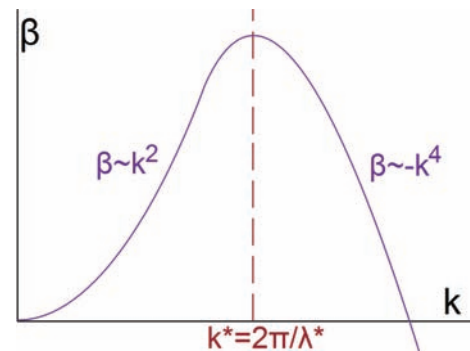


Figure 12.2: Growth rate β as a function of wavenumber k for the system depicted in Fig. 12.1.

12.3 Rupture of a Soap Film (Culick 1960, Taylor 1960)

We assume $\mathcal{O}h = \frac{\mu\nu}{\sigma R} \ll 1$, so that viscous effects are negligible. The driving curvature force is thus resisted principally by fluid inertia. Assume dynamics is largely 2D (true for a planar film, or for bubble burst for $r(t) \gg h$).

Retraction of a Planar Sheet

Note: Force/ length acting on the rim may be calculated exactly via Frenet-Serret

$$\mathbf{F}_C = \int_C \sigma (\nabla \cdot \mathbf{n}) \mathbf{n} dl \tag{12.15}$$

where $(\nabla \cdot \mathbf{n}) \mathbf{n} = \frac{dt}{dl}$

$$\Rightarrow \mathbf{F}_C = \int_C \sigma \frac{dt}{dl} dl = \sigma (t_1 - t_2) = 2\sigma \hat{x} \tag{12.16}$$

At time $t = 0$, planar sheet of thickness h punctured at $x = 0$, and retracts in \hat{x} direction owing to \mathbf{F}_C .

Observation: The rim engulfs the film, and there is no upstream disturbance.

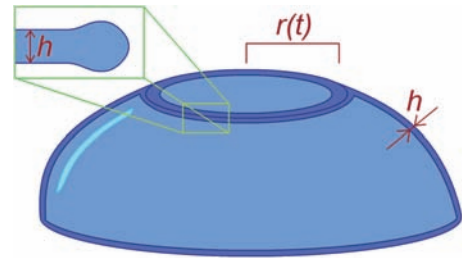


Figure 12.3: Rupture of a soap film of thickness h .

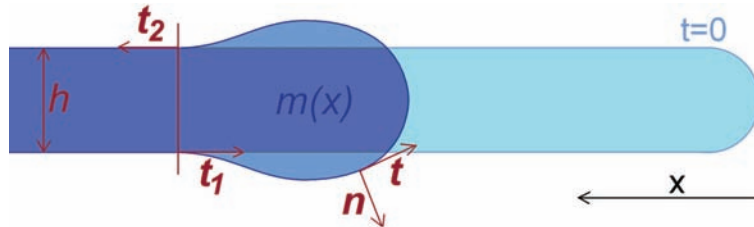


Figure 12.4: Surface-tension-induced retraction of a planar sheet of uniform thickness h released at time $t = 0$.

Rim mass: $m(x) = \rho hx$ and speed $v = \frac{dx}{dt}$.

Since the inertial force on the rim is equal to the rate of change of rim momentum

$$F_I = \frac{d}{dt}(mv) = v \frac{d}{dx}mv = v^2 \frac{dm}{dx} + mv \frac{dv}{dx} = \frac{1}{2}v^2 \frac{dm}{dx} + \frac{1}{2} \frac{d}{dx}(mv^2) . \tag{12.17}$$

The force balance us between the curvature force and the inertial force

$$2\sigma = \frac{d}{dx} \left(\frac{1}{2}mv^2 \right) + \frac{1}{2}\rho hv^2 \tag{12.18}$$

Integrate from 0 to x :

$$2\sigma x = \frac{1}{2}\rho hxv^2 + \frac{1}{2}\rho h \int_0^x v^2 dx \tag{12.19}$$

The first term is the surface energy released per unit length, the 2nd term the K.E. of the rim, and the 3rd term the energy required to accelerate the rim. Now we assume v is independent of x (as observed in experiments), thus $\int_0^x v^2 dx = xv^2$ and the force balance becomes $2\sigma x = \rho hxv^2 \Rightarrow$

$$v = \left(\frac{2\sigma}{\rho h} \right)^{1/2} \text{ is the retraction speed (Taylor-Culick speed)} \tag{12.20}$$

E.g. for water-soap film, $h \sim 150\mu m \Rightarrow v \sim 10^2 \text{ cm/s}$.

Note: Surface area of rim/ length: $p = 2\pi R$ where $m = \rho hx = \pi\rho R^2 \Rightarrow R = \sqrt{\frac{hx}{\pi}}$ where R is the rim radius. Therefore the rim surface energy is $\sigma P = \sigma 2\pi\sqrt{\frac{hx}{\pi}} = 2\sigma\sqrt{hx\pi}$. Total surface energy of the system is $\sigma [2x + 2(\pi hx)^{1/2}]$.

Scale: $\frac{SA_{rim}}{SA_{sheet}} \sim \frac{2\sqrt{hx\pi}}{2x} \sim \left(\frac{hx}{x}\right)^{1/2} \ll 1$ for $x \gg h$.

The rim surface area is thus safely neglected once the sheet has retracted a distance comparable to its thickness.

Some final comments on soap film rupture.

1. for dependence on geometry and influence of μ , see *Savva & Bush (JFM 2009)*.
2. form of sheet depends on $\sqrt{\mathcal{O}h} = \frac{\mu}{\sqrt{2h\rho\sigma}}$.
3. The growing rim at low $\mathcal{O}h$ is subject to Ra-Plateau \Rightarrow scalloping of the retracting rim \Rightarrow rim pinches off into drops
4. At very high speed, air-induced shear stress leads to flapping. The sheet thus behaves like a flapping flag, but with Marangoni elasticity.

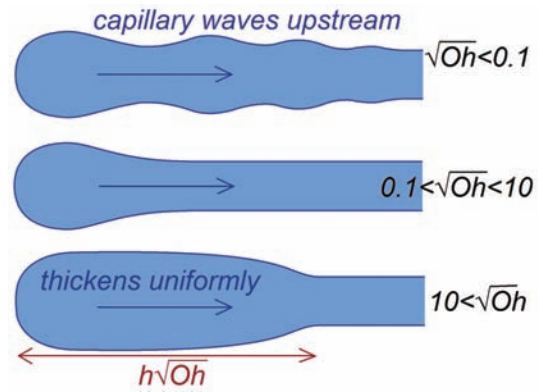


Figure 12.5: The different shapes of a retracting sheet and rim depend on the value of $\mathcal{O}h$.

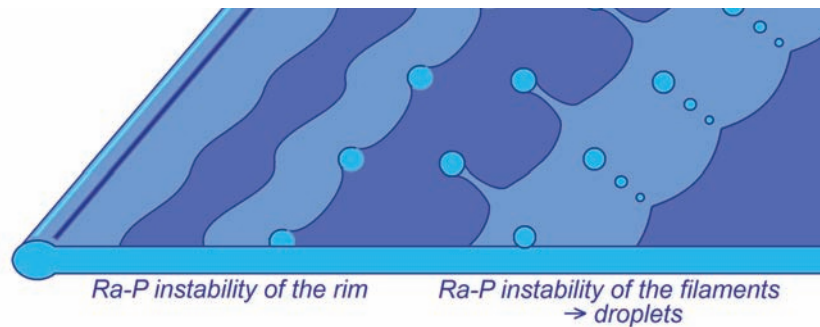


Figure 12.6: The typical evolution of a retracting sheet. As the rim retracts and engulfs fluid, it eventually becomes Rayleigh-Plateau unstable. Thus, it develops variations in radius along its length, and the retreating rim becomes scalloped. Filaments are eventually left by the retracting rim, and pinch off through a Rayleigh-Plateau instability, the result being droplets.

13. Fluid Sheets

13.1 Fluid Sheets: shape and stability

The dynamics of high-speed fluid sheets was first considered by *Savart (1833)* after his early work on electromagnetism with Biot, and was subsequently examined by *Rayleigh (1879)*, then in a series of papers by Taylor (*Proc. Roy. Soc., 1959*). They have recently received a great deal of attention owing to their relevance in a number of spray atomization processes. Such sheets may be generated from a variety of source conditions, for example, the collision of jets on rigid impactors, and jet-jet collisions. There is generally a curvature force acting on the sheet edge which acts to contain the fluid sheet. For a 2D (planar) sheet, the magnitude of this curvature force is given by

$$\mathbf{F}_c = \int_C \sigma (\nabla \cdot \mathbf{n}) \mathbf{n} dl \quad (13.1)$$

Using the first Frenet-Serret equation (Lecture 2, Appendix B),

$$(\nabla \cdot \mathbf{n}) \mathbf{n} = \frac{dt}{dl} \quad (13.2)$$

thus yields

$$\mathbf{F}_c = \int_C \sigma \frac{dt}{dl} dl = \sigma (\mathbf{t}_1 - \mathbf{t}_2) = 2\sigma \mathbf{x} \quad (13.3)$$

There is thus an effective force per unit length 2σ along the length of the sheet rim acting to contain the rim. We now consider how this result may be applied to compute sheet shapes for three distinct cases: i) a circular sheet, ii) a lenticular sheet with unstable rims, and iii) a lenticular sheet with stable rims.

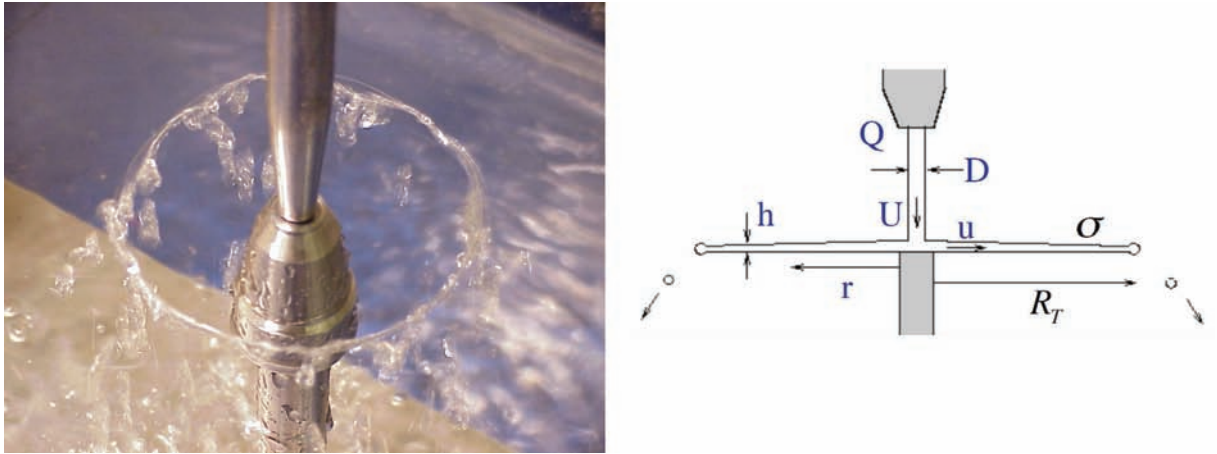


Figure 13.1: A circular fluid sheet generated by the impact of a water jet on a circular impactor. The impacting circle has a diameter of 1 cm.

13.2 Circular Sheet

We consider the geometry considered in Savart's original experiment. A vertical fluid jet strikes a small horizontal circular impactor. If the flow rate is sufficiently high that gravity does not influence the sheet shape, the fluid is ejected radially, giving rise to a circular free fluid sheet (Fig. 13.1).

For $We = \frac{\rho U^2 D}{\sigma} > 1000$, the circular sheet is subject to the flapping instability. We thus consider $We < 1000$, for which the sheet is stable. Scaling: $Re = \frac{UR}{\nu} \sim \frac{30 \cdot 10}{0.01} \sim 3 \cdot 10^4 \gg 1$. $Fr = \frac{U^2}{gR} \sim \frac{30^2}{10^3 \cdot 10} \sim 0.1$ so inertia dominates gravity.

The sheet radius is prescribed by a balance of radial forces; specifically, the inertial force must balance the curvature force:

$$\rho u^2 h = 2\sigma \quad (13.4)$$

Continuity requires that the sheet thickness h depend on the speed u , jet flux Q and radius r as

$$h(r) = \frac{Q}{2\pi r u} \sim \frac{1}{r} \quad (13.5)$$

Experiments (specifically, tracking of particles suspended within the sheet) indicate that the sheet speed u is independent of radius; consequently, the sheet thickness decreases as $1/r$. Substituting the form (13.5) for h into the force balance (13.4) yields the sheet radius, or so-called Taylor radius:

$$R_T = \frac{\rho Q u}{4\pi\sigma} \quad (13.6)$$

The sheet radius increases with source flux and sheet speed, but decreases with surface tension. We note that the fluid proceeds radially to the sheet edge, where it accumulates until going unstable via a modified Rayleigh-Plateau instability, often referred to as the Rayleigh-Plateau-Savart instability, as it was first observed on a sheet edge by Savart.

13.3 Lenticular sheets with unstable rims (Taylor 1960)

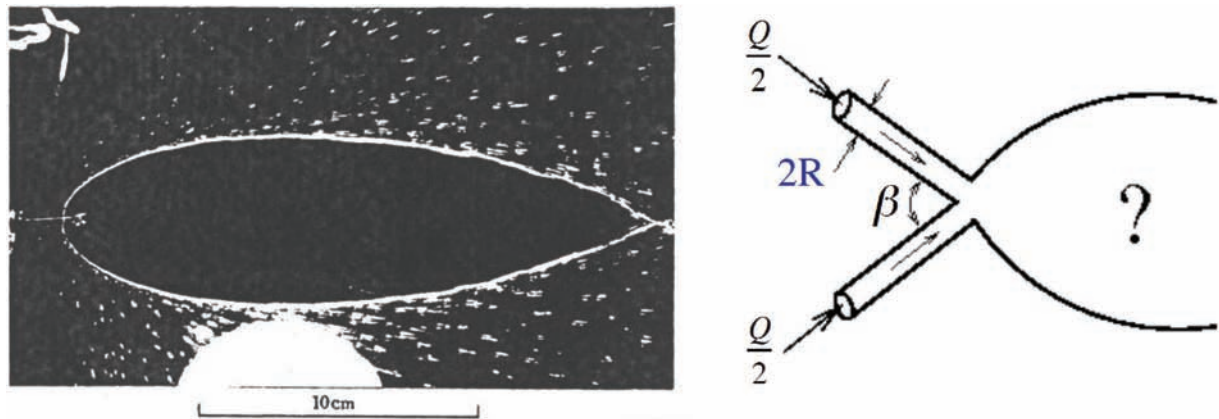


Figure 13.2: A sheet generated by the collision of water jets at left. The fluid streams radially outward in a thinning sheet; once the fluid reaches the sheet rim, it is ejected radially in the form of droplets. From *G.I. Taylor (1960)*.

We now consider the non-axisymmetric fluid , such as may be formed by the oblique collision of water jets (see Fig. 13.2), a geometry originally considered by *Taylor (1960)*. Fluid is ejected radially from the origin into a sheet with flux distribution given by $Q(\theta)$, so that the volume flux flowing into the sector between θ and $\theta + d\theta$ is $Q(\theta)d\theta$. As in the previous case of the circular sheet, the sheet rims are unstable, and fluid drops are continuously ejected therefrom. The sheet shape is computed in a similar manner, but now depends explicitly on the flux distribution within the sheet, $Q(\theta)$. The normal force balance on the sheet edge now depends on the normal component of the sheet speed, u_n :

$$\rho u_n^2(\theta)h(\theta) = 2\sigma \quad (13.7)$$

The sheet thickness is again prescribed by (13.5), but now $Q = Q(\theta)$, so the sheet radius $R(\theta)$ is given by the Taylor radius

$$R(\theta) = \frac{\rho u_n^2 Q(\theta)}{4\pi\sigma u} \quad (13.8)$$

Computing sheet shapes thus relies on either experimental measurement or theoretical prediction of the flux distribution $Q(\theta)$ within the sheet.

13.4 Lenticular sheets with stable rims

In a certain region of parameter space, specifically, with fluids more viscous than water, one may encounter fluid sheets with stable rims (see www-math.mit.edu/~bush/bones.html). The force balance describing the sheet shape must change accordingly. When rims are stable, fluid entering the rim proceeds along the rim. As a result, there is a centripetal force normal to the fluid rim associated with flow along the curved rim that must be considered in order to correctly predict the sheet shapes.

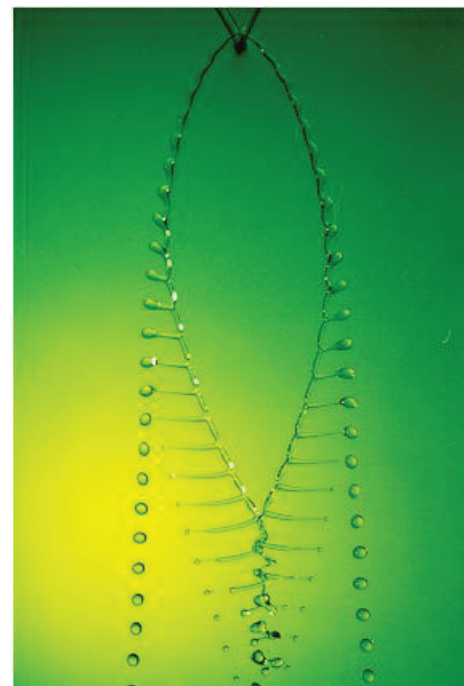


Figure 13.3: The “Fluid fishbone” formed by the collision of two jets of a glycerine-water solution. *Bush & Hasha (2004)*.

The relevant geometry is presented in Fig. 13.4. $r(\theta)$ is defined to be the distance from the origin to the rim centreline, and $u_n(\theta)$ and $u_t(\theta)$ the normal and tangential components of the fluid velocity in the sheet where it contacts the rim. $v(\theta)$ is defined to be the velocity of flow in the rim, $R(\theta)$ the rim radius, and $\Psi(\theta)$ the angle between the position vector \mathbf{r} and the local tangent to the rim centreline. Finally, $r_c(\theta)$ is defined to be the radius of curvature of the rim centreline, and s the arc length along the rim centreline. The differential equations governing the shape of a stable fluid rim bounding a fluid sheet may be deduced by consideration of conservation of mass in the rim and the local normal and tangential force balances at the rim.

For a steady sheet shape, continuity requires that the volume flux from the sheet balance the tangential gradient in volume flux along the rim:

$$0 = u_n h - \frac{\partial}{\partial s} (v \pi R^2) \quad (13.9)$$

The normal force balance requires that the curvature force associated with the rim's surface tension balance the force resulting from the normal flow into the rim from the fluid sheet and the centripetal force resulting from the flow along the curved rim:

$$\rho u_n^2 h + \frac{\rho \pi R^2 v^2}{r_c} = 2\sigma \quad (13.10)$$

Note that the force balance (13.7) appropriate for sheets with unstable rims is here augmented by the centripetal force. The tangential force balance at the rim requires a balance between tangential gradients in tangential momentum flux, tangential gradients in curvature pressure, viscous resistance to stretching of the rim, and the tangential momentum flux arriving from the sheet. For most applications involving high-speed sheets, the Reynolds number characterizing the rim dynamics is sufficiently large that viscous resistance may be safely neglected. Moreover, the curvature term $\nabla \cdot \hat{\mathbf{n}}$ generally depends on θ ; however, accurate to $O(R/r_c)$, we may use $\nabla \cdot \hat{\mathbf{n}} = 1/R$. One thus obtains:

$$\frac{\partial}{\partial s} (\pi R^2 v^2) = h u_t u_n - \frac{\pi R^2 \sigma}{\rho} \frac{\partial}{\partial s} \left(\frac{1}{R} \right). \quad (13.11)$$

Equations (13.9)-(13.11) must be supplemented by the continuity relation,

$$h(r, \theta) = \frac{Q(\theta)}{u_0 r} \quad (13.12)$$

in addition to a number of relations that follow directly from the system geometry:

$$u_n = u_0 \sin \Psi \quad , \quad u_T = u_0 \cos \Psi \quad , \quad \frac{1}{r_c} = \frac{\sin \Psi}{r} \left(\frac{\partial \Psi}{\partial \theta} + 1 \right) \quad (13.13)$$

The system of equations (13.9-13.13) may be nondimensionalized, and reduce to a set of coupled ordinary equations in the four variables $r(\theta)$, $v(\theta)$, $R(\theta)$ and $\Psi(\theta)$. Given a flux distribution, $Q(\theta)$, the system may be integrated to deduce the sheet shape.

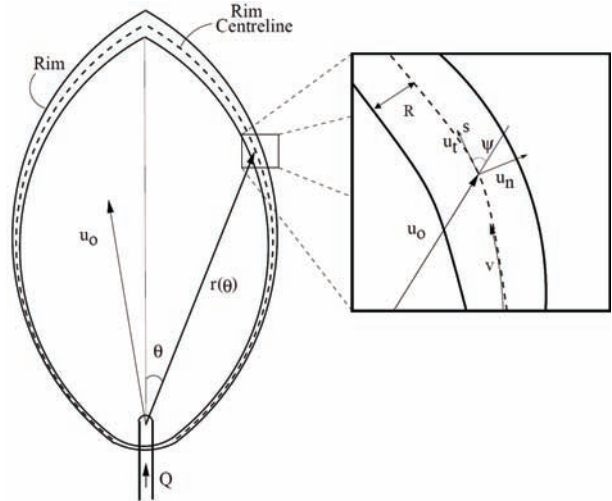


Figure 13.4: A schematic illustration of a fluid sheet bound by stable rims.

13.5 Water Bells

All of the fluid sheets considered thus far have been confined to a plane. In §13.1, we considered circular sheets generated from a vertical jet striking a horizontal impactor. The sheet remains planar only if the flow is sufficiently fast that the fluid reaches its Taylor radius before sagging substantially under the influence of gravity. Decreasing the flow rate will make this sagging more pronounced, and the sheet will no longer be planar. While one might expect the sheet to fall along a parabolic trajectory, the toroidal curvature of the bell induces curvature pressures that act to close the sheet. Consequently, the sheet may close upon itself, giving rise to a water bell, as illustrated in Fig. 13.5. A recent review of the dynamics of water bells has been written by *Clanet (Ann.Rev.)*. We proceed by outlining the theory required to compute the shapes of water bells.

We consider a fluid sheet extruded radially at a speed u_0 and subsequently sagging under the influence of a gravitational field $\mathbf{g} = -g\hat{\mathbf{z}}$. The inner and outer sheet surfaces are characterized by a constant surface tension σ . The sheet has constant density ρ and thickness $t(r, z)$. Q is the total volume flux in the sheet. The characteristic Re is assumed to be sufficiently high so that the influence of viscosity is negligible.

We define the origin to be the center of the impact plate; r and z are, respectively, the radial and vertical distances from the origin. u is the sheet speed, and ϕ the angle made between the sheet and the vertical. r_c is the local radius of curvature of a meridional line, and s the arc length along a meridional line measured from the origin. Finally, ΔP is the pressure difference between the outside and inside of the bell as may be altered experimentally.

Flux conservation requires that

$$Q = 2\pi r t u \quad (13.14)$$

while Bernoulli's Theorem indicates that

$$u^2 = u_0^2 + 2gz \quad (13.15)$$

The total curvature force acting normal to the bell surface is given by

$$2\sigma \nabla \cdot \mathbf{n} = 2\sigma \left(\frac{1}{r_c} + \frac{\cos \phi}{r} \right) \quad (13.16)$$

Note that the factor of two results from there being two free surfaces. The force balance normal to the sheet thus takes the form:

$$\frac{2\sigma}{r_c} + \frac{2\sigma \cos \phi}{r} - \Delta P + \rho g t \sin \phi - \frac{\rho t u^2}{r_c} = 0 \quad (13.17)$$

Equations (13.14), (13.15) and (13.17) may be appropriately nondimensionalized and integrated to determine the shape of the bell.

Note:

- the bell closes due to the out-of-plane curvature
- the influence of g is reflected in top-bottom asymmetry. Note that g is not significant in Fig. 13.5. The relevant control parameter is $\mathcal{F}r = \text{INERTIA}/\text{GRAVITY} = U^2/gL \sim 1$
- if deflected upwards by the impactor, the bell will also close due to σ



Figure 13.5: A water bell produced by the impact of a descending water jet on a solid impactor. The impactor radius is 1 cm. Fluid is splayed radially by the impact, then sags under the influence of gravity. The sheet may close on itself owing to the azimuthal curvature of the bell.

13.6 Swirling Water Bell

Consider the water bell formed with a swirling jet (*Bark et al. 1979*).

Observation: Swirling bells don't close. Why not?

Conservation of angular momentum: as r decreases, v increases as does $F_C \sim v^2/r$.

Sheet velocity:

$$\mathbf{v} = \underbrace{u\hat{e}_s}_{\text{in plane}} + \underbrace{v\hat{e}_\theta}_{\text{swirl}} \quad (13.18)$$

$$\text{Continuity: } Q = 2\pi rhu \quad (13.19)$$

$$\text{Conservation of Angular Momentum: } vr = v_0r_0 \quad (13.20)$$

$$\text{Energy conservation: } u^2 + v^2 = 2gz + u_0^2 + v_0^2 \quad (13.21)$$

$$\text{Normal force balance: } \frac{2\sigma}{R} + \frac{2\sigma \cos \phi}{r} + \rho gh \sin \phi = \Delta P + \frac{\rho hu^2}{R} + \frac{\rho hv^2 \cos \phi}{r} \quad (13.22)$$

Evidently, the bell fails to close owing to the influence of the centripetal forces induced by the swirl.

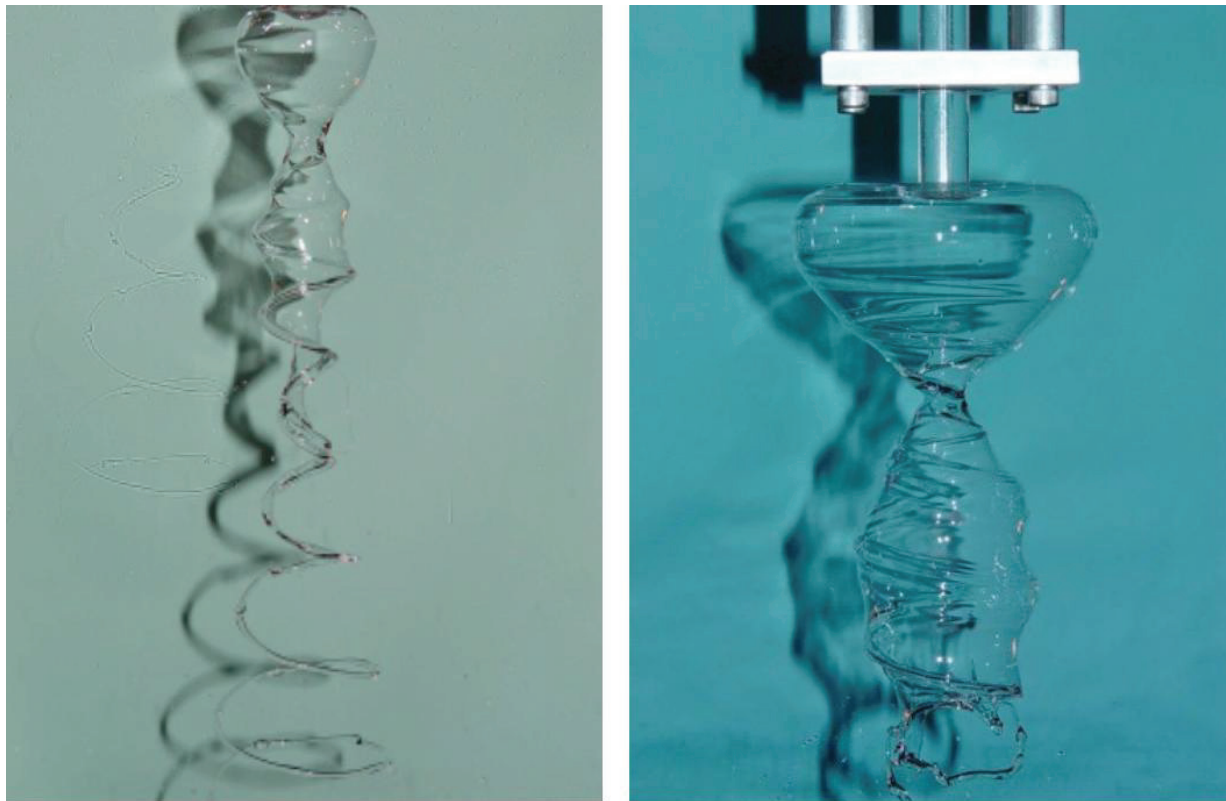


Figure 13.6: Swirling water bells extruded from a rotating nozzle.

14. Instability of Superposed Fluids

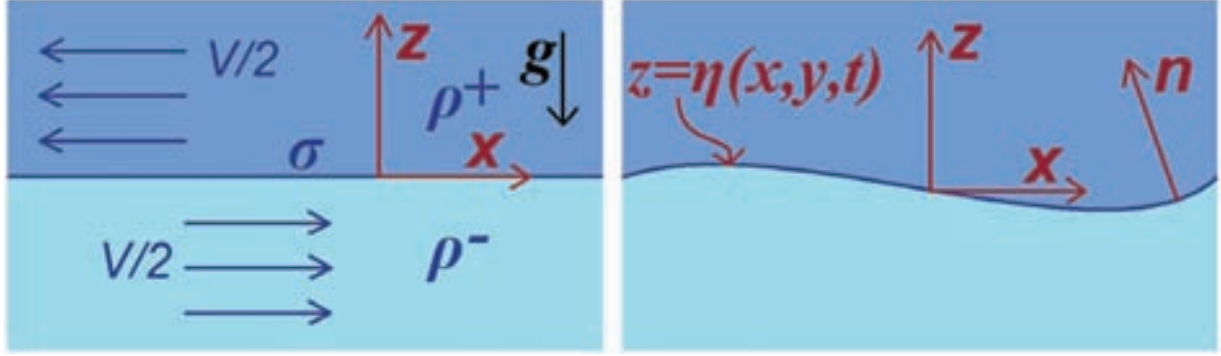


Figure 14.1: Wind over water: A layer of fluid of density ρ^+ moving with relative velocity V over a layer of fluid of density ρ^- .

Define interface: $h(x, y, z) = z - \eta(x, y) = 0$ so that $\nabla h = (-\eta_x, -\eta_y, 1)$.
The unit normal is given by

$$\hat{\mathbf{n}} = \frac{\nabla h}{|\nabla h|} = \frac{(-\eta_x, -\eta_y, 1)}{(\eta_x^2 + \eta_y^2 + 1)^{1/2}} \quad (14.1)$$

Describe the fluid as inviscid and irrotational, as is generally appropriate at high $\mathcal{R}e$.

Basic state: $\eta = 0$, $\mathbf{u} = \nabla \phi$, $\phi = \mp \frac{1}{2} V x$ for $z \pm$.

Perturbed state: $\phi = \mp \frac{1}{2} V x + \phi_{\pm}$ in $z \pm$, where ϕ_{\pm} is the perturbation field.

Solve

$$\nabla \cdot \mathbf{u} = \nabla^2 \phi_{\pm} = 0 \quad (14.2)$$

subject to BCs:

1. $\phi_{\pm} \rightarrow 0$ as $z \rightarrow \pm\infty$
2. **Kinematic BC:** $\frac{\partial \eta}{\partial t} = \mathbf{u} \cdot \mathbf{n}$,
where

$$\mathbf{u} = \nabla \left(\mp \frac{1}{2} V x + \phi_{\pm} \right) = \mp \frac{1}{2} V \hat{\mathbf{x}} + \frac{\partial \phi_{\pm}}{\partial x} \hat{\mathbf{x}} + \frac{\partial \phi_{\pm}}{\partial y} \hat{\mathbf{y}} + \frac{\partial \phi_{\pm}}{\partial z} \hat{\mathbf{z}} \quad (14.3)$$

from which

$$\frac{\partial \eta}{\partial t} = \left(\mp \frac{1}{2} V + \frac{\partial \phi_{\pm}}{\partial x} \right) (-\eta_x) + \frac{\partial \phi_{\pm}}{\partial y} (-\eta_y) + \frac{\partial \phi_{\pm}}{\partial z} \quad (14.4)$$

Linearize: assume perturbation fields η , ϕ_{\pm} and their derivatives are small and therefore can neglect their products.

Thus $\hat{\eta} \approx (-\eta_x, -\eta_y, 1)$ and $\frac{\partial \eta}{\partial t} = \pm \frac{1}{2} V \eta_x + \frac{\partial \phi_{\pm}}{\partial z} \Rightarrow$

$$\frac{\partial \phi_{\pm}}{\partial z} = \frac{\partial \eta}{\partial t} \mp \frac{1}{2} V \frac{\partial \eta}{\partial x} \quad \text{on } z = 0 \quad (14.5)$$

3. **Normal Stress Balance:** $p_- - p_+ = \sigma \nabla \cdot \mathbf{n}$ on $z = \eta$.
Linearize: $p_- - p_+ = -\sigma (\eta_{xx} + \eta_{yy})$ on $z = 0$.

We now deduce p_{\pm} from time-dependent Bernoulli:

$$\rho \frac{\partial \phi}{\partial t} + \frac{1}{2} \rho u^2 + p + \rho g z = f(t) \quad (14.6)$$

where $u^2 = \frac{1}{4} V^2 \mp V \frac{\partial \phi_{\pm}}{\partial x} + H.O.T.$

Linearize:

$$\rho_{\pm} \frac{\partial \phi_{\pm}}{\partial t} + \frac{1}{2} \rho_{\pm} \left(\mp V \frac{\partial \phi_{\pm}}{\partial x} \right) + p_{\pm} + \rho_{\pm} g \eta = G(t) \quad (14.7)$$

so

$$p_- - p_+ = (\rho_+ - \rho_-) g \eta + (\rho_+ \frac{\partial \phi_{\pm}}{\partial t} - \rho_- \frac{\partial \phi_{\pm}}{\partial t}) + \frac{V}{2} (\rho_- \frac{\partial \phi_-}{\partial x} + \rho_+ \frac{\partial \phi_+}{\partial x}) = -\sigma (\eta_{xx} + \eta_{yy}) \quad (14.8)$$

is the linearized normal stress BC. Seek normal mode (wave) solutions of the form

$$\eta = \eta_0 e^{i\alpha x + i\beta y + \omega t} \quad (14.9)$$

$$\phi_{\pm} = \phi_{0\pm} e^{\mp k z} e^{i\alpha x + i\beta y + \omega t} \quad (14.10)$$

where $\nabla^2 \phi_{\pm} = 0$ requires $k^2 = \alpha^2 + \beta^2$.

Apply kinematic BC: $\frac{\partial \phi_{\pm}}{\partial z} = \frac{\partial \eta}{\partial t} \mp \frac{1}{2} V \frac{\partial \eta}{\partial x}$ at $z = 0 \Rightarrow$

$$\mp k \phi_{0\pm} = \omega \eta_0 \mp \frac{1}{2} i \alpha V \eta_0 \quad (14.11)$$

Normal stress BC:

$$k^2 \sigma \eta_0 = -g(\rho_- - \rho_+) \eta_0 + \omega(\rho_+ \phi_{0+} - \rho_- \phi_{0-}) + \frac{1}{2} i \alpha V (\rho_+ \phi_{0+} + \rho_- \phi_{0-}) \quad (14.12)$$

Substitute for $\phi_{0\pm}$ from (14.11):

$$-k^3 \sigma = \omega \left[\rho_+ \left(\omega - \frac{1}{2} i \alpha V \right) + \rho_- \left(\omega + \frac{1}{2} i \alpha V \right) \right] + g k (\rho_- - \rho_+) + \frac{1}{2} i \alpha V \left[\rho_+ \left(\omega - \frac{1}{2} i \alpha V \right) + \rho_- \left(\omega + \frac{1}{2} i \alpha V \right) \right]$$

so

$$\omega^2 + i \alpha V \left(\frac{\rho_- - \rho_+}{\rho_- + \rho_+} \right) \omega - \frac{1}{4} \alpha^2 V^2 + k^2 C_0^2 = 0 \quad (14.13)$$

where $C_0^2 \equiv \left(\frac{\rho_- - \rho_+}{\rho_- + \rho_+} \right) \frac{g}{k} + \frac{\sigma}{\rho_- + \rho_+} k$.

Dispersion relation: we now have the relation between ω and k

$$\omega = \frac{1}{2} i \left(\frac{\rho_+ - \rho_-}{\rho_- + \rho_+} \right) \mathbf{k} \cdot \mathbf{V} \pm \left[\frac{\rho_- - \rho_+}{(\rho_- + \rho_+)^2} (\mathbf{k} \cdot \mathbf{V})^2 - k^2 C_0^2 \right]^{1/2} \quad (14.14)$$

where $\mathbf{k} = (\alpha, \beta)$, $k^2 = \alpha^2 + \beta^2$.

The system is UNSTABLE if $\mathcal{R}e(\omega) > 0$, i.e. if

$$\frac{\rho_+ \rho_-}{\rho_- + \rho_+} (\mathbf{k} \cdot \mathbf{V})^2 > k^2 C_0^2 \quad (14.15)$$

Squires Theorem:

Disturbances with wave vector $\mathbf{k} = (\alpha, \beta)$ parallel to \mathbf{V} are most unstable. This is a general property of shear flows.

We proceed by considering two important special cases, Rayleigh-Taylor and Kelvin-Helmholtz instability.

14.1 Rayleigh-Taylor Instability

We consider an initially static system in which heavy fluid overlies light fluid: $\rho_+ > \rho_-$, $V = 0$. Via (14.15), the system is unstable if

$$C_0^2 = \frac{\rho_- - \rho_+}{\rho_+ \rho_-} \frac{g}{k} + \frac{\sigma}{\rho_- + \rho_+} k < 0 \tag{14.16}$$

i.e. if $\rho_+ - \rho_- > \frac{\sigma k^2}{g} = \frac{4\pi^2 \sigma}{g \lambda^2}$.

Thus, for instability, we require: $\lambda > 2\pi\lambda_c$ where $\lambda_c = \sqrt{\frac{\sigma}{\Delta\rho g}}$ is the capillary length.

Heuristic Argument:

Change in Surface Energy:

$$\Delta E_S = \sigma \cdot \underbrace{\Delta l}_{\text{arc length}} = \sigma \left[\int_0^\lambda ds - \lambda \right] = \frac{1}{4} \sigma \epsilon^2 k^2 \lambda.$$

Change in gravitational potential energy:

$$\Delta E_G = \int_0^\lambda -\frac{1}{2} \rho g (h^2 - h_0^2) dx = -\frac{1}{4} \rho g \epsilon^2 \lambda.$$

When is the total energy decreased?

When $\Delta E_{total} = \Delta E_S + \Delta E_G < 0$, i.e. when $\rho g > \sigma k^2$, so $\lambda > 2\pi\lambda_c$.

The system is thus unstable to long λ .

Note:

1. The system is stabilized to small λ disturbances by σ
2. The system is always unstable for suff. large λ
3. In a finite container with width smaller than $2\pi\lambda_c$, the system may be stabilized by σ .
4. System may be stabilized by temperature gradients since Marangoni flow acts to resist surface deformation. E.g. a fluid layer on the ceiling may be stabilized by heating the ceiling.

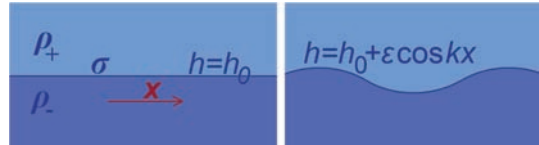


Figure 14.2: The base state and the perturbed state of the Rayleigh-Taylor system, heavy fluid over light.

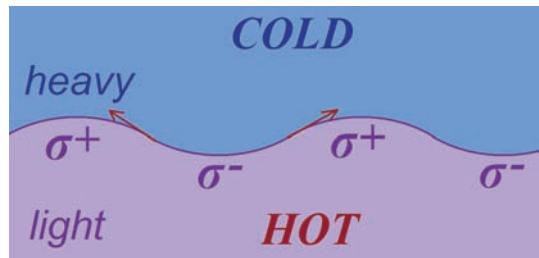


Figure 14.3: Rayleigh-Taylor instability may be stabilized by a vertical temperature gradient.

14.2 Kelvin-Helmholtz Instability

We consider shear-driven instability of a gravitationally stable base state. Specifically, $\rho_- \geq \rho_+$ so the system is gravitationally stable, but destabilized by the shear.

Take \mathbf{k} parallel to \mathbf{V} , so $(\mathbf{V} \cdot \mathbf{k})^2 = k^2 V^2$ and the instability criterion becomes:

$$\rho_- \rho_+ V^2 > (\rho_- - \rho_+) \frac{g}{k} + \sigma k \quad (14.17)$$

Equivalently,

$$\rho_- \rho_+ V^2 > (\rho_- - \rho_+) g \frac{\lambda}{2\pi} + \sigma \frac{2\pi}{\lambda} \quad (14.18)$$

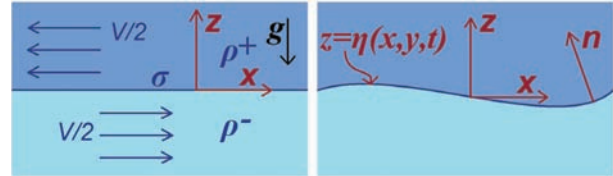


Figure 14.4: Kelvin-Helmholtz instability: a gravitationally stable base state is destabilized by shear.

Note:

1. System stabilized to short λ disturbances by surface tension and to long λ by gravity.
2. For any given λ (or k), one can find a critical V that destabilizes the system.

Marginal Stability Curve:

$$V(k) = \left(\frac{\rho_- - \rho_+}{\rho_- \rho_+} \frac{g}{k} + \frac{1}{\rho_- \rho_+} \sigma k \right)^{1/2} \quad (14.19)$$

$V(k)$ has a minimum where $\frac{dV}{dk} = 0$, i.e. $\frac{d}{dk} V^2 = 0$.

This implies $-\frac{\Delta\rho}{k^2} + \sigma = 0 \Rightarrow k_c = \sqrt{\frac{\Delta\rho g}{\sigma}} = \frac{1}{l_{cap}}$.

The corresponding $V_c = V(k_c) = \frac{2}{\rho_- \rho_+} \sqrt{\Delta\rho g \sigma}$ is the minimal speed necessary for waves.

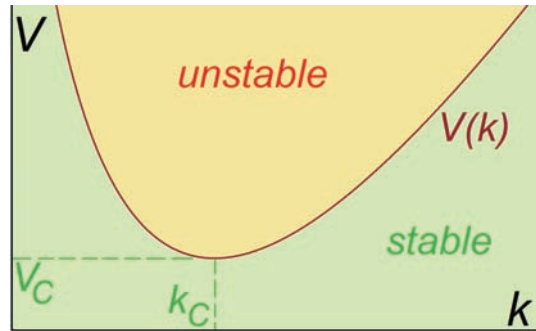


Figure 14.5: Fluid speed $V(k)$ required for the growth of a wave with wavenumber k .

E.g. Air blowing over water: (cgs)

$V_c^2 = \frac{2}{1.2 \cdot 10^{-3}} \sqrt{1 \cdot 10^3 \cdot 70} \Rightarrow V_c \sim 650 \text{cm/s}$ is the minimum wind speed required to generate waves.

These waves have wavenumber $k_c = \sqrt{\frac{1 \cdot 10^3}{70}} \approx 3.8 \text{ cm}^{-1}$, so $\lambda_c = 1.6 \text{cm}$. They thus correspond to capillary waves.

15. Contact angle hysteresis, Wetting of textured solids

Recall: In Lecture 3, we defined the equilibrium contact angle θ_e , which is prescribed by Young's Law: $\cos \theta_e = (\gamma_{SV} - \gamma_{SL}) / \gamma$ as deduced from the horizontal force balance at the contact line. Work done by a contact line moving a distance dx :

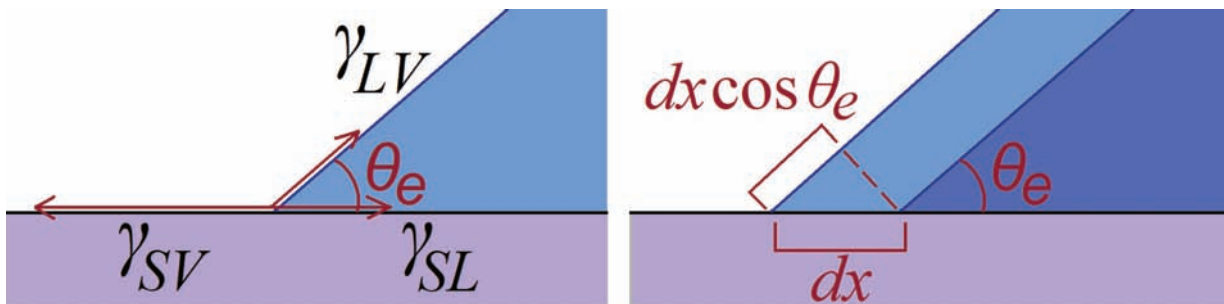


Figure 15.1: Calculating the work done by moving a contact line a distance dx .

$$dW = \underbrace{(\gamma_{SV} - \gamma_{SL}) dx}_{\text{contact line motion}} - \underbrace{\gamma \cos \theta_e dx}_{\text{from creating new interface}} \quad (15.1)$$

In equilibrium: $dW = 0$, which yields Young's Law. It would be convenient if wetting could be simply characterized in terms of this single number θ_e . Alas, there is:

15.1 Contact Angle Hysteresis

For a given solid wetting a given liquid, there is a range of possible contact angles: $\theta_r < \theta < \theta_a$, i.e. the contact angle lies between the retreating and advancing contact angles; θ_r and θ_a , respectively. That is, many θ values may arise, depending on surface, liquid, roughness and history.

Filling a drop

- begin with a drop in equilibrium with $\theta = \theta_e$
- fill drop slowly with a syringe
- θ increases progressively until attaining θ_a , at which point the contact line advances

Draining a drop

- begin with a drop in equilibrium with $\theta = \theta_e$
- drain drop slowly with a syringe
- θ decreases progressively until attaining θ_r , at which point the contact line retreats

Origins: Contact line pinning results from surface heterogeneities (either chemical or textural), that present an energetic impediment to contact line motion.

The pinning of a contact line on impurities leads to increased interfacial area, and so is energetically costly. Contact line motion is thus resisted.

Contact Line Pinning at Corners

A finite range of contact angles can arise at a corner $\theta_1 < \theta < \pi - \phi + \theta_1$; thus, an advancing contact line will generally be pinned at corners. Hence surface texture increases contact angle hysteresis.

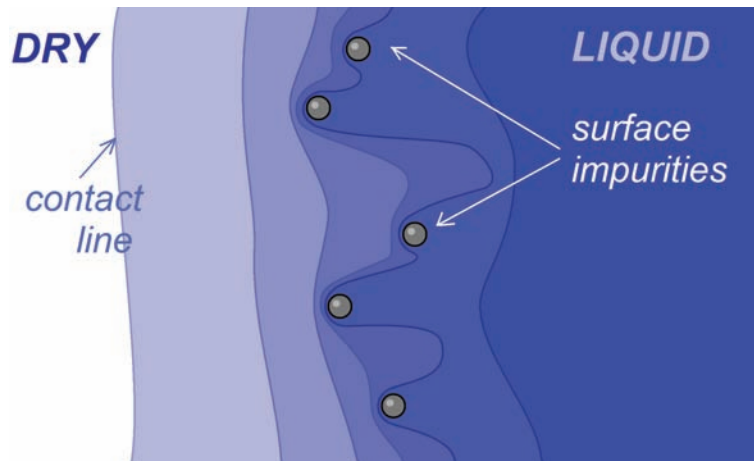


Figure 15.2: Pinning of a contact line retreating from left to right due to surface impurities.

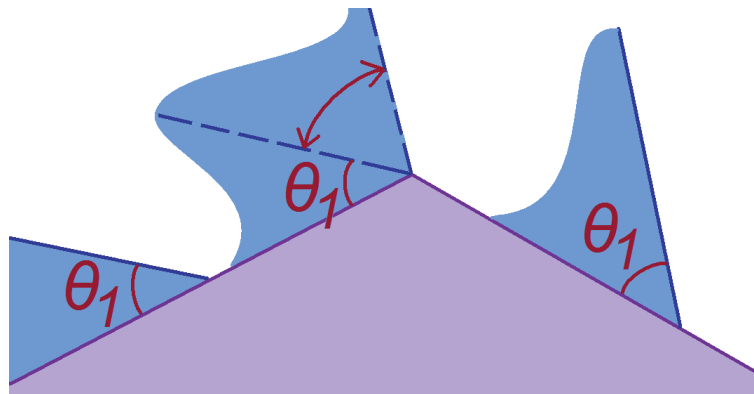


Figure 15.3: A range of contact angles is possible at a corner.

Manifestations of Contact Angle Hysteresis

I. Liquid column trapped in a capillary tube.

θ_2 can be as large as θ_a ; θ_1 can be as small as θ_r . In general $\theta_2 > \theta_1$, so there is a net capillary force available to support the weight of the slug.

$$\underbrace{2\pi R\sigma(\cos\theta_1 - \cos\theta_2)}_{\text{max contact force}} = \underbrace{\rho g\pi R^2 H}_{\text{weight}} \quad (15.2)$$

Force balance requires:

$$\frac{2\sigma}{R}(\cos\theta_1 - \cos\theta_2) = \rho g H \quad (15.3)$$

Thus, an equilibrium is possible only if $\frac{2\sigma}{R}(\cos\theta_r - \cos\theta_a) > \rho g H$.

Note: if $\theta_a = \theta_r$ (no hysteresis), there can be no equilibrium.

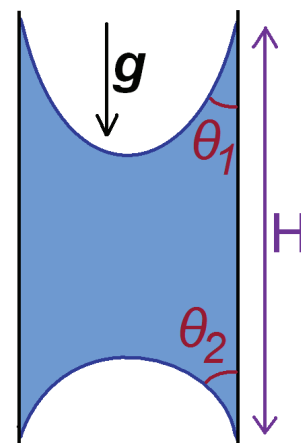


Figure 15.4: A heavy liquid column may be trapped in a capillary tube despite the effects of gravity.

II. Raindrops on window panes (*Dussan+Chow 1985*)

If $\theta_1 = \theta_2$ then the drop will fall due to unbalanced gravitational force. θ_2 can be as large as θ_a , θ_1 as small as θ_r . Thus, the drop weight may be supported by the capillary force associated with the contact angle hysteresis.

Note: $F_g \sim \rho R^3 g$, $F_c \sim 2\pi R\sigma(\cos \theta_1 - \cos \theta_2)$ which implies that $\frac{F_g}{F_c} \sim \frac{\rho g R^2}{\sigma} \equiv \mathcal{B}o$. In general, drops on a window pane will increase in size by accretion until $\mathcal{B}o > 1$ and will then roll downwards.

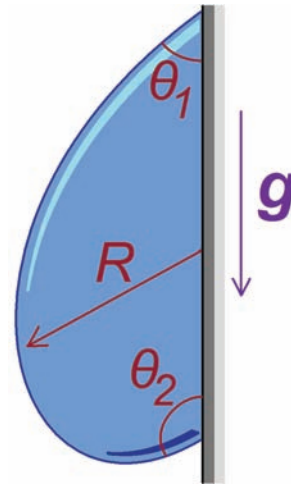


Figure 15.5: A raindrop may be pinned on a window pane.

15.2 Wetting of a Rough Surface

Consider a fluid placed on a rough surface.

Define: roughness parameters

$$r = \frac{\text{Total Surface Area}}{\text{Projected Surf. Area}} > 1 \quad \phi_S = \frac{\text{Area of islands}}{\text{Projected Area}} < 1 \tag{15.4}$$

The change in surface energy associated with the fluid front advancing a distance dz :

$$dE = (\gamma_{SL} - \gamma_{SV})(r - \phi_S)dz + \gamma(1 - \phi_S)ds \tag{15.5}$$

Spontaneous Wetting (demi-wicking) arises when $dE < 0$

i.e. $\cos \theta_e = \frac{\gamma_{SV} - \gamma_{SL}}{\gamma} > \frac{1 - \phi_S}{r - \phi_S} \equiv \cos \theta_c$, i.e. when $\theta_e < \theta_c$. **Note:**

1. can control θ_e with chemistry, r and ϕ_S with geometry, so can prescribe wettability of a solid.
2. if $r \gg 1$, $\theta_c = \frac{\pi}{2}$, so one expects spontaneous wicking when $\theta_e < \pi/2$
3. for a flat surface, $r \sim 1$, $\theta_c = 0$: wicking requires $\cos \theta_e > 1$ which never happens.
4. most solids are rough (except for glass which is smooth down to $\sim 5\text{\AA}$).

Wetting of Rough Solids with Drops

Consider a drop placed on a rough solid. **Define:** Effective contact angle θ^* is the contact angle apparent on a rough solid, which need not correspond to θ_e . **Observation:**

$\theta^* < \theta_e$ when $\theta_e < \pi/2$ (hydrophilic)

$\theta^* > \theta_e$ when $\theta_e > \pi/2$ (hydrophobic).

The intrinsic hydrophobicity or hydrophilicity of a solid, as prescribed by θ_e , is **enhanced** by surface roughening.

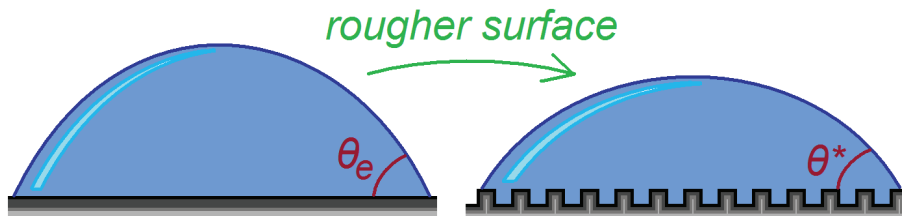


Figure 15.6: A drop wetting a rough solid has an effective contact angle θ^* that is generally different from its equilibrium value θ_e .

15.3 Wenzel State (1936)

A Wenzel state arises when the fluid impregnates the rough solid. The change in wetting energy associated with a fluid front advancing a distance dx (see Fig. 15.7) is

$$dE_W = r(\gamma_{SL} - \gamma_{SV})dx + \gamma \cos \theta^* dx \quad (15.6)$$

If $r = 1$ (smooth surface), Young's Law emerges.

If $r > 1$: $\cos \theta^* = r \cos \theta_e$

Note:

1. wetting tendencies are amplified by roughening, e.g. for hydrophobic solid ($\theta_e > \pi/2$, $\cos \theta_e < 0 \Rightarrow \theta_e \gg \pi/2$ for large r)
2. for $\theta_e < \theta_c$ (depends on surface texture) \Rightarrow demi-wicking / complete wetting
3. Wenzel state breaks down at large $r \Rightarrow$ air trapped within the surface roughness \Rightarrow Cassie State

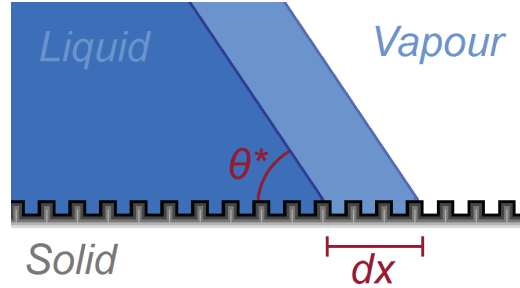


Figure 15.7: The wetting of a rough solid in a Wenzel state.

15.4 Cassie-Baxter State

In a Cassie state, the fluid does not impregnate the rough solid, leaving a trapped vapour layer. A fluid placed on the rough surface thus sits on roughness elements (e.g. pillars or islands), and the change of energy associated with its front advancing a distance dx is

$$dE_c = \phi_S (\gamma_{SL} - \gamma_{SV}) dx + (1 - \phi_S) \gamma dx + \gamma \cos \theta^* dx \quad (15.7)$$

For equilibrium ($dE_c/dx = 0$), we require:

$$\cos \theta^* = -1 + \phi_S + \phi_S \cos \theta_e \quad (15.8)$$

Note:

1. as pillar density $\phi_S \rightarrow 0$, $\cos \theta^* \rightarrow -1$, i.e. $\theta^* \rightarrow \pi$
2. drops in a Cassie State are said to be in a “fakir state”.
3. contact angle hysteresis is greatly increased in the Wenzel state, decreased in the Cassie.
4. the maintenance of a Cassie state is key to water repellency.

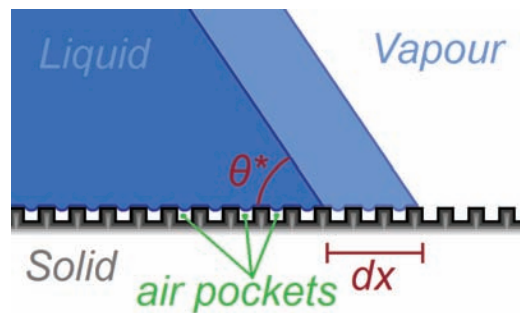


Figure 15.8: The wetting of a rough solid in a Cassie-Baxter state.

Crossover between Wenzel and Cassie states:

For $dE_W > dE_c$, we require $-r \cos \theta_e + \cos \theta^* > -\phi_S \cos \theta_e + (1 - \phi_S) + \cos \theta^*$, i.e. $\cos \theta_e < \frac{-1 + \phi_S}{r - \phi_S} = \cos \theta_c$, i.e. one expects a Cassie state to emerge for $\cos \theta_e > \cos \theta_c$. Therefore, the criterion for a Wenzel State giving way to a Cassie state is identical to that for spontaneous wicking.

Summary:

Hydrophilic: Wenzel's Law ceases to apply at small θ_e when demi-wicking sets in, and the Cassie state emerges.

Hydrophobic: Discontinuous jump in θ^* as θ_e exceeds $\pi/2 \Rightarrow$ Cassie state. Jump is the largest for large roughness (small ϕ_S)

Historical note:

1. early studies of wetting motivated by insecticides
2. chemists have since been trying to design superhydrophobic (or oliophobic) surfaces using combinations of chemistry and texture
3. recent advances in microfabrication have achieved $\theta^* \sim \pi$, $\Delta\theta \sim 0$ (e.g. Lichen surface *McCarthy*)

16. More forced wetting

Some clarification notes on **Wetting**.



Figure 16.1: Three different wetting states.

Last class, we discussed the Cassie state only in the context of drops in a Fakir state, i.e. suspended partially on a bed of air. There is also a “wet Cassie” state. More generally, the Cassie-Baxter model applies to wetting on a planar but chemically heterogeneous surfaces.

Consider a surface with 2 species, one with area fraction f_1 and equilibrium contact angle θ_1 , another with area fraction f_2 and angle θ_2 . Energy variation associated with the front advancing a distance dx :

$$dE = f_1(\gamma_{SL} - \gamma_{SV})_1 dx + f_2(\gamma_{SL} - \gamma_{SV})_2 dx + \gamma \cos \theta^* dx.$$

Thus, $dE = 0$ when

$$\cos \theta^* = f_1 \cos \theta_1 + f_2 \cos \theta_2 \quad (\text{Cassie-Baxter relation}) \quad (16.1)$$

Special Case: in the Fakir state, the two phases are the solid ($\theta_1 = \theta_e$ and $f_1 = \theta_S$) and air ($\theta_2 = \pi$, $f_2 = 1 - \theta_S$) so we have

$$\cos \theta^* = \theta_S \cos \theta_e - 1 + \theta_S \quad (16.2)$$

as previously. As before, in this hydrophobic case, the Wenzel state is energetically favourable when $dE_W < dE_C$, i.e. $\cos \theta_C < \cos \theta_e < 0$

where $\cos \theta_C = (\theta_S - 1)/(r - \theta_S)$, i.e. θ_C is between $\pi/2$ and θ_e .

However, experiments indicate that even in this regime, air may remain trapped, so that a *metastable Cassie* state emerges.

16.1 Hydrophobic Case: $\theta_e > \pi/2$, $\cos \theta_e < 0$

In the Fakir state, the two phases are the solid ($\theta = \theta_e$, $f_1 = \phi$) and vapour ($\theta_2 = \pi$, $f_2 = 1 - \phi_s$).

Cassie-Baxter:

$$\cos \theta^* = \pi_S \cos \theta_e - 1 + \phi_s \quad (16.3)$$

as deduced previously. As previously, the Wenzel state is energetically favourable when $dE_W < dE_L$, i.e. $\cos \theta_C < \cos \theta_e < 0$ where $\cos \theta_C = \frac{\phi_s - 1}{r - \phi_s}$. Experiments indicate that even in this region, air may remain trapped, leading to a meta-stable Fakir state.

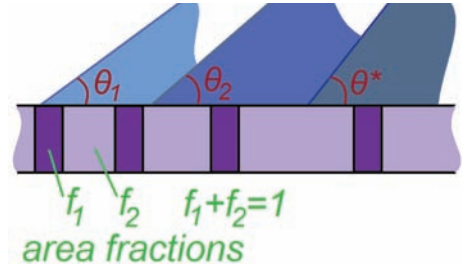


Figure 16.2: Wetting of a tiled (chemically heterogeneous) surface.

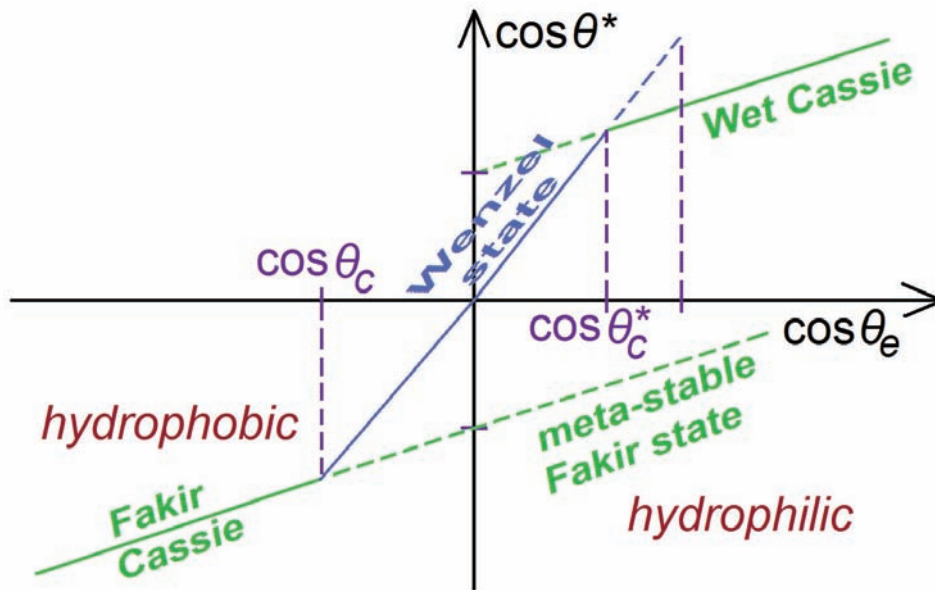


Figure 16.3: Relationship between $\cos \theta^*$ and $\cos \theta_e$ for different wetting states.

16.2 Hydrophilic Case: $\theta_e < \pi/2$

Here, the Cassie state corresponds to a tiled surface with 2 phases corresponding to the solid ($\theta_1 = \theta_e$, $f_1 = \phi_S$) and the fluid ($\theta_2 = 0$, $f_2 = 1 - \phi_S$).

Cassie-Baxter $\Rightarrow \cos \theta^* = 1 - \phi_S + \phi_S \cos \theta_e$, which describes a “Wet Cassie” state. Energy variation: $dE = (r - \phi_S)(\gamma_{SL} - \gamma_{SV})dx + (1 - \phi_S)\gamma dx$.

$$\Rightarrow dE = 0 \text{ if } \cos \theta_e = \frac{\gamma_{SL} - \gamma_{SV}}{\gamma} > \frac{1 - \phi_S}{r - \phi_S} \equiv \cos \theta_c^* \tag{16.4}$$

For $\theta_e < \theta_c$, a film will impregnate the rough solid. Criteria for this transition can also be deduced by equating energies in the Cassie and Wenzel states, i.e. $r \cos \theta_e = 1 - \phi_S + \phi_S \cos \theta_e \Rightarrow \theta_e = \theta_C$. Therefore, when $\pi/2 > \theta_e > \theta_C$, the solid remains dry ahead of the drop \Rightarrow Wenzel applies \Rightarrow when $\theta_e < \theta_C \Rightarrow$ film penetrates texture and system is described by “Wet Cassie” state.

Johnson + Dettre (1964) examined water drops on wax, whose roughness they varied by baking. They showed an increase and then decrease of $\Delta\theta = \theta_a - \theta_r$ as the roughness increased, and system went from smooth to Wenzel to Cassie states.

Water-repellency: important for corrosion-resistance, self-cleaning, drag-reducing surfaces. It requires the maintenance of a Cassie State. This means the required impregnation pressure must be exceeded by the curvature pressure induced by roughness.

E.g.1 Static Drop in a Fakir State

The interface will touch down if $\delta > h$. Pressure balance: $\frac{\sigma}{R} \sim \sigma \frac{\delta}{l^2}$ so $\delta > h \Rightarrow \frac{l^2}{R} > h$ i.e. $R < \frac{l^2}{h}$. Thus taller pillars maintain Fakir State. (see Fig. 16.5)

E.g.2 Impacting rain drop: impregnation pressure $\Delta P \sim \rho U^2$ or $\rho U c$ where c is the speed of sound in water.

E.g.3 Submerged surface, e.g. on a side of a boat. $\Delta P = \rho g z$ is impregnation pressure.

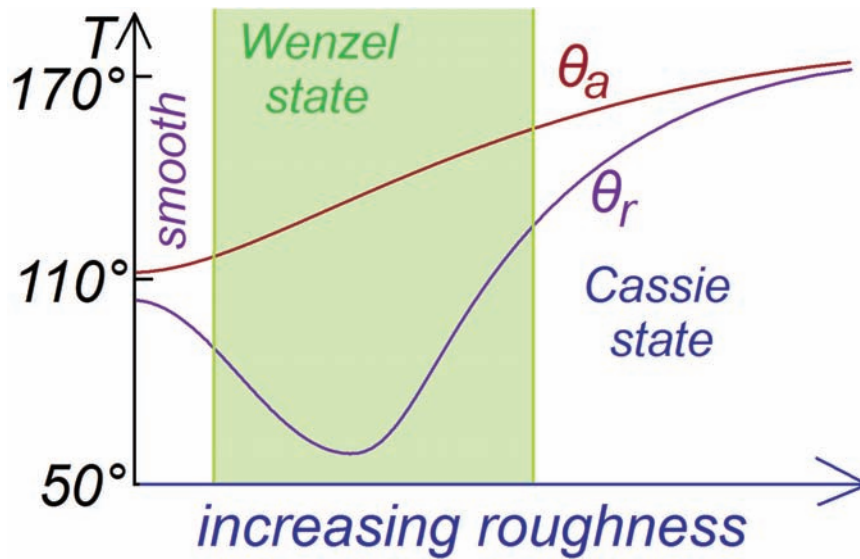


Figure 16.4: Contact angle as a function of surface roughness for water drops on wax.

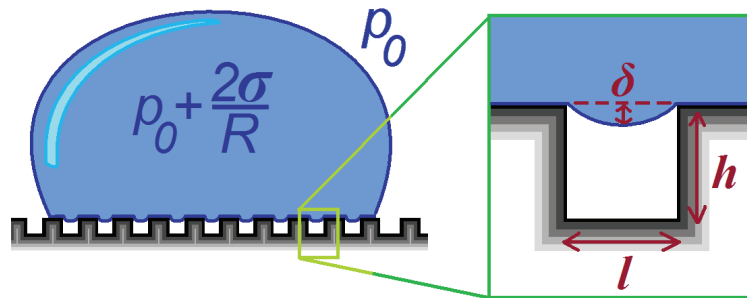


Figure 16.5: To remain in a Cassie state, the internal drop pressure $P_0 + 2\sigma/R$ must not exceed the curvature pressure induced by the roughness, roughly σ/l .

16.3 Forced Wetting: the Landau-Levich-Derjaguin Problem

Withdraw a plate from a viscous fluid with constant speed. What is the thickness of the film that coats the plate? Consider a static meniscus.

For relatively thick films ($Ca \sim 1$), balancing viscous stresses and gravity: $\mu \frac{V}{h} \sim \rho gh \Rightarrow$

$$h \sim \left(\frac{\mu V}{\rho g} \right)^{1/2} \sim \ell_c Ca^{1/2} \quad (\text{Derjaguin 1943}) \tag{16.5}$$

where $\ell_c = \sqrt{\frac{\sigma}{\rho g}}$ and $Ca = \frac{\mu V}{\sigma} = \frac{\text{viscous}}{\text{curvature}}$ is the Capillary number.

But this scaling is not observed at low Ca , where the coating is resisted principally by curvature pressure rather than gravity. Recall static meniscus (Lecture 6): $\eta(x) = \sqrt{2}\ell_c (1 - \sin \theta(x))$ and internal pressure: $p(x) = p_0 - \rho g \eta(x)$. As $x \rightarrow 0$, $\eta(x) \rightarrow \sqrt{2}\ell_c$ and $p(x) \rightarrow p_0 - \sqrt{2}\rho g \ell_c$. It is this capillary suction inside the meniscus that resists the rise of thin films.

Thin film wetting

We describe the flow in terms of two distinct regions:

Region I: Static meniscus. The balance is between gravity and curvature pressures: $\rho g \eta \sim \sigma \nabla \cdot \mathbf{n}$ so curvature $\nabla \cdot \mathbf{n} \sim 1/\ell_c$.

Region II: Dynamic meniscus (coating zone). The balance here is between viscous stresses and curvature pressure. Define this region as the zone over which film thickness decreases from $2h$ to h , whose vertical extent L to be specified by pressure matching. In region II, curvature $\nabla \cdot \mathbf{n} \sim h/L^2$. Matching pressure at point A: $p_0 - \frac{\sigma h}{L^2} \sim p_0 - \rho g \ell_c \Rightarrow L^2 \sim \frac{\sigma h}{\rho g \ell_c} \sim \ell_c h \Rightarrow L = \sqrt{\ell_c h}$ is the geometric mean of ℓ_c and h .

Force balance in Zone II: viscous stress vs. curvature pressure: $\mu \frac{V}{h^2} \sim \frac{\Delta P}{L} \sim \sigma \frac{h}{L^2} \frac{1}{L}$.

Substitute in for $L \Rightarrow h^3 \sim \frac{\mu V}{\sigma} L^3 \sim Ca \ell_c^{3/2} h^{3/2} \Rightarrow h \sim \ell_c Ca^{2/3}$ where $\ell_c = \sqrt{\frac{\sigma}{\rho g}}$, $Ca = \frac{\mu V}{\sigma}$.

Implicit in above: $h \ll L$, $L \ll \ell_c$, $\rho g \ll \frac{\sigma h}{L^3}$, or equivalently $Ca^{1/3} \ll 1$. Matched asymptotics give $h \approx 0.94 \ell_c Ca^{2/3}$.

E. g. 1 Jump out of pool at 1m/s: $Ca \sim 10^{-2}$ so $h \sim 0.1\text{mm} \Rightarrow \sim 300\text{g}$ entrained.

E. g. 2 Drink water from a glass, $V \sim 1\text{cm/s} \Rightarrow Ca \sim 10^{-4}$.

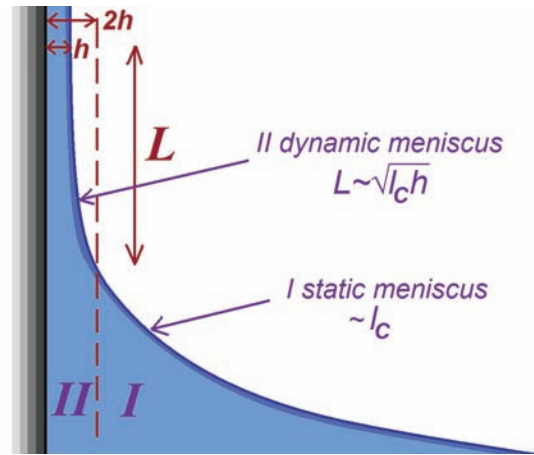


Figure 16.6: The two regions of the meniscus next to a moving wall.

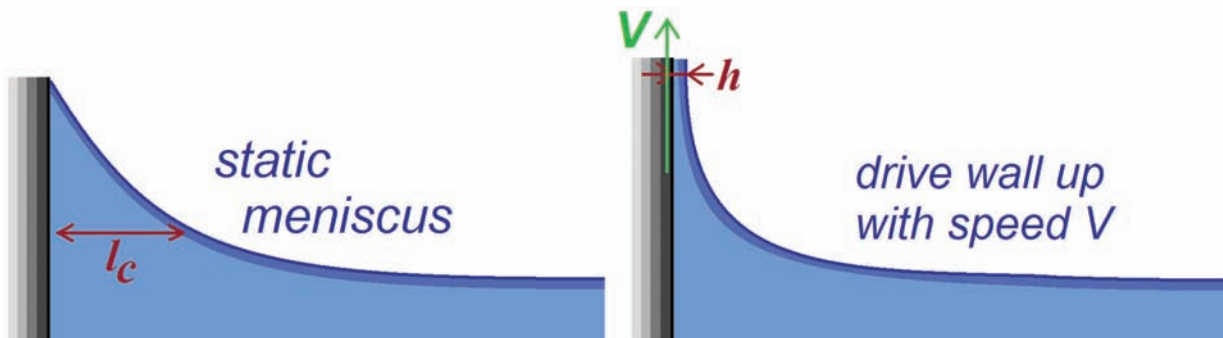


Figure 16.7: Left: A static meniscus. Right: Meniscus next to a wall moving upwards with speed V .

17. Coating: Dynamic Contact Lines

Last time we considered the Landau-Levich-Derjaguin Problem and deduced

$$h \sim \ell_c Ca^{2/3} \text{ for } Ca = \frac{\mu V}{\sigma} < 10^{-3}$$

$$h \sim \ell_c Ca^{1/3} \text{ for } Ca \rightarrow 1.$$

The influence of surfactants

Surfactants decrease σ which affects h slightly. But the principle effect is to generate Marangoni stresses that increase fluid emplacement: h typically doubles.

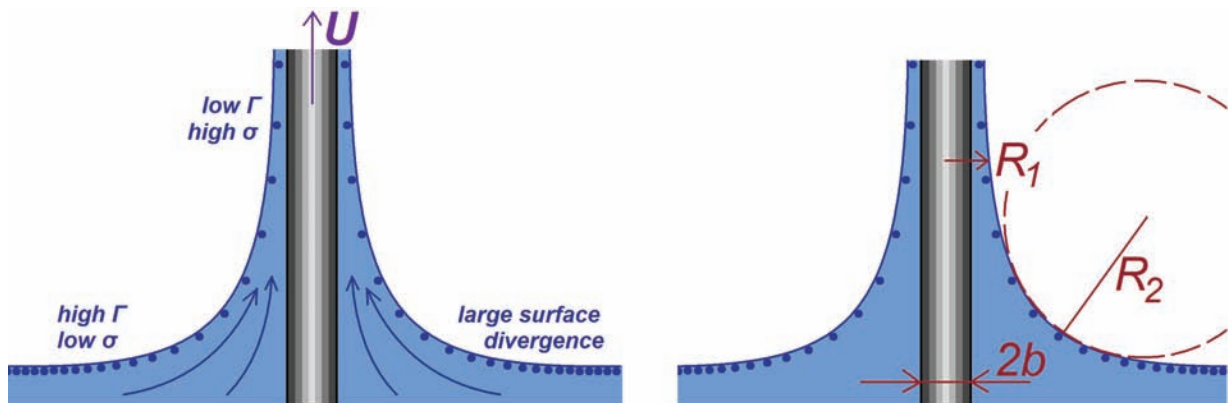


Figure 17.1: The influence of surfactants on fiber coating. Gradients in Γ induce Marangoni stresses that enhance deposition.

Fiber coating:

$$\text{Normal stress: } p_0 + \sigma \left(\frac{1}{R_1} + \frac{1}{R_2} \right) = p_0 - \rho g z.$$

If $b \ll \ell_c$, $\frac{1}{R_1} \sim \frac{1}{b} \Rightarrow$ curvature pressures dominant, can't be balanced by gravity.

Thus, the interface must take the form of a catenoid: $\frac{1}{R_1} + \frac{1}{R_2} = 0$.

For wetting, $\theta_e = 0 \Rightarrow r(z) = b \cosh\left(\frac{z-h}{b}\right)$ where $h \approx b \ln(2\ell_c/b)$.

Note:

1. gravity prevents meniscus from extending to $\infty \Rightarrow h$ deduced by cutting it off at ℓ_c .
2. h is just a few times b ($h \ll \ell_c$) \Rightarrow lateral extent greatly exceeds its height.

Forced wetting on fibers e.g. optical fiber coating.

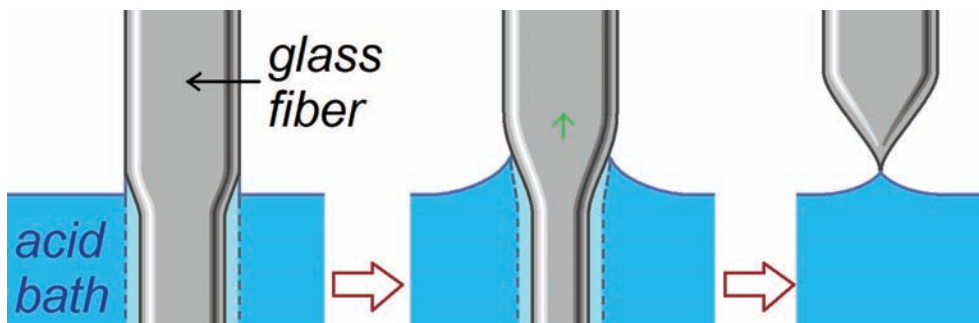


Figure 17.2: Etching of the microtips of Atomic Force Microscopes. As the fiber is withdrawn from the acid bath, the meniscus retreats and a sharp tip forms.

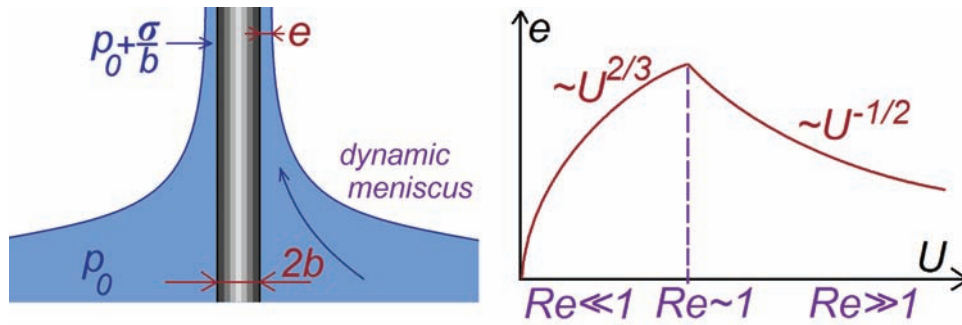


Figure 17.3: *Left*: Forced wetting on a fiber. *Right*: The coating thickness as a function of the Reynolds number Re .

$$p_{film} \sim p_0 + \frac{\sigma}{b}, p_{meniscus} \sim p_0 \Rightarrow \Delta p \sim \frac{\sigma}{b} \text{ resists entrainment.}$$

$$\text{Force balance: } \mu \frac{U}{e^2} \sim \frac{\Delta p}{L} = \frac{\sigma}{bL}.$$

$$\text{Pressure match: } \frac{e}{L^2} \sim \frac{1}{b} \Rightarrow L \sim \sqrt{be}, \text{ substitute into the previous equation to find}$$

$$e \approx bCa^{2/3} \quad (\text{Bretherton's Law}) \quad (17.1)$$

Note:

- this scaling is valid when $e \ll b$, i.e. $Ca^{2/3} \ll 1$.
- At higher Ca , film is the viscous boundary layer that develops during pulling: $\delta \sim \left(\frac{\mu}{\rho} \frac{L_s}{U}\right)^{1/2}$, where L_s is the submerged length.

Displacement of an interface in a tube

E.g. air evacuating a water-filled pipette, pumping oil out of rock with water.

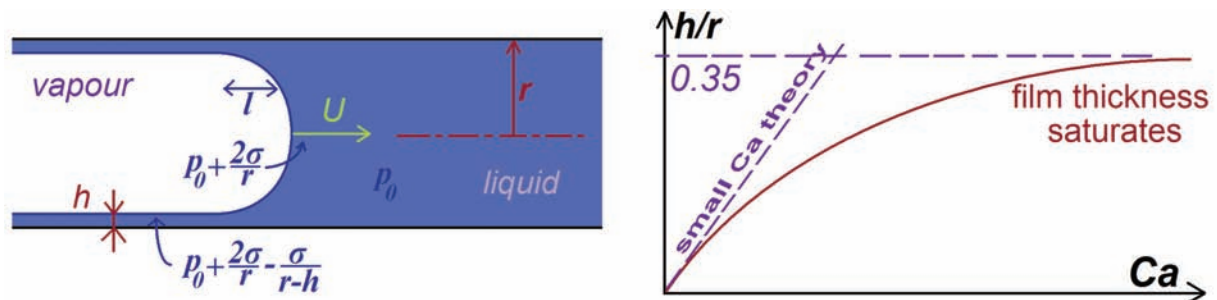


Figure 17.4: *Left*: Displacing a liquid with a vapour in a tube. *Right*: The dependence of the film thickness left by the intruding front as a function of $Ca = \mu U / \sigma$.

In the limit of $h \ll r$, the pressure gradient in the meniscus $\nabla p \sim \frac{\sigma}{rl}$, where l is the extent of the dynamic meniscus.

As on a fiber, pressure matching: $p_0 + \frac{2\sigma}{r} - \frac{\sigma}{r-h} \sim p_0 + \frac{\sigma h}{l^2} \Rightarrow l \sim (hr)^{1/2}$ when $h \ll r$.

$$\text{Force balance: } \underbrace{\mu U / h^2}_{\text{viscous}} \sim \underbrace{\sigma / rl}_{\text{curvature}} \sim \sigma / r(hr)^{1/2} \Rightarrow$$

$$h \sim rCa^{2/3} \quad (\text{Bretherton 1961}) \quad (17.2)$$

where $Ca = \frac{\mu U}{\sigma}$.

Thick films: what if $h = \text{ord}(r)$? For $h \sim r$, Taylor (1961) found $h \sim (r-h)Ca^{2/3}$.

17.1 Contact Line Dynamics

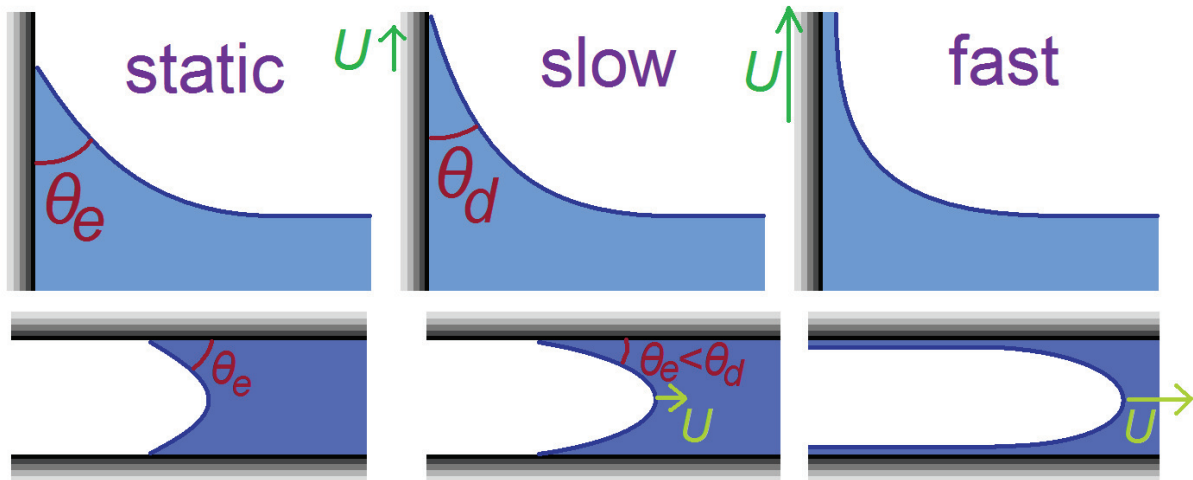


Figure 17.5: The form of a moving meniscus near a wall or inside a tube for three different speeds.

We consider the withdrawal of a plate from a fluid bath (Fig. 16.6) or fluid displacement within a cylindrical tube. **Observations:**

- at low speeds, the contact line advances at the dynamic contact angle $\theta_d < \theta_e$
- dynamic contact angle θ_d decreases progressively as U increases until $U = U_M$.
- at sufficiently high speed, the contact line cannot keep up with the imposed speed and a film is entrained onto the solid.

Now consider a clean system free of hysteresis.

Force of traction pulling liquid towards a dry region:

$$F(\theta_d) = \gamma_{SV} - \gamma_{SL} - \gamma \cos \theta_d.$$

Note:

- $F(\theta_e) = 0$ in equilibrium. How does F depend on U ? What is $\theta_d(U)$?
- the retreating contact line ($F < 0$) was examined with retraction experiments e.g. plate withdrawal.
- the advancing contact line ($F > 0$) was examined by *Hoffmann (1975)* for the case of $\theta_e = 0$.
- he found $\theta_d \sim U^{1/3} \sim Ca^{1/3}$ (Tanner's Law)

Dussan (1979): drop in vicinity of contact line advances like a tractor tread

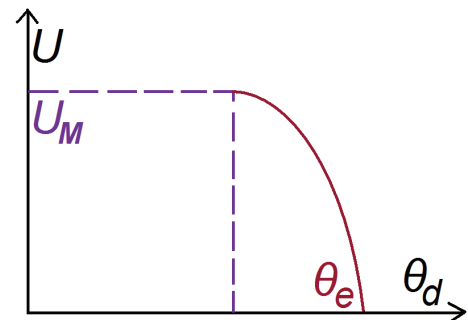


Figure 17.6: Dynamic contact angle θ_d as a function of the differential speed U . For $U > U_M$, the fluid wets the solid.

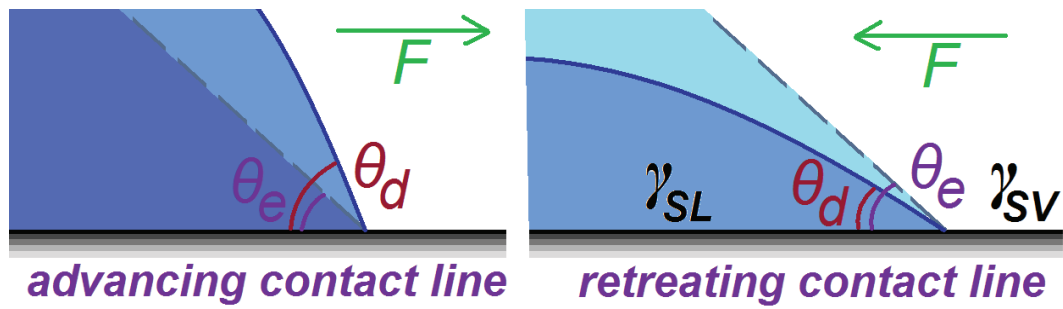


Figure 17.7: The advancing and retreating contact angles of a drop.

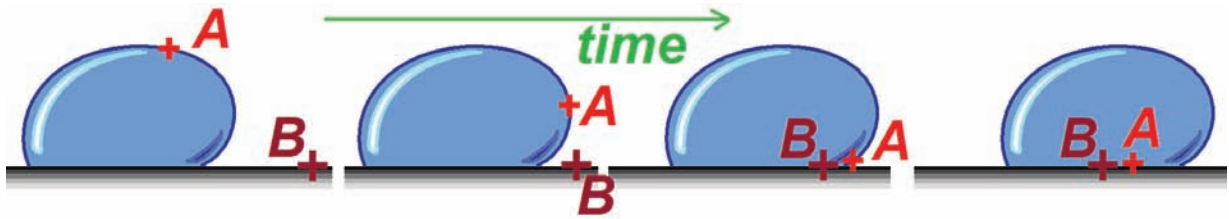


Figure 17.8: A drop advancing over a solid boundary behaves like a tractor tread (Dussan 1979), advancing through a rolling motion.

Flow near advancing contact line

We now consider the flow near the contact line of a spreading liquid ($\theta_d > \theta_e$):

- consider $\theta_d \ll 1$, so that slope $\tan \theta_d = \frac{z}{x} \approx \theta_d \Rightarrow z \approx \theta_d x$.
- velocity gradient: $\frac{dU}{dz} \approx \frac{U}{\theta_d x}$
- rate of viscous dissipation in the corner

$$\Phi = \int \int_{corner} \mu \left(\frac{dv}{dz} \right)^2 dU = \mu \int_0^\infty dx \int_0^{z_{max}=\theta_d x} \frac{U^2}{\theta_d^2 x^2} dz \tag{17.3}$$

$$\Phi = 3\mu \int_0^\infty \frac{U^2}{\theta_d^2 x^2} \theta_d x dx = \frac{3\mu U^2}{\theta_d} \int_0^\infty \frac{dx}{x} \tag{17.4}$$

de Gennes' approximation: $\int_0^\infty \frac{dx}{x} \approx \int_a^L \frac{dx}{x} = \ln L/a \equiv \ell_D$

where L is the drop size and a is the molecular size. From experiments $15 < \ell_D < 20$.

Energetics:

$$FU = \Phi = \frac{3\mu \ell_D}{\theta_d} \cdot U^2 \tag{17.5}$$

rate of work done by surface forces equals the rate of viscous dissipation.

Recall:

- $F = \gamma_{SV} - \gamma_{SL} - \gamma \cos \theta_d = \gamma (\cos \theta_e - \cos \theta_d)$
- in the limit $\theta_e < \theta_d \ll 1$, $\cos \theta \approx 1 - \frac{\theta^2}{2} \Rightarrow F \approx \frac{\gamma}{2} (\theta_d^2 - \theta_e^2)$
- substitute F into the energetics equation to get the contact line speed:

$$U = \frac{U^*}{6\ell_D} \theta_d (\theta_d^2 - \theta_e^2) \tag{17.6}$$

where $U^* = \frac{\gamma}{\mu} \approx 30\text{m/s}$.

Note:

1. rationalizes Hoffmann's data (obtained for $\theta_e = 0$) $\Rightarrow U \sim \theta_D^3$
2. $U = 0$ for $\theta_d = \theta_e$ (static equilibrium)
3. $U = 0$ as $\theta_d \rightarrow 0$: dissipation in sharp wedge impedes motion.
4. $U(\theta_d)$ has a maximum when $\frac{dU}{d\theta_d} = \frac{U^*}{6\ell_D} (3\theta_d^2 - \theta_e^2) \Rightarrow \theta_d = \frac{\theta_e}{\sqrt{3}} \Rightarrow U_{max} = \frac{U^*}{9\sqrt{3}\ell_D} \theta_e^3$

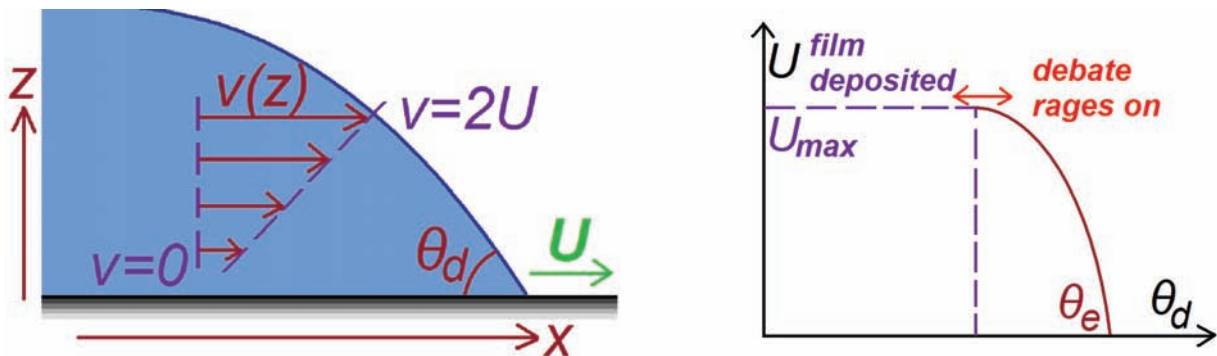


Figure 17.9: *Left*: Schematic illustration of the flow in the vicinity of an advancing contact line. *Right*: The dependence of the dynamic contact angle on the speed of withdrawal.

E.g. In water, $U^* = 70\text{m/s}$. With $\theta_e = 0.1$ radians and $\ell_D = 20$, $U_{max} = 0.2\text{mm/s}$
 \Rightarrow sets upper bound on extraction speed for water coating flows.

18. Spreading

Recall: gravity currents, the spreading of heavy fluid under the influence of gravity.

further reading: **John E. Simpson - Gravity Currents: In the Environment and the Laboratory.**

Stage I: $Re \gg 1$

Flow forced by gravity, and resisted by fluid inertia:

$$\frac{\Delta \rho g h}{R} \sim \rho \frac{U^2}{R} \Rightarrow U \sim \sqrt{g'h} \quad \text{where } g' = \frac{\Delta \rho}{\rho} g.$$

$$\begin{aligned} \text{Continuity: } V = \pi R^2(t)h(t) = \text{const.} &\Rightarrow h(t) \sim \frac{V}{R^2(t)} \\ \Rightarrow U \equiv \frac{dR}{dt} \sim \sqrt{g'V} \frac{1}{R} &\Rightarrow R dR \sim \sqrt{g'V} dt \Rightarrow R(t) \sim \\ (g'V)^{1/4} t^{1/2} \end{aligned}$$

Note: $U \sim \sqrt{g'h}$ decreases until $Re = \frac{UR}{\nu} \leq 1$.

Stage II: $Re \ll 1$

Flow forced by gravity, resisted by viscosity: $\frac{\partial p}{\partial r} = \nu \frac{\partial^2 u}{\partial z^2} \Rightarrow \frac{\Delta \rho g h}{R} \sim \nu \frac{U}{h^2}$
now substitute for $h(t) = V/R^2(t)$ to obtain:

$$U = \frac{dR}{dt} \sim \frac{R}{t} \sim \frac{\rho g' V^3}{\nu R^7} \Rightarrow R \sim \left(\frac{\rho g' V^3}{\nu} \right)^{1/8} t^{1/8} \quad (18.1)$$

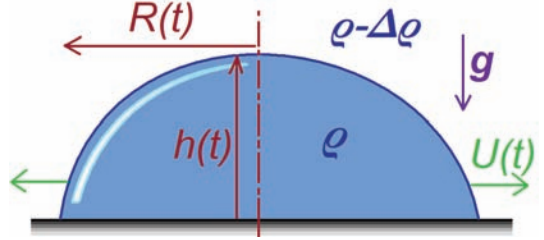


Figure 18.1: Spreading of a fluid volume under the influence of gravity.

18.1 Spreading of small drops on solids

For a drop of undeformed radius R placed on a solid substrate, spreading will in general be driven by both gravity and curvature pressure.

Gravity: $\nabla p_g \sim \frac{\rho g h}{R}$, Curvature: $\nabla p_c \sim \frac{\gamma h}{R^3}$.

Continuity $V = \pi R^2(t)h(t) = \text{const.}$

Which dominates? $\frac{\Delta p_g}{\Delta p_c} \sim \frac{\rho g R^2}{\gamma} = \text{Bond number. } \mathcal{Bo} = \frac{\rho g V}{\gamma h} \sim \frac{1}{h} \Rightarrow$ gravity becomes progressively more important as the drop spreads !?

Recall:

- drop behaviour depends on $S = \gamma_{SV} - \gamma_{SL} - \gamma$.
- When $S < 0$: Partial wetting. Spreading arises until a puddle forms.
- When $S > 0$: Complete wetting. Here, one expects spreading forced by the unbalanced tension at the contact line.

$$\underbrace{\frac{\mu U}{h}}_{\text{viscous stress}} \cdot \underbrace{\pi R^2}_{\text{drop area}} \sim \underbrace{S}_{\text{contact line force}} \cdot \underbrace{2\pi R}_{\text{perimeter}} \quad (18.2)$$

Thus, we expect $R \frac{dR}{dt} \sim \frac{S}{\mu} h \sim \frac{S}{\mu} \frac{U}{R^2} \Rightarrow R^3 \frac{dR}{dt} \sim \frac{SU}{\mu}$

$$\Rightarrow R \sim \left(\frac{SU}{\mu} \right)^{1/4} t^{1/4} \quad (18.3)$$

But this is not observed; instead, one sees $R \sim t^{1/10}$. **Why?**

Hardy (1919) observed a precursor film, the evidence of which was the disturbance of dust ahead of the drop. This precursor film is otherwise invisible, with thickness $e \sim 20\text{\AA}$. Its origins lie in the force imbalance at the contact line ($S > 0$) and its stability results from interactions between the fluid and solid (e.g. Van der Waals)

Physical picture

Force at Apparent Contact Line: $F = \gamma + \gamma_{SL} - \gamma \cos \theta_d - \gamma_{SL} = \gamma(1 - \cos \theta_d) \approx \gamma \frac{\theta_d^2}{2}$ for small θ_d .

Note: $F \ll S$. Now recall from last class: $FU = \frac{3\mu\ell_D}{\theta_d} U^2$.

Letting $F \rightarrow \frac{\gamma\theta_d^2}{2}$, we find $U = \frac{dR}{dt} = \frac{\theta_d}{3\ell_D\mu} F = \frac{U^*}{6\ell_D} \theta_d^3$, where $U^* = \frac{\gamma}{\mu}$. Since the drop is small, it is a section of a sphere, so that

$$U = \frac{\pi}{4} R^3 \theta_d \tag{18.4}$$

Hence $\frac{3}{R} \frac{dR}{dt} = -\frac{1}{\theta_d} \frac{d\theta_d}{dt}$. Substituting in $\frac{dR}{dt}$ from above, we find:

$$\frac{1}{\theta_d} \frac{d\theta_d}{dt} = -\frac{U^*}{R} \theta_d^3$$

Now substitute $R = L\theta_d^{-1/3} \approx (U/\theta_d)^{1/3}$ and $L \equiv U^{1/3} \Rightarrow \frac{d\theta_d}{dt} = -\frac{U^*}{L} \theta_d^{13/3} \Rightarrow$

$$\theta_d = \left(\frac{L}{U^*t} \right)^{3/10} \quad (\text{Tanner's Law}) \tag{18.5}$$

so using (18.4) yields $R \sim L \left(\frac{U^*t}{L} \right)^{1/10}$, which is consistent with observation.

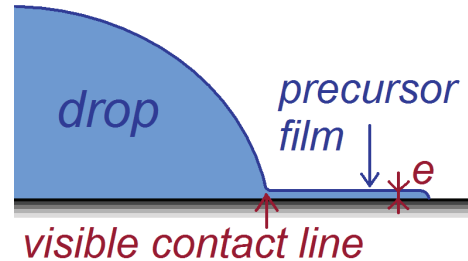


Figure 18.2: The precursor film of a spreading drop.

18.2 Immiscible Drops at an Interface *Pujado & Scriven 1972*

Gravitationally unstable configurations can arise ($\rho_a < \rho_b < \rho_c$ or $\rho_c < \rho_a < \rho_b$).

- weight of drops supported by interfacial tensions.
- if drop size $R < l_{bc} \sim \sqrt{\frac{\gamma_{bc}}{(\rho_b - \rho_c)g}}$, it can be suspended by the interface.

Sessile Lens, $\rho_a < \rho_c < \rho_b$: stable for drops of any size, e.g. oil on water.

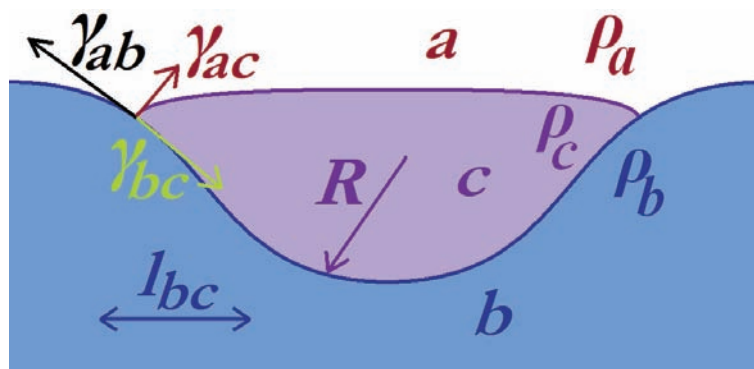


Figure 18.3: An immiscible liquid drop floats on a liquid bath.

18.3 Oil Spill

3 Distinct phases:

Phase I Inertia vs. Gravity: $U \sim \sqrt{g'h(t)} \Rightarrow R(t) \sim (g'U_0)^{1/4} t^{1/2}$

Phase II Viscosity vs. Gravity : as previously, $R \sim \left(\frac{\rho g' V_0^3}{\nu}\right)^{1/8} t^{1/8}$

Phase III Line tension vs. Viscosity: For $S < 0$, an equilibrium configuration arises \Rightarrow drop takes the form of a sessile lens. For $S > 0$ the oil will completely cover the water, spreading to a layer of molecular thickness.

Phase IIIa Viscous resistance from dissipation within oil. As previously:

$$\frac{\mu U}{h} \pi R^2 \sim 2\pi R S \Rightarrow R \sim \left(\frac{SU}{\mu}\right)^{1/4} t^{1/4}$$

Phase IIIb Spreading driven by S , resisted by viscous dissipation in the underlying fluid.

Blasius boundary layer grows on base of spreading current like $\delta \sim \sqrt{\nu t}$.

$$\mu \frac{U}{\delta} \pi R^2 \sim S \cdot 2\pi R \text{ where } \delta \sim \sqrt{\nu t} \Rightarrow R \frac{dR}{dt} \sim \frac{S}{\mu} \sqrt{\nu t}^{1/2} \Rightarrow R \sim \left(\frac{S}{\mu}\right)^{1/2} \nu^{1/4} t^{3/4}.$$

18.4 Oil on water: A brief review

When an oil drop is emplaced on the water surface, its behaviour will depend on the spreading coefficient

$$S \equiv \sigma_{aw} - \sigma_{oa} - \sigma_{ow} \quad (18.6)$$

For $S > 0$, the droplet will completely wet the underlying liquid, and so spread to a layer of molecular thickness.

References: *Franklin (1760); Fay (1963); DePietro & Cox (1980); Foda & Cox (1980); Joanny (1987); Brochard-Wyart et al. (1996); Fraaije & Cazabat (1989).*

For $S < 0$, an equilibrium configuration arises: the drop assumes the form of a sessile lens.

The statics of the sessile lens have been considered by *Langmuir (1933)* and *Pujado & Scriven (1972)*. their dynamics has been treated by *Wilson & Williams (1997)* and *Miksis & Vanden-Broeck (2001)*.

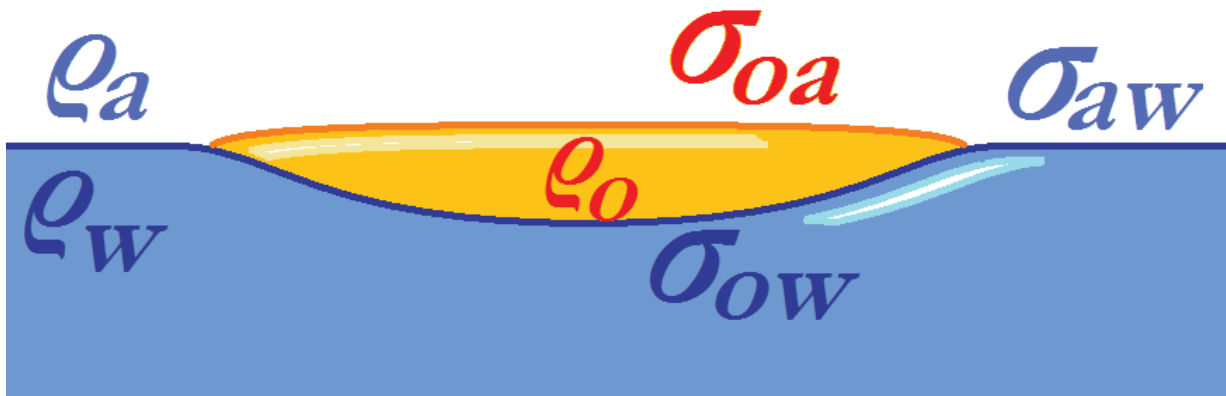


Figure 18.4: An oil drop spreading on the water surface.

18.5 The Beating Heart *Stocker & Bush (JFM 2007)*

When a drop of mineral oil containing a small quantity of non-ionic, water-insoluble surfactant (Tergitol)



Figure 18.5: An oil drop oscillates on the water surface. Note the ring of impurities that marks the edge of the internal circulation.

is so emplaced, a sessile lens with $S < 0$ is formed. However, **no equilibrium shape emerges**; the lens is characterized by periodic fluctuations in radius, and so resembles a beating heart.

The phenomenon was first reported by *Buetschli (1894)*, a professor of Zoology at the University of Heidelberg, in his treatise *Investigations on Protoplasm*. It was subsequently described qualitatively by *Sebba (1979, 1981)*.

Motivation: “*The ultimate goal of physiologists is to be able to explain living behaviour in terms of physicochemical forces. Thus, any expansion of our knowledge of such forces, based on inanimate systems, should be examined to see whether this might not offer insight into biological behaviour*”. Sebba (1979).

Many biological systems exhibit periodic behaviour; e.g. oscillations of cells of nerves and muscle tissue, oscillations in mitochondria, and biological clocks. Conversion of chemical into mechanical energy is one of the main processes in biological movements; e.g. chloroplast movements and muscle contraction.

Observations:

- lens behaviour is independent of water depth, strongly dependent on surfactant concentration Γ
- for $\Gamma = 0$ no beating - stable sessile lens
- for moderate Γ steady beating observed
- for high Γ drop edges become unstable to fingers
- for highest Γ , lens explodes into a series of smaller beating lenses.
- beating marked by slow expansion, rapid retraction
- odour of Tergitol always accompanies beating

- placing lid on the chamber suppresses the oscillations \Rightarrow evaporation is a critical ingredient.

Physical picture

Stage I: Slow expansion of drop.

Adsorption of surfactant onto oil-water interface $\Rightarrow \sigma_{ow}$ decreases. Evaporation of surfactant from air-water surface $\Rightarrow \sigma_{aw}$ increases.

Stage II: Rapid retraction.

Flushing of surfactant onto air-water interface $\Rightarrow \sigma_{aw}$ decreases and σ_{ow} increases. BUT WHY?

Internal circulation: confined to the outer extremities of the lens, absent in the flat central region. Marangoni flow associated with gradient in Γ - indicates Γ is lowest at the drop edge. Consistent with radial gradient in adsorption flux along surface. Reflects geometric constraint - less surfactant available to corners than bulk.



Such **Marangoni shear layers** are unstable to longitudinal rolls or *transverse waves* (as in the wine glass).

Figure 18.6: Internal circulation of the “beating heart”.

The flushing events are associated with breaking Marangoni waves (*Frenkel & Halpern 2005*).

Another surfactant-induced auto-oscillation: The Spitting Drop (*Fernandez & Homsy 2004*)

- chemical reaction produces surfactant at drop surface
- following release of first drop, periodic spitting
- rationalized in terms of *tip-streaming* (Taylor 1934), which arises only in the presence of surfactant (de Bruijn 1993) for $\mu/\mu_d \approx 10^4$ and $Ca = \mu G/\sigma > 0.4$

19. Water waves

We consider waves that might arise from disturbing the surface of a pond.

We define the normal to the surface: $\mathbf{n} = \frac{(-\zeta_x, 1)}{(1+\zeta_x^2)^{1/2}}$

Curvature: $\nabla \cdot \mathbf{n} = \frac{-\zeta_{xx}}{(1+\zeta_x^2)^{3/2}}$

We assume the fluid motion is inviscid and irrotational: $\mathbf{u} = \nabla\phi$. Must deduce solution for velocity potential ϕ satisfying $\nabla^2\phi = 0$.

B.C.s:

1. $\frac{\partial\phi}{\partial z} = 0$ on $z = -h$

2. Kinematic B.C.:

$\frac{D\zeta}{Dt} = u_z \Rightarrow \frac{\partial\zeta}{\partial t} + \frac{\partial\phi}{\partial x} \frac{\partial\zeta}{\partial x} = \frac{\partial\phi}{\partial z}$ on $z = \zeta$.

3. Dynamic B.C. (time-dependent Bernoulli applied at free surface):

$\rho \frac{\partial\phi}{\partial t} + \frac{1}{2}\rho |\nabla\phi|^2 + \rho g\zeta + p_s = f(t)$, independent of x

where $p_s = p_0 + \sigma \nabla \cdot \mathbf{n} = p_0 - \sigma \frac{\zeta_{xx}}{(1+\zeta_x^2)^{3/2}}$ is the surface pressure.

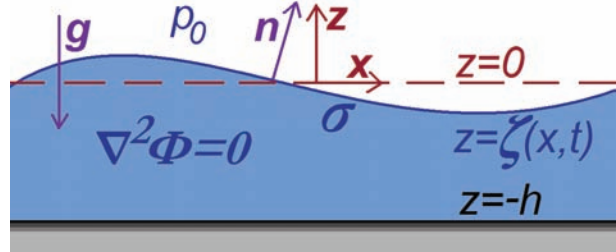


Figure 19.1: Waves on the surface of an inviscid irrotational fluid.

Recall: unsteady inviscid flows Navier-Stokes:

$$\rho \frac{\partial\mathbf{u}}{\partial t} + \rho \left[\nabla \left(\frac{1}{2}u^2 \right) - \mathbf{u} \times (\nabla \times \mathbf{u}) \right] = -\nabla(p + \Phi) \quad (19.1)$$

For irrotational flows, $\mathbf{u} = \nabla\phi$, so that $\mathbf{u} \cdot \nabla \left[\rho \frac{\partial\phi}{\partial t} + \frac{1}{2}\rho |\nabla\phi|^2 + p + \Phi \right] = 0$.

Time-dependent Bernoulli: $\rho \frac{\partial\phi}{\partial t} + \frac{1}{2}\rho |\nabla\phi|^2 + p + \Phi = F(t)$ only.

Now consider small amplitude waves and **linearize** the governing equations and BCs (assume ζ, ϕ are small, so we can neglect the nonlinear terms $\phi^2, \zeta^2, \phi\zeta$, etc.)

$\Rightarrow \nabla^2\phi = 0$ in $-h \leq z \leq 0$.

Must solve this equation subject to the **B.C.s**

1. $\frac{\partial\phi}{\partial z} = 0$ on $z = -h$

2. $\frac{\partial\zeta}{\partial t} = \frac{\partial\phi}{\partial z}$ on $z = 0$.

3. $\rho \frac{\partial\phi}{\partial t} + \rho g\zeta + p_0 - \sigma\zeta_{xx} = f(t)$ on $z = 0$.

Seek solutions: $\zeta(x, t) = \hat{\zeta} e^{ik(x-ct)}$, $\phi(x, z, t) = \hat{\phi}(z) e^{ik(x-ct)}$

i.e. travelling waves in x -direction with phase speed c and wavelength $\lambda = 2\pi/k$.

Substitute ϕ into $\nabla^2\phi = 0$ to obtain $\hat{\phi}_{zz} - k^2\hat{\phi} = 0$

Solutions: $\hat{\phi}(z) = e^{kz}, e^{-kz}$ or $\sinh(z), \cosh(z)$.

To satisfy B.C. 1: $\frac{\partial\hat{\phi}}{\partial z} = 0$ on $z = -h$ so choose $\hat{\phi}(z) = A \cosh k(z+h)$.

From B.C. 2:

$$ikc\hat{\zeta} = Ak \sinh kh \quad (19.2)$$

From B.C. 3: $(-ikc\rho A \cosh kh + \rho g\hat{\zeta} + k^2\sigma\hat{\zeta}) e^{ik(x-ct)} = f(t)$, independent of x , i.e.

$$-ikc\rho A \cosh kh + \rho g\hat{\zeta} + k^2\sigma\hat{\zeta} = 0 \quad (19.3)$$

(19.2) $\Rightarrow A = \frac{ic\hat{\zeta}}{\sinh kh} \Rightarrow$ into (19.3) $\Rightarrow c^2 = \left(\frac{g}{k} + \frac{\sigma k^3}{\rho} \right) \tanh kh$ defines the phase speed $c = \omega/k$.

Dispersion Relation:

$$\omega^2 = \left(gk + \frac{\sigma k^3}{\rho} \right) \tanh kh \quad (19.4)$$

Note: as $h \rightarrow \infty$, $\tanh kh \rightarrow 1$, and we obtain deep water dispersion relation deduced in our wind-over-water lecture.

Physical Interpretation

- relative importance of σ and g is prescribed by the Bond number $\mathbb{B}o = \frac{\rho g}{\sigma k^2} = \frac{\sigma(2\pi)^2}{\rho g \lambda^2} = (2\pi)^2 \frac{\ell_c^2}{\lambda^2}$ where $\ell_c = \sqrt{\sigma/\rho g}$ is the capillary length.
- for air-water, $\mathbb{B}o \sim 1$ for $\lambda \sim 2\pi\ell_c \sim 1.7\text{cm}$.
- $\mathbb{B}o \gg 1$, $\lambda \gg 2\pi\ell_c$: surface effects negligible \Rightarrow gravity waves.
- $\mathbb{B}o \ll 1$: $\lambda \ll 2\pi\ell_c$: influence of g is negligible \Rightarrow capillary waves.

Special Cases: deep and shallow water. Can expand via Taylor series: For $kh \ll 1$, $\tanh kh = kh - \frac{1}{3}(kh)^3 + O((kh)^5)$, and for $kh \gg 1$, $\tanh kh \approx 1$.

A. Gravity waves $\mathbb{B}o \gg 1$: $c^2 = \frac{g}{k} \tanh kh$.

Shallow water ($kh \ll 1$) $\Rightarrow c = \sqrt{gh}$. All wavelengths travel at the same speed (i.e. non-dispersive), so one can only surf in shallow water.

Deep water ($kh \gg 1$) $\Rightarrow c = \sqrt{g/k}$, so longer waves travel faster, e.g. drop large stone into a pond.

B. Capillary Waves: $\mathbb{B}o \ll 1$, $c^2 = \frac{\sigma k}{\rho} \tanh kh$.

Deep water $kh \gg 1 \Rightarrow c = \sqrt{\sigma k/\rho}$ so short waves travel fastest, e.g. raindrop in a puddle.

Shallow water $kh \ll 1 \Rightarrow c = \sqrt{\frac{\sigma h k^2}{\rho}}$.

An interesting note: in lab modeling of shallow water waves ($kh \ll 1$) $c^2 \approx \left(\frac{g}{k} + \frac{\sigma k}{\rho}\right) \left(kh - \frac{1}{3}k^3h^3 + O((kh)^5)\right) = gh + \left(\frac{\sigma h}{\rho} - \frac{1}{3}gh^2\right)k^2 + O((kh)^4)gh$. In ripple tanks, choose $h = \left(\frac{3\sigma}{\rho g}\right)^{1/2}$ to get a good approximation to nondispersive waves. In water, $\left(\frac{3\sigma}{\rho g}\right)^{1/2} \sim \left(\frac{3 \cdot 70}{10^3}\right)^{1/2} \sim 0.5\text{cm}$.

From $c(k)$ can deduce $c_{min} = \left(\frac{4g\sigma}{\rho}\right)^{1/4}$ for $k_{min} = \left(\frac{\rho g}{\sigma}\right)^{1/2}$.

Group velocity: when $c = c(\lambda)$, a wave is called dispersive since its different Fourier components (corresponding to different k or λ) separate or disperse, e.g. deep water gravity waves: $c \sim \sqrt{\lambda}$. In a dispersive system, the energy of a wave component does not propagate at $c = \omega/k$ (phase speed), but at the **group velocity**:

$$c_g = \frac{d\omega}{dk} = \frac{d}{dk}(ck) \quad (19.5)$$

Deep gravity waves: $\omega = ck = \sqrt{gk}$. $c_g = \frac{\partial \omega}{\partial k} = \frac{\partial}{\partial k} \sqrt{gk} = \frac{1}{2} \sqrt{g/k} = \frac{c}{2}$.

Deep capillary wave: $c = \frac{\sigma/\rho}{k}^{1/2}$, $\omega = \sqrt{\sigma/\rho} k^{3/2} \Rightarrow c_g = \frac{\partial \omega}{\partial k} = \frac{3}{2} \sqrt{\sigma/\rho} k^{1/2} = \frac{3}{2}c$.



Figure 19.2: Deep water capillary waves, whose speed increases as wavelength decreases.

Image courtesy of Andrew Davidhazy. Used with permission.

Flow past an obstacle.

If $U < c_{min}$, no steady waves are generated by the obstacle.

If $U > c_{min}$, there are two k -values, for which $c = U$:

1. the smaller k is a gravity wave with $c_g = c/2 < c \Rightarrow$ energy swept downstream.
2. the larger k is a capillary wave with $c_g = 3c/2 > c$, so the energy is swept upstream.

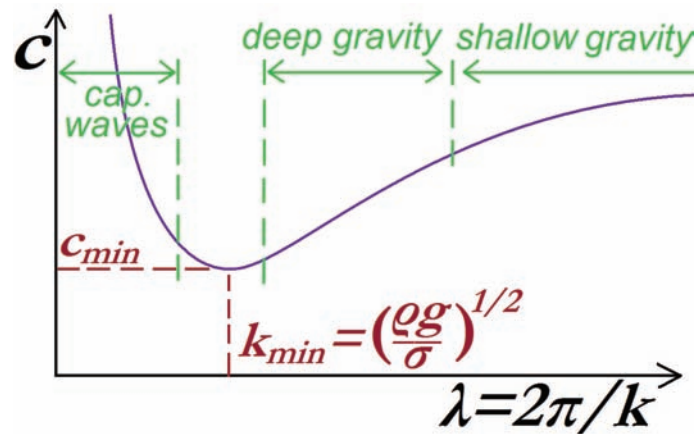


Figure 19.3: Phase speed c of surface waves as a function of their wavelength λ .

MIT OpenCourseWare
<http://ocw.mit.edu>

357 Interfacial Phenomena
Fall 2010

For information about citing these materials or our Terms of Use, visit: <http://ocw.mit.edu/terms>.